

**UNIVERSITÉ DE BELGRADE**

Faculté de chimie



**UNIVERSITÉ BORDEAUX 1**



Ecole doctorale des Sciences Chimiques

**Milena MILUTINOVIC**

**IMMOBILISATION D'HYDROGEL REDOX POUR LA DETECTION  
PAR ELECTROCHIMILUMINESCENCE**

**- Mémoire de thèse -**

**Membres du jury:**

Dr. Alexander KUHN	Professeur, ENSCBP, Université Bordeaux 1	Président du jury
Dr. Frédéric KANOUI	Directeur de recherche, CNRS, Paris	Rapporteur
Dr. Radmila DZUDOVIC	Professeur, Faculté de chimie, Université de Kragujevac	Rapporteur
Dr. Goran ROGLIC	Professeur, Faculté de chimie, Université de Belgrade	Examineur
Dr. Dragan MANOJLOVIC	Professeur, Faculté de chimie, Université de Belgrade	Directeur de thèse
Dr. Neso SOJIC	Professeur, ENSCBP, Université Bordeaux 1	Directeur de thèse

**Décembre 2011.**

**УНИВЕРЗИТЕТ У БЕОГРАДУ**

Хемијски факултет



**УНИВЕРЗИТЕТ БОРДО 1**



Докторска школа хемијских наука

**Милена Милутиновић**

**ЕЛЕКТРОГЕНЕРИСАНА ХЕМИЛУМИНИСЦЕНТНА ДЕТЕКЦИЈА  
ЗАСНОВАНА НА РЕДОКС ХИДРОГЕЛУ ИМОБИЛИЗОВАНОМ  
УНАПРЕЂЕНИМ МЕТОДАМА**

**- докторска дисертација –**

**Чланови комисије:**

Dr. Alexander Kuhn	Professeur, ENSCBP, Université Bordeaux 1	Председник комисије
Dr. Frédéric Kanoufi	Directeur de recherche, CNRS, Paris	Известилац
др Радмила Цудовић	Професор, Хемијски факултет, Универзитет у Крагујевцу	Известилац
др Горан Роглић	Професор, Хемијски факултет, Универзитет у Београду	Испитивач
др Драган Манојловић	Професор, Хемијски факултет, Универзитет у Београду	Ментор
Dr. Neso SOJC	Професор, ENSCBP, Универзитет Бордо 1	Ментор

**Децембар 2011.**

**UNIVERSITY OF BELGRADE**

Faculty of Chemistry



**UNIVERSITY BORDEAUX 1**



Doctoral school of Chemical Sciences

**Milena Milutinovic**

**ELECTROGENERATED CHEMILUMINESCENCE DETECTION  
BASED ON ADVANCED IMMOBILISED REDOX HYDROGEL**

**- Doctoral dissertation -**

**Members of the jury:**

Dr. Alexander Kuhn	Professor, ENSCBP, University Bordeaux 1	President of the jury
Dr. Frédéric Kanoufi	Director of research, CNRS, Paris	Reviewer
Dr. Radmila Dzudovic	Professor, Faculty of Chemistry, University of Kragujevac	Reviewer
Dr. Goran Roglic	Professor, Faculty of Chemistry, University of Belgrade	Examiner
Dr. Dragan Manojlovic	Professor, Faculty of Chemistry, University of Belgrade	Supervisor
Dr. Neso Sojic	Professor, ENSCBP, University Bordeaux 1	Supervisor

**December 2011.**

## ACKNOWLEDGMENT

---

The work presented in this doctoral dissertation was realised as co-tutoring thesis between the Analytical department of the Faculty of Chemistry, University of Belgrade in Serbia and the group Analytical Nanosystems of the Institute of Molecular Sciences, University Bordeaux 1 in France.

My special thanks belong to my supervisors Prof. Dr. Dragan Manojlovic and Prof. Dr. Neso Sojic. Their exceptional help, a lot of advices and fruitful discussions have enabled this doctoral dissertation to be realised. Желела бих да им се захвалим на изузетно доброј сарадњи, на њиховом залагању и непроцењиво великој помоћи током целе израде доктората. Захваљујем им се на указаном поверењу као и прилици да радим докторат у сарадњи између двеју земаља и тиме проширим своје видике, упознам једну нову земљу, културу и језик. Посебно им се захваљујем на подршци коју су ми пружили и у професионалном и у приватном животу. Својим саветима и смерницама омогућили су ми да се развијем у професионалном смислу. Својим личним примером били су мој узор. Они су ме увели у свет науке и омогућили да постанем оно што јесам и оно што ћу бити и ја им се на томе од срца захваљујем.

It is my great pleasure to thank to Dr. Frédéric Kanoufi and Prof. Dr. Radmila Dzudović for accepting to be the reviewers for my doctoral dissertation and to be a part of the jury for my defence.

I would also like to thank to Ministry of Education and Science and Ministry of Youth and Sport of the Republic of Serbia, to Innovation Center of the Faculty of Chemistry in Belgrade, to Ministry of Foreign Affairs of the French Republic, Eiffel excellence scholarship programme and French Institute in Belgrade for the financial support.

Je souhaite remercier les Dr. Nicolas Mano et Dr. Emmanuel Suraniti du Centre de Recherche Paul Pascal pour leur entière coopération durant mon travail de thèse. Leurs conseils, idées et soutiens ont été très importants dans le déroulement de ce projet.

Je tiens par ailleurs à remercier les différentes personnes du Groupe NanoSystèmes Analytiques (NsysA) avec qui j'ai passé des années scientifiquement et humainement magnifiques.

Tout d'abord, je voudrais remercier le Prof. Dr. Alexander Kuhn pour son accueil chaleureux au sein du laboratoire et pour son soutien continu durant ma thèse. Je tiens également à lui exprimer ma gratitude pour avoir accepté d'être le président du jury de ma soutenance de thèse.

Je voudrais ensuite chaleureusement remercier Stéphane Arbault pour avoir collaboré avec moi. De ses conseils et de nos discussions, j'ai beaucoup appris. Je remercie également Dodzi Zigah et Laurent Bouffier pour leurs expertises dans le domaine de l'électrochimie et au-delà. Je souhaite également adresser mes remerciements à Valérie Ravaine, Isabelle Gosse, Sandra Pinet, Véronique Lapeyre, Bertrand Goudeau, Anne-Marie Dorthé et Anne Thienpont.

Je voudrais spécialement remercier Patrick Garrigue pour toute l'aide qu'il a pu m'apporter, et il a su me guider de façon pertinente durant mon travail.

Je voudrais également exprimer ma gratitude à Aline Simon-Lalande sans qui je n'aurais pu m'en sortir d'un point administratif surtout au début de ma thèse. Merci pour sa disponibilité et sa patience à mon égard.

Enfin, je voudrais exprimer mes profonds remerciements à tous les étudiants et chercheurs du laboratoire NsysA avec qui j'ai passé de merveilleux moments à la fois dans et hors de notre laboratoire. Ils ont grandement contribué à ce que mes années de thèse à Bordeaux restent à jamais gravés dans ma mémoire. Merci à Catherine, Léa, Lisa, Zahra et Gabriel, Laurent, Salem et Suresh pour tous les moments de joie que nous avons partagé ensemble et pour le soutien et la compréhension qu'ils m'ont apporté. Je voudrais spécialement remercier Yémima et Matthias qui ont partagé ces années de thèse avec moi. Ils ont toujours été à mes côtés dans les bons comme dans les mauvais moments et ont su distiller de précieux conseils pour surmonter les différentes étapes qui nous faisaient faces.

Je tiens également à remercier Emeline, Hélène, Nina, Jérôme, Florent, Chawawait, Churalat et tous les étudiants présents dans le laboratoire durant ma thèse pour tous les moments que nous avons partagés ensemble. J'ai également une pensée pour les doctorants qui ont permis mon intégration dans le laboratoire : merci à Frédérique, Christophe et Emilie pour leur accueil chaleureux et leur aide. Enfin, je souhaiterais remercier Veronika et Jennifer avec qui j'ai passé une période de ma thèse inoubliable.

Такође, хтела бих да се захвалим свим члановима лабораторије 538 као и осталим професорима и истраживачима на Хемијском факултету у Београду који су били уз мене за време израде моје докторске дисертације. Пре свега, хтела бих да се захвалим

проф. др Горану Роглићу на конструктивним разговорима и корисним саветима као и на прихватању обавезе и одговорности да буде члан комисије приликом одбране моје докторске дисертације. Такође, хтела бих да се захвалим др Јелени Мутић на помоћи приликом писања дисертације и др Биљани Дојчиновић на великој подршци и разумевању. Исто тако, захваљујем се др Маји Груден Павловић, др Александру Николићу и мр Војину Крсмановићу на пријатној сарадњи током израде мог доктората.

Такође, хтела бих да се захвалим свим докторантима на изузетно пријатној атмосфери и свима онима који су ме уз њих испраћали и дочекивали и који су учинили да се у нашој лабораторији осећам као код куће. Захваљујем се Маријани, Јелени, Ивану и Далибору на изузетно пријатним разговорима, разумевању и подршци. Такође се захваљујем Дејану, Ференцу, Хиосу, Бекију и Бранку на пријатном друђењу.

Посебно се захваљујем Милицы Сентић која ће у сарадњи између Хемијског факулета у Београду и Института молекуларних наука у Бордоу наставити са проучавањем у области којом сам се бавила.

На крају, најтоплије и најискреније се захваљујем својој породици, родитељима и брату, на њиховом разумевању и пажњи коју су ми поклањали и на безграничној подршци и подстреку који су ми све време несебично пружали.

Enfin, je tiens à remercier mon copain Romain pour son soutien, ses encouragements et pour tous les moments de ma thèse qu'ils soient heureux ou difficiles, que nous avons partagé ensemble.

*“What the result of these investigations will be the future will tell; but whatever they may be, and to whatever this principle may lead, I shall be sufficiently recompensed if later it will be admitted that I have contributed a share, however small, to the advancement of science.”*

*Nikola Tesla  
In The Electrical Engineer, 1888, p. 583*

*„Шта ће бити резултат ових истраживања време ће показати, али шта год то може бити и чему год овај принцип водио, биће ми добовљно узвраћено ако буде било признато да и ја имам допринос, ма колико мали, у унапређењу науке.“*

*Никола Тесла  
У The Electrical Engineer, 1888, p. 583*

## RÉSUMÉ

---

Ce travail de thèse a pour objectif l'étude de l'électrochimiluminescence (ECL) et son application pour le développement de nouvelles techniques analytiques.

De par son importante sensibilité, l'ECL est une technique performante pour des applications telles que les diagnostics cliniques ou la chimie environnementale (présence d'agents contaminants dans l'eau ou la nourriture). L'immobilisation du luminophore ECL est réalisée généralement sur une phase solide. Cette étape constitue une phase essentielle pour obtenir une méthode d'immobilisation rapide, simple, flexible et efficace de ces luminophores ECL, tout en permettant une utilisation pour des systèmes variés.

La première partie de ce travail présente l'optimisation de la déposition électrochimique de films de métalpolymère de ruthénium et son application pour la détection enzymatique. Un film d'épaisseur micrométrique de cet hydrogel redox a été préparé par voltamétrie cyclique. Cet hydrogel immobilisé a permis la détection d'un substrat modèle (le glucose) en utilisant l'enzyme glucose déshydrogénase.

La seconde partie se concentre sur le développement d'une nouvelle méthode de photodéposition d'un polymère. Celle-ci permet l'immobilisation de centres actifs sur des régions sélectives. En utilisant les techniques de photolithographie, les figures du masque sont projetées sur la surface des électrodes. Cela permet la réalisation de spots micrométriques dont la taille, forme et épaisseur sont modulables. Les propriétés électrochimiques des films nanométriques obtenus sont comparables à ceux obtenus par électrodéposition. De même, les spectres ECL réalisés avec polymères immobilisés par ces deux stratégies sont identiques. Ces résultats montrent que les états excités induits lors de l'ECL sont identiques avec les deux techniques d'immobilisation. Le développement d'un tel procédé constitue une alternative prometteuse pour la réalisation de réseaux de spots ECL différenciés et permettant la détection multiplexée par imagerie ECL.

Dans la troisième partie de ce travail, nous avons associé la spectroélectrochimie et l'imagerie ECL pour contribuer à l'étude des mécanismes ECL au niveau d'une bille micrométrique fonctionnalisée par des complexes de ruthénium. En combinant microscopie de fluorescence et imagerie ECL, la distribution des sites électroactifs et des sites ECL a pu être mise en évidence. A partir de cette étude, nous pouvons clarifier les mécanismes conduisant à l'émission ECL au niveau de ces billes fonctionnalisées.

Mots-clés : électrochimiluminescence, hydrogel, électrodéposition, photodéposition, réseaux de microspots, photopatterning, imagerie ECL, enzymes, biodétection



# ИЗВОД

---

Циљ ове докторске дисертације био је проучавање електрогенерисане хемилуминисценције (Electrogenerated ChemiLuminescence ECL) и њене примене у развоју нових аналитичких техника.

Због изузетно високе осетљивости електрогенерисана хемилуминисценција представља изузетно моћну методу која је нашла широку примену у клиничкој дијагностици и хемији животне средине (испитивање присуства загађивача у води и храни). Имобилизација ECL луминофоре углавном се изводи на чврстим фази. Овај корак је од суштинског значаја за добијање технике за брзу, једноставну, флексибилну и ефикасну имобилизацију ECL луминофора применљиву у различитим конфигурацијама.

Први део овог рада представља оптимизацију електрохемијске депозиције рутенијумовог металополимера и његову примену у ензимској детекцији. Хидрогел филм микрометарске дебљине припремљен је применом цикличне волтаметрије. Овај имобилизовани хидрогел омогућава детекцију модел супстрата (глукозе) применом глукоза дехидрогеназе.

Други део ове дисертације фокусиран је на развој нове методе фотодепозиције за имобилизацију ECL полимера. Ова метода омогућава регионселективну имобилизацију активних центара. Применом фотолитографске методе, фигуре се са маске пројектују на површину електроде. То омогућава формирање микрометарских спотова чија величина, облик и дебљина могу да се подешавају. Електрохемијске особине добијених нанометарских филмова упоредиве су са особинама добијеним за електродепоноване филмове. Такође, ECL спектри добијени помоћу обе имобилизационе стратегије су идентични. То показује да су ECL ексцитована стања иста. Добијени фотопатерни снимани су применом ECL-а. Развој оваквог процеса представља алтернативу за добијање различитих мрежа ECL спотова и омогућава мултиплексну детекцију применом ECL снимања.

У трећем делу овог рада удружили смо електрохемију и ECL снимање за проучавање ECL механизма на нивоу једне микросфере, функционализоване рутенијумовим комплексом. Комбиновањем флуоресцентне микроскопије и ECL снимањем утврђена је дистрибуција електроактивних и ECL центара. Из ове студије може да се утврди механизам који доводи до ECL емисије на нивоу функционализованих микросфера.

Кључне речи: електрогенерисана хемилуминисценција, хидрогел, електродепозиција, фотодепозиција, мрежа микроспотова, фотопатернинг, ECL снимање, ензими, биодетекција.

## ABSTRACT

---

The main goal of this thesis was to study electrogenerated chemiluminescence (ECL) and its application in development of new analytical techniques.

Due to its high sensitivity, ECL presents a powerful method for applications in clinical diagnostic and environmental chemistry (presence of contaminants in water or food). The immobilisation of an ECL luminophore is usually performed on a solid phase. This step is an essential point to obtain a technique for fast, simple, flexible and effective immobilisation of ECL luminophores with possibility of applications in various configurations.

The first part of this work presents the optimisation of the electrochemical deposition of a ruthenium metallopolymer and its application in enzymatic detection. A redox hydrogel film with micrometric thickness was prepared using cyclic voltammetry. This immobilised hydrogel allows the detection of model substrate (glucose) using enzyme glucose dehydrogenase.

The second part of this thesis is focused on the development of a new photodeposition method for the ECL polymer immobilisation. This method allows region-selective immobilisation of active centres. Using photolithographic methods, the figures from the mask are projected on the electrode surface. This allows the formation of micrometric spots which size, shape and thickness is modulated. Electrochemical properties of obtained nanometric films are comparable with those of electrodeposited films. Also, ECL spectra recorded with both immobilisation strategies are identical. It shows that the ECL excited state is the same. The obtained photopatterns were imaged using ECL. The development of such process presents an alternative for realisation of different ECL spot arrays and allows multiplexed detection by ECL imaging.

In the third part of this work we have associated spectroelectrochemistry and ECL imaging to study the ECL mechanisms at the level of a single microbead, functionalised with ruthenium complex. Combining fluorescence microscopy and ECL imaging, the distribution of electroactive and ECL sites have been highlighted. From this study we can clarify the mechanism that leads to ECL emission at the level of functionalised beads.

**Keywords:** electrogenerated chemiluminescence, hydrogel, electrodeposition, photodeposition, microspot arrays, photopatterning, ECL imaging, enzymes, biodetection

# CONTENT

---

<b>List of abbreviations.....</b>	<b>14</b>
<b>Introduction .....</b>	<b>16</b>
<b>Chapter 1: Introduction to electrogenerated chemiluminescence .....</b>	<b>18</b>
1.1. Historical overview .....	19
1.2. Luminescent types .....	20
1.2.1. Photoluminescence.....	20
1.2.2. Chemiluminescence .....	22
1.2.3. Electrogenerated chemiluminescence .....	23
1.3. Ion Annihilation ECL.....	23
1.4. Coreactant ECL .....	27
1.4.1. Typical coreactant ECL systems and their mechanisms .....	28
1.4.1.1. Example of oxidative-reduction ECL (Oxalate ( $\text{Ru}(\text{bpy})_3^{2+}/\text{C}_2\text{O}_4^{2-}$ ) system) 28	
1.4.1.2. Example of reductive-oxidation ECL (Peroxydisulfate (persulfate) ( $\text{Ru}(\text{bpy})_3^{2+}/\text{S}_2\text{O}_8^{2-}$ ) system) .....	29
1.4.1.3. A model ECL system (Tri-n-propylamine ( $\text{Ru}(\text{bpy})_3^{2+}/\text{TPrA}$ ) system).....	30
1.4.2. ECL Luminophores .....	33
1.4.2.1. Inorganic systems .....	33
1.4.3. ECL Coreactants .....	41
1.5. ECL application.....	43
1.5.1. Application in CE, HPLC and FIA systems.....	44
1.5.2. Solid Phase ECL Assay .....	45
1.6. Conclusion.....	49
References .....	51
<b>Chapter 2: New sensing approach based on electrodeposited ECL redox polymer .....</b>	<b>56</b>
2.1. Immobilisation of $\text{Ru}(\text{bpy})_3^{2+}$ and its derivatives.....	58
2.1.1. Immobilisation in cation exchange polymers.....	58
2.1.2. Immobilisation in Silica Sol-Gel films.....	59
2.1.4. Immobilisation in self assembled monolayer.....	61
2.1.5. Covalent attachment of the luminophore .....	61
2.2. Electrodeposition of $[\text{poly}(4\text{-vinylpyridine})\text{-Ru}(2,2'\text{-bipyridine})_2\text{Cl}]^{+/2+}$ .....	62
2.2.1. Electrochemical immobilisation of PVP- $\text{Ru}(\text{bpy})_2^{2+}$ on the electrode surface .....	63
2.2.2. Characterisation of the electrodeposited redox hydrogel.....	65
2.3. Glucose sensing .....	70

2.4. Conclusion.....	76
References .....	78
<b>Chapter 3: Photodeposition and photopatterning of ultrathin electrochemiluminescent redox hydrogel films.....</b>	<b>81</b>
3.1. Multiplexed assays .....	82
3.1.1 Microarray-based assays .....	84
3.1.2. Bead-based assays .....	85
3.2. Photodeposition .....	86
3.2.1 Photopolymerisation of PEGDA .....	86
3.2.2. Photodeposition of [poly(4-vinylpyridine)-Ru(2,2'-bipyridine) <sub>2</sub> Cl] <sup>+2+</sup> .....	90
3.2.3. Electrochemical characterisation of photodeposited redox hydrogel .....	91
3.2.4 ECL characterisation of the photodeposited redox hydrogel .....	93
3.3. Photopatterning .....	94
3.3.1. Fabrication of ultrathin ECL photopatterns .....	95
3.3.2. ECL imaging .....	96
3.3.3. Effect of the film thickness .....	98
3.4. Conclusion.....	102
Refereces .....	103
<b>Chapter 4: ECL imaging at the single bead level.....</b>	<b>106</b>
4.1 Reported mechanisms of Ru(bpy) <sub>3</sub> <sup>2+</sup> /TPrA ECL pair .....	108
4.2. The concept of single bead imaging.....	115
4.2.1. Electrochemical characterisation.....	117
4.2.2. Photoluminescence imaging.....	118
4.2.3. ECL imaging .....	119
4.3. Conclusion.....	124
References .....	125
<b>General conclusion .....</b>	<b>127</b>
<b>Experimental part .....</b>	<b>130</b>
1. Electrogenerated chemiluminescence on electrodeposited redox hydrogel.....	131
1.1. Electrodeposition of [poly(4-vinylpyridine)-Ru(2,2'-bipyridine) <sub>2</sub> Cl] <sup>+2+</sup> on the electrode surface.....	131
1.2. Electrochemical characterisation.....	133
1.3. ECL experiments.....	133
1.3.1. ECL characterisation of the electrodeposited film.....	133
1.3.2. ECL detection of glucose .....	134
1.3.3. The ECL spectra recording .....	135

2. Photodeposition and photopatterning.....	135
2.1. Preparation of electrodes.....	135
2.2. Polymer solution preparations.....	135
2.3. Photodeposition and photopatterning.....	136
2.4. Electrochemical characterization.....	136
2.5. PL and ECL imaging.....	136
2.6. AFM imaging.....	139
3. ECL imaging at the single bead level.....	139
3.1. Beads surface modification.....	139
3.2. Beads immobilisation at the electrode surface.....	140
3.3. PL and ECL imaging by epifluorescence microscopy.....	140
3.4. PL imaging by confocal microscopy.....	141

## LIST OF ABBREVIATIONS

---

AFM	atomic force microscopy
AFP	alpha-fetoprotein
BNAH	1-benzyl-1,4-dihydronicotinamide
BSA	bovine serum albumin
CCD	charge coupled device
CE	capillary electrophoresis
CL	chemiluminescence
CNTs	carbon nanotubes
CRP	C-reactive protein
CV	cyclic voltammetry
DBAE	2-(dibutylamino) ethanol
DMF	dimethylformamide
DMPA	2,2-dimethoxy-2-phenylacetophenone
DNA	deoxyribonucleic acid
DPA	9,10-diphenylanthracene
ds-DNA	double-strand DNA
ECL	electrogenerated chemiluminescence
EM-CCD	electron multiplying charge coupled device
FIA	flow injection analysis
GC	glassy carbon
GDH	glucose dehydrogenase
HOMO	highest occupied molecular orbital
HPLC	high performance liquid chromatography
IL-6	interleukin-6
IL-8	interleukin-8
ITO	indium tin oxide
LB	Langmuir-Blodgett
LC	ligand centered excited states
LECs	light-emitting electrochemical cells
LS	Langmuir-Schaefer

LUMO	lowest unoccupied molecular orbital
MB	magnetic beads
MC	metal centered excited states
MLCT	metal-to-ligand charge transfer
NAD <sup>+</sup>	β-nicotinamide adenine dinucleotide hydrate
NADH	β-nicotinamide adenine dinucleotide reduced salt
NPs	nanoparticles
PAHs	polycyclic aromatic hydrocarbons
PBS	phosphate buffered saline
PEG	poly(ethylene glycol)
PEGDA	poly(ethylene glycol) diacrylate
PEGDMA	poly(ethylene glycol) dimethacrylate
PEGTA	poly(ethylene glycol) tetraacrylate
PETA	pentaerythritol triacrylate
PL	photoluminescence
PMT	photomultiplier tube
PSA	prostate specific antigen
PSB	polystyrene beads
RNA	ribonucleic acid
SAMs	self-assembled monolayers
SCE	saturated calomel electrode
SECM	scanning electrochemical microscopy
SEM	scanning electron microscopy
ss-DNA	single-strand DNA
SWCNTs	single-wall carbon nanotubes
TEOS	tetraethoxysilane
TMOS	tetramethoxysilane
TMPD	N,N,N,N-tetramethyl-p-phenylenediamine
TPrA	tri-n-propylamine
TRAP	telomere repeat amplification protocol
TTA	triplet-triplet annihilation

## INTRODUCTION

---

The need to analyse complex analytical and bioanalytical samples in fast, inexpensive and reliable way lead to the expansion of analytical techniques and detection methods. Electrogenenerated chemiluminescence (ECL) is a powerful analytical technique which applications daily increase. It offers very sensitive detection. For example,  $\text{Ru}(\text{bpy})_3^{2+}$  labels can be detected at subpicomolar concentrations with an extremely wide dynamic range greater than six orders of magnitude. The instrumentation for ECL experiments is not expensive. It consists of electrochemical cell with transparent window, a potentiostat and a light detector. In most of the cases, the light detector is a photomultiplier tube (PMT) but it can be also a CCD camera. As there is no need of light source, the system is simple and it can be easily combined with other technologies such as microfluidics and capillary electrophoresis to obtain complete detection systems. For these reasons, ECL finds various applications in analytical chemistry. It is used in immunoassays, DNA probe assays, in aptamer and DNAzyme biosensors and for detection of coreactants. ECL is a commercially successful analytical technique. There are a large number of commercially available assay kits based on different technologies. For example, the assays based on magnetic beads technology for different applications in life sciences, high-throughput drug screening, and food, water, and animal health testing are available. There are also developed assays based on multi-array platforms that can be used for single and multiplexed assays in different fields of clinical analysis such as immunology, toxicology, inflammation, metabolic disorders etc.

The distinguished feature of ECL techniques, the popularisation of the commercial ECL instrumentation and the demand in various fields leads to a large increase in the development of new assays. In most of the applications, the ECL luminophore is immobilised on the solid phase. Thus, many efforts have been focused on the immobilisation of  $\text{Ru}(\text{bpy})_3^{2+}$  on the electrode surface: in composite films, in polymer films, in ceramic carbon materials, in the form of monolayers, in silica sol-gels, or using various techniques such as Langmuir–Blodgett (LB).

This doctoral dissertation deals with study of ECL and development of new strategies for immobilisation of an ECL luminophore. This step presents the base for development of new ECL systems for different kind of applications.



In the first part of this thesis the general principles of ECL are presented. Basically two different natures of ECL generation, annihilation ECL and coreactant ECL are explained in details. As the coreactant ECL has more applications, the most used ECL luminophores and coreactants are also presented. In the last part of this chapter, the principal applications of ECL are briefly described.

The second chapter of this thesis is dedicated to immobilisation of a ruthenium metallopolymer. In the first part of the chapter some already reported methods for immobilisation of an ECL luminophore are presented. Then, the optimisation of electrochemical immobilisation of the metallopolymer and its application in enzymatic systems are described. The procedure of electrodeposition as well as electrochemical and ECL characterisation are presented. Electrodeposited polymer was applied for the detection of glucose (model substrate) in the presence of glucose dehydrogenase.

In the third part of this thesis, a completely new method based on photodeposition and photopatterning of redox polymer has been developed. Photopatterning is based on photolithography which allows the immobilisation of the polymer in the form of patterns, which have not been reported so far to the best of our knowledge. The properties of obtained ultrathin films were characterised using electrochemical and ECL methods. Obtained ECL patterns were revealed by ECL imaging and may find application in multiplexed bioassays. For this reason one part of this chapter is dedicated to already reported multiplexed systems and its application in analytical and clinical research.

The last chapter deals with the study of ECL mechanisms and their influence on ECL emission. Spectroelectrochemistry and ECL imaging was combined to observe the ECL emission at the level of a single microbead, functionalised with ruthenium complex. This presents a new approach for investigation of the mechanisms which are involved in an ECL reaction.

~ ~ ~

## CHAPTER 1:

# INTRODUCTION TO ELECTROGENERATED CHEMILUMINESCENCE

~ ~ ~

*Electrogenerated ChemiLuminescence (ECL) is the light emitted after the reaction of species which are previously generated at the electrode surface.*<sup>1-4</sup>

ECL is similar in nature to chemiluminescence (CL) but the reagents are produced electrochemically *in situ*.<sup>5</sup> It presents the synergy of electrochemical and spectroscopic methods which brings many potential advantages. First, some reactants are electrochemically regenerated at the electrode which greatly enhances the sensitivity of the technique. For example, Ru(bpy)<sub>3</sub><sup>2+</sup> is very sensitively detected at subpicomolar concentrations with an extremely wide dynamic range of greater than six orders of magnitude.<sup>3</sup> Second, as ECL is initiated and controlled by changing an electrode potential, it offers time and position control. By controlling the time, light emission is delayed until events such as immuno or enzyme-catalysed reactions have taken place.<sup>1</sup> Since the ECL emission is close to the electrode surface, the emission region can be located with respect to the detector improving sensitivity and signal to noise ratio.<sup>1</sup> Third, comparing with fluorescence methods, ECL does not involve an external light source thus problems with scattering light and luminescent impurities can be avoided.<sup>1, 6</sup> Finally, ECL allows the simultaneous measurements of two experimental parameters, light intensity and Faradaic current *vs.* potential which facilitates the investigation of light emission mechanism and enables the ECL and electrochemical detection simultaneously. Due to these properties, ECL finds place in a wide range of analytical applications. Commercial immunoassays and DNA probe assays have been widely used in the areas of clinical diagnostic, food and water testing, environmental monitoring, biowarfare agent detection and scientific research.<sup>1, 2, 6-12</sup> ECL has also been exploited for the determination of numerous analytes by combining with high performance liquid chromatography (HPLC), flow injection analysis (FIA) and capillary electrophoresis (CE).<sup>13-</sup>

17

Since the work performed in this thesis is based on ECL detection, the first chapter deals with principles of ECL and its application.

### 1.1. HISTORICAL OVERVIEW

For the first time ECL has been reported as a light emitted during an electrochemical reaction.<sup>18, 19</sup> Although the first reports date back to 1920s, the first detailed ECL studies started in 1960s reporting the luminescence of aromatic hydrocarbons.<sup>20, 21</sup> The first experiments which were done applying alternating current gave the suggestion of mechanism

and the first theory about electron transfer in ECL. In 1972 it has been reported that [Ru(byp)<sub>3</sub>Cl<sub>2</sub>] can also emit the light due to cycling of potential on Pt electrode and that maximum of emission is exactly the same as the maximum of emission observed upon photoexcitation.<sup>22</sup> A real breakthrough was the ECL generation with coreactant species in 1977. It was found that characteristic emission occurs during the simultaneous oxidation of oxalate and some fluorophore like rubrene, 9,10-diphenylanthracene and bipyridyl chelates of ruthenium(II) and osmium(II).<sup>23</sup> Ten years later aliphatic amines especially tri-n-propylamine has been found to be one of the most efficient ECL coreactants.<sup>5, 24</sup> Finally, starting from early 1990s, ECL has been applied in bioassays. Nowadays thanks to the high sensitivity and good selectivity, ECL presents powerful analytical technique widely used in areas such as clinical diagnostic, food and water tasting and biowarfare agent detection.<sup>1, 2, 6</sup>

## 1.2. LUMINESCENT TYPES

ECL corresponds to light emission from a luminescent molecule after the electrochemical reaction initiated on the electrode surface. In order to explain the principles of ECL emission and to distinguish the ECL from other types of luminescence, the principles of photoluminescence (PL) and chemiluminescence (CL) are also described.

### 1.2.1. Photoluminescence

Photoluminescence is the process in which excited state of a molecule is generated after the absorption of light which wavelength (energy) corresponds to the difference between energy levels of the highest occupied molecular orbital (HOMO) and the lowest unoccupied molecular orbital (LUMO). Various energy states available to a molecule can be presented by energy level diagram like that in Figure 1. It shows electronic and vibrational (but not rotational) states.<sup>4</sup> S<sub>0</sub>, S<sub>1</sub> and T<sub>1</sub> present ground singlet state, excited singlet state and the lowest triplet state respectively while the vibrational levels for each of the states are numbered  $v = 0, 1, 2, \dots$

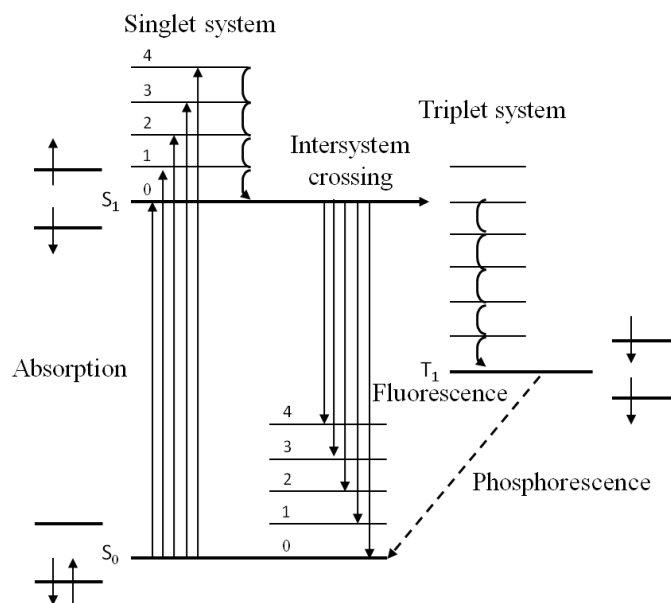


Figure 1. Energy level diagram during the absorption and emission of radiation

The absorption from  $S_0$  to  $S_1$  involves transitions from ground vibrational state  $\nu = 0$  of  $S_0$  to various vibration levels in  $S_1$ . The lifetime of an excited vibration state in the solution is very short (in the range of picoseconds) thus excited vibration states in  $S_1$  rapidly decay to  $\nu = 0$  vibrational level. Emission then occurs from  $\nu = 0$  of  $S_1$  to the different vibration levels of  $S_0$ . Obviously, the energy of emission is lower than energy of excitation and excitation wavelength is longer compared with the wavelength of absorption. In all chemical compounds that have a colour, the difference in energy of their HOMO and LUMO correspond to visible light. For example, the complex  $[\text{Ru}(\text{bpy})_3]\text{Cl}_2$  exposed to the white light absorbs blue light (450 nm)<sup>25</sup> which enables the excitation of an electron from HOMO to LUMO. For this reason this complex has orange-red colour (610 nm).

The radiative lifetime of excited singlet state is relatively short in order of nanoseconds but that of triplet state is much longer, in order of millisecond, because transition from triplet state to singlet state is “forbidden”. Emission from the triplet state results in phosphorescence but this can be rarely seen for organic molecules in solution. Indeed, these molecules are readily quenched by the solution species before emission. However, the emission from triplet state is found for metal chelates which have much shorter lifetime than organic molecules. In this case, triplet state can produce excited singlet state by triplet-triplet annihilation, process which involved energy transfer between two triplet states leading to one excited singlet state and one ground singlet state.<sup>26</sup> The emission from generated excited singlet state is then fast resulting in delayed fluorescence.

### 1.2.2. Chemiluminescence

Chemiluminescence is the process in which the excited state is generated by highly energetic electron-transfer reaction between two reacting species. The reaction occurs by simple mixing of reagents. By comparison with photoluminescence where the light energy is used to obtain an excited state, in chemiluminescence electron-transfer reaction provides chemical energy used to generate an excited state. In both mentioned cases, the way to achieve excited state is different but the relaxation process and mechanism of light emission is the same. Chemiluminescence of luminol is a common example. It has been used as a detection method in liquid chromatography, immunoassays and hybridisation assays. Chemiluminescent reaction of luminol is an oxidation reaction which is carried out either in aprotic solvents (dimethyl sulfoxide (DMSO), *N,N*-dimethylformamide) or protic solvents (water, lower alcohols).<sup>27</sup> Chemiluminescence reaction of luminol in protic media occurs in a basic solution to generate an energy-rich intermediate with subsequent light emission from 3-aminophthalic acid (Figure 2). To obtain chemiluminescence from luminol in an aqueous solution, a chemioxidising reagent, such as hydrogen peroxide, is needed. The oxidation reaction of luminol is catalysed by metal ions such as Co(II), Cu(II) and Fe(III) or by an enzyme such as horseradish peroxidase and microperoxidase. In the aqueous solution luminol shows emission at 424 nm.<sup>28</sup>

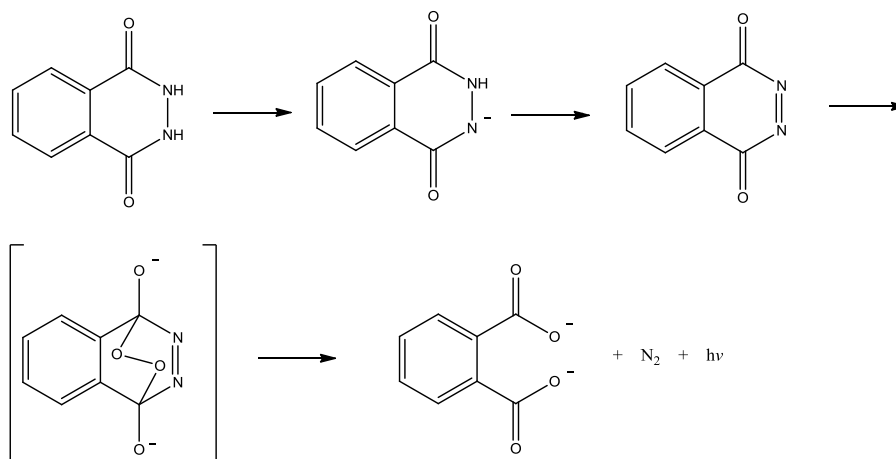


Figure 2. Chemiluminescence reaction of luminol

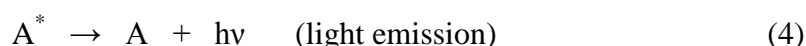
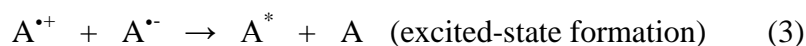
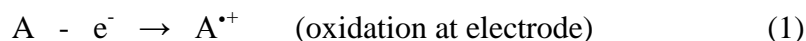
$\text{Ru}(\text{bpy})_3^{3+}$  may also take a part in a chemiluminescent reaction. If solution of  $\text{Ru}(\text{bpy})_3^{3+}$  is mixed with an aliphatic amine such as tri-*n*-propylamine (TPrA), a yellow-orange light is generated.<sup>24</sup> It was found that observed chemiluminescence is generated due to oxidation of amine to short-lived radical cation  $\text{TPrA}^{\cdot+}$  by  $\text{Ru}(\text{bpy})_3^{3+}$ .<sup>24</sup> Radical cation rapidly loses one proton forming strongly reducing agent  $\text{TPrA}^{\cdot}$  which can further reduce  $\text{Ru}(\text{bpy})_3^{3+}$  to excited state  $\text{Ru}(\text{bpy})_3^{2+*}$ . Relaxing from excited to ground state the complex emits the light.

### 1.2.3. Electrogenerated chemiluminescence

ECL is the process in which excited state occurs thanks to the highly energetic electron-transfer reaction of molecules which are previously generated on the electrode surface. Comparing with the chemiluminescence (CL) where light emission is initiated by mixing of necessary reagents and can be controlled by careful manipulation of fluid flow, light emission in ECL is initiated and controlled by application of electrode potential. An example comparable with the previous can be presented. In this case, if the solution of  $\text{Ru}(\text{bpy})_3^{2+}$  and TPrA is mixed together nothing will happen. Then, electrodes are immersed in the solution to form three-electrode cell and a voltammetric scan is applied. During the cyclic voltammogram scan the light is emitted but only in the anodic part of the scan. Emission of the light can be explained by oxidation of  $\text{Ru}(\text{bpy})_3^{2+}$  to  $\text{Ru}(\text{bpy})_3^{3+}$  that can further react in the same way like in previous case. Actually, the mechanism of presented ECL reaction is much more complex, and it corresponds to an active area of investigation.<sup>29-31</sup> The mechanism is detailed in the paragraph 1.4.1.3. and 4.1.

### 1.3. ION ANNIHILATION ECL

Although modern ECL applications are mainly based on coreactant ECL, the first ECL studies started with ion annihilation. Ion annihilation ECL involves the formation of an excited state as a result of an electron-transfer reaction between an oxidised and a reduced species. Both were generated at an electrode by alternate pulsing of the electrode potential.<sup>1, 2</sup> If the potential of the working electrode is quickly changed between two different values, species A can be oxidised to  $\text{A}^{*+}$  (eq 1) and reduced to  $\text{A}^{*-}$  (eq 2) at the same electrode. These species react in the Nernst diffusion layer and form an excited state  $\text{A}^*$  (eq 3) which emits the light when it relaxes to the ground state (eq 4).<sup>2</sup>

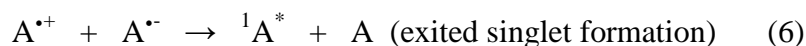


Annihilation reaction (eq 3) also can occur in “mixed systems” where the radical cation and radical anion are from different molecules. Such a system is presented later.

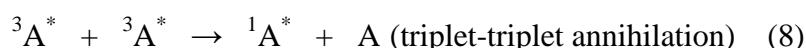
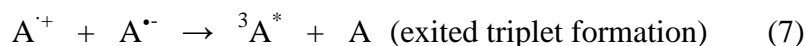
To obtain successful ECL emission some energy requirements should be met. Depending on the energy available in the annihilation reaction, the produced  $A^*$  can be either in the lowest excited singlet state  $^1A^*$  or in the triplet state  $^3A^*$ . The enthalpy which is directly related to the energy available in eq 3 can be calculated (eq 5) from the redox potential for the reactions 1 and 2.<sup>1</sup>

$$-\Delta H_{\text{ann}} = \Delta G + T\Delta S = E_p(A/A^{\bullet+}) - E_p(A/A^{\bullet-}) - 0.16 \quad (5)$$

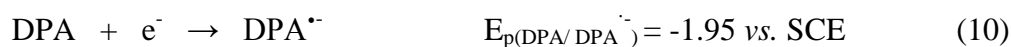
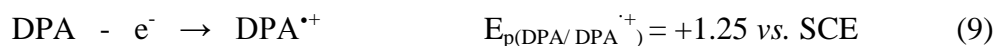
Where  $-\Delta H_{\text{ann}}$  (in eV) is the enthalpy for ion annihilation,  $E_p$  is the peak potential for electrochemical oxidation or reduction. The value 0.16 is the entropy approximation term ( $T\Delta S$ ) estimated to be  $\sim 0.1$  eV with an addition of 0.057 eV resulting from the difference between two reversible peak potentials of the redox reaction.<sup>1, 32</sup> If the enthalpy of annihilation is larger than the energy ( $E_s$ ) required to produce the lowest excited singlet state, it is possible to directly generate  $^1A^*$ . This system is called energy-sufficient system and the reaction follows the S-route (eq 6):



If  $-\Delta H_{\text{ann}}$  is smaller than the energy of singlet excited state  $E_s$ , but larger than the energy of triplet excited state ( $E_t$ )<sup>3</sup> a triplet excited state  $A^*$  is formed (eq 7). Emission from the triplet state is rarely seen because transition from triplet to singlet state is forbidden but  $^3A^*$  can be transformed to  $^1A^*$  by triplet-triplet annihilation (TTA) (eq 8). This system is called energy-deficient system and reaction is said to follow the T-route:



A classic example of energy sufficient system (system which follows S-route) involves 9,10-diphenylanthracene (DPA) which is one of the first studied ECL systems. In the first experiments, the working electrodes were platinum coaxial helices or parallel pairs of gold foils. ECL observations were carried out in dimethylformamide (DMF) applying alternating current.<sup>20</sup> During potential changes DPA was oxidized and reduced. Both produced species reacted resulting in light emission.







The study of anodic and cathodic processes of DPA were done by cyclic voltammetry giving the reduction peak at -1.95 V vs SCE and oxidation peak at +1.25 V vs. SCE. According to these results and equation (5) it can be calculated that enthalpy for the electron-transfer reaction is 3.04 eV. When we compare it with the energy of emitted light at 435 nm and 410 nm (2.85 and 3.02 eV respectively, eq 13) we can see that emitting state is accessible.  $^1\text{DPA}^*$  can be populated directly in the reaction so it follows the S-route.

$$E = h\nu = hc/\lambda \quad (13)$$

Where h is the Plank constant ( $6.626 \times 10^{-34}$  J's),  $\nu$  is frequency (Hz), c is speed of light ( $2.99 \times 10^8$  m/s) and  $\lambda$  is wavelength of emission (m).

As it is mentioned above, ECL may be generated using two different precursors. ECL is achieved via “cross-reaction” between the radical cation of one species and the radical anion of a different species. A classic example is the electron-transfer reaction between the anion radical of 9,10-diphenylanthracene (DPA) and cation radical of N,N,N,N-tetramethyl-p-phenylenediamine (TMPD) in dimethylformamide:<sup>33-35</sup>



In theory, light may be emitted from either  $\text{DPA}^*$  or  $\text{TMPD}^*$ . However, the emitted light generated via ECL is identical to DPA photoluminescence indicating that  $\text{DPA}^*$  is the ultimate product of charge transfer.<sup>34</sup> The enthalpy for the electron-transfer reaction is 1.97 eV which is less than required to reach the emitting single state for DPA (3.02 eV). So it was surprising that this system undergoes ECL generation. As singlet excited state is not possible to reach directly, such systems are called energy-deficient systems. The proposed mechanism involved triplet intermediates, the so called T-route.



The singlet excited state is generated by “triplet-triplet annihilation” where the energy from two electron-transfer reaction is pooled to provide sufficient energy to form the singlet excited state (eq 19).<sup>36</sup>

If the enthalpy of electron-transfer reaction is marginal to the energy of singlet excited state, the T-route can contribute to the formation of  $^1A^*$  in addition to the S-route, so called ST-route. A typical example is the rubrene anion-cation annihilation.<sup>37</sup>

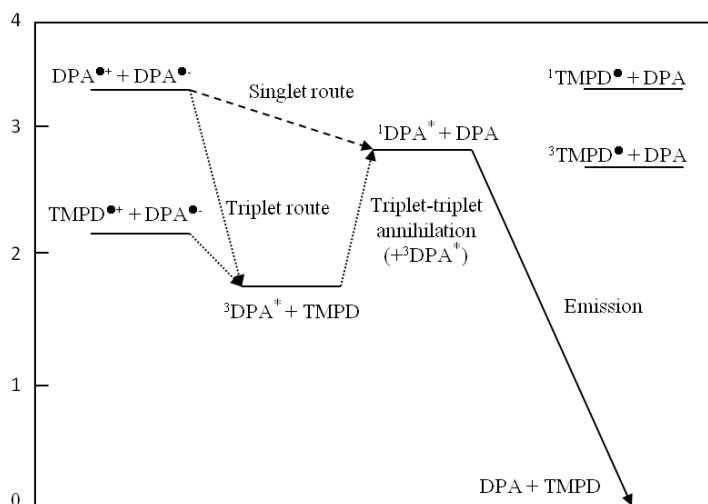


Figure 3. Energy level diagram for DPA-DPA and TMPD-DPA ECL systems

If one considers the presented examples, there are few requirements for successful annihilation ECL. First is generation of both radicals (anion and cation) at the electrode surface. For singlet systems, parent species in this type of reactions must undergo both oxidation and reduction within a potential range that is accessible in the employed solvent. Once formed, the radical ions must be sufficiently long-lived to allow them to diffuse, encounter each others, and undergo electron transfer. These electrochemical properties can be evaluated by cyclic voltammetry. Photoluminescence efficiencies and high photoluminescence lifetime is required which often can be evaluated from the fluorescent experiment. Finally, sufficient energy in the reaction of annihilation is required to form one of the excited states mentioned above.

As the energy for visible range emission (~400-700 nm) covers from 3.1 to 1.8 eV (eq 13) the potential window of an electrochemical system should be wide enough (from ~3.3 to 2 V) (eq 5). Thus ion annihilation ECL is mainly performed in non-aqueous media, such as acetonitrile, dimethyl-sulfoxide or methylene-chloride with tetra-n-butylammonium perchlorate or tetraethylammonium perchlorate as supporting electrolyte.

Despite its application in light-emitting electrochemical cells (LECs)<sup>3</sup> annihilation ECL has important limitations. It requires the use of rigorously purified and deoxygenated non-aqueous solvents because the available potential range in water is too narrow to generate the required energetic precursors. Water and oxygen are harmful to these experiments because they can quench ECL.<sup>2</sup> Thus, cells and electrodes have to be constructed to allow transfer of solvents and degassing on high-vacuum line or in inert-atmosphere (glove-boxes).<sup>2</sup>

#### 1.4. COREACTANT ECL

The discovery of coreactants presents an important moment in history of ECL development. Compared with ion annihilation ECL which requires strict conditions, usually non-aqueous solution and inert atmosphere, coreactant ECL is more comfortable for work not only in aqueous media and in the air but also in physiological conditions (pH ~ 7.4). Thus, most of ECL applications are based on coreactant ECL.

Annihilation ECL requires generation of both oxidised and reduced precursor at the same electrode alternating between two potentials. Using coreactant, ECL is generated in a single potential step where reagents are only oxidised or reduced. The ECL generation occurs in solution which contains luminophore species (“emitter”) and deliberately added reagent (coreactant). Depending on the polarity of the applied potential, both luminophore and the coreactant can be first oxidised or reduced at the electrode. Coreactants form radicals as intermediates decompose producing a powerful reducing or oxidising species. These species then react with the oxidised or reduced luminophore to produce the excited state that emits light.<sup>1</sup> Thus, a coreactant is a species that, after electrochemical oxidation or reduction, immediately undergoes chemical decomposition to form a strong reducing or oxidising intermediate that can react with oxidised or reduced ECL luminophore. Depending on the case, if the luminophore is first oxidised at the electrode surface and then reduced by strongly reducing intermediate, the corresponding ECL is called “oxidative-reduction” ECL. If applied potential leads to reduction of the luminophore which is after oxidised by oxidised coreactant intermediate, the corresponding ECL is called “reductive-oxidation” ECL.

Considering one potential step generation, coreactant ECL shows several advantages over annihilation ECL. First, there is no need for wide potential window so other solvents with a narrow potential window and aqueous solution can be also used. Further, there is no need of rigorously purified and deoxygenated solvents because oxygen and water quenching is less

efficient. Thus reaction can be carried out in air. Finally, the use of coreactant makes ECL possible even for some fluorophores that have only a reversible electrochemical oxidation or reduction while annihilation ECL in general requires both of them.

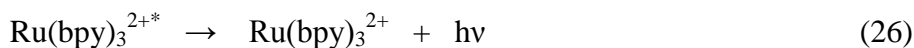
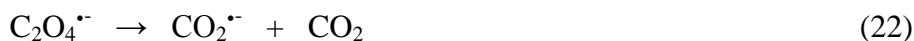
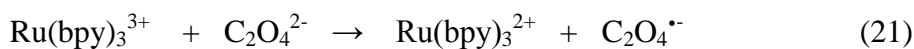
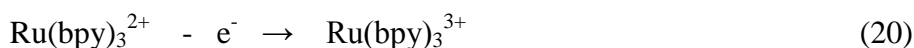
#### 1.4.1. Typical coreactant ECL systems and their mechanisms

$\text{Ru}(\text{bpy})_3^{2+}$  is the first inorganic complex that shows ECL. Because of its excellent chemical, electrochemical and photochemical properties, it is still the most used ECL luminophore. From this reason most of the examples of coreactant ECL given here will include  $\text{Ru}(\text{bpy})_3^{2+}$  as an luminophore.

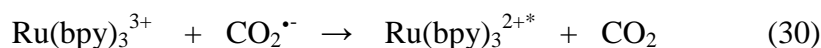
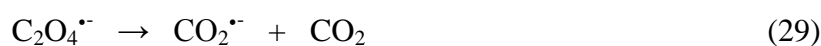
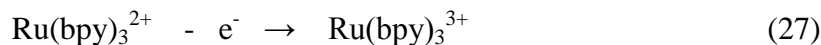
##### 1.4.1.1. Example of oxidative-reduction ECL (Oxalate ( $\text{Ru}(\text{bpy})_3^{2+}/\text{C}_2\text{O}_4^{2-}$ ) system)

Oxalate ion was the first discovered ECL coreactant. A lot of studies investigating its mechanism have been reported by Bard and co-workers.<sup>23, 38-42</sup> The first experiments were performed in acetonitrile<sup>23</sup> and later in aqueous solutions.<sup>43</sup>

In an aqueous solution upon the anodic potential,  $\text{Ru}(\text{bpy})_3^{2+}$  is first oxidised to  $\text{Ru}(\text{bpy})_3^{3+}$ . The cation is then capable to oxidise oxalate ( $\text{C}_2\text{O}_4^{2-}$ ) in the diffusion layer close to the electrode surface to form an oxalate radical anion ( $\text{C}_2\text{O}_4^{\bullet-}$ ) which decomposes to form highly reducing radical anion ( $\text{CO}_2^{\bullet-}$ ) and carbon dioxide. The reducing radical anion is then capable to reduce both  $\text{Ru}(\text{bpy})_3^{3+}$  to excited state  $\text{Ru}(\text{bpy})_3^{2+*}$  and to reduce non oxidised  $\text{Ru}(\text{bpy})_3^{2+}$  to  $\text{Ru}(\text{bpy})_3^+$  that is then able to react with  $\text{Ru}(\text{bpy})_3^{3+}$  to generate again  $\text{Ru}(\text{bpy})_3^{2+*}$ .

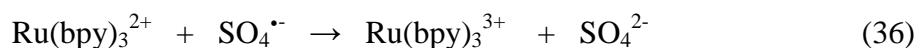
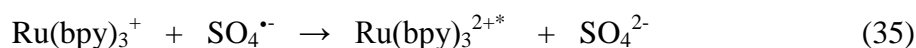
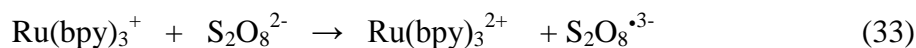
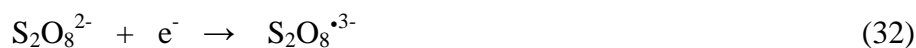
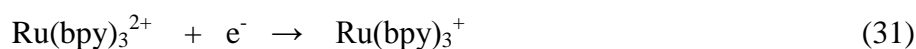


In the previous case oxalate species were oxidised by a catalytic way. In acetonitrile, oxalate may be oxidised directly on the electrode surface, thus the mechanism is more simplified.<sup>23</sup> The oxalate ( $C_2O_4^{2-}$ ) is oxidised to oxalate radical anion ( $C_2O_4^{\bullet-}$ ) that decomposes to reducing radical anion ( $CO_2^{\bullet-}$ ) which then reacts with  $Ru(bpy)_3^{3+}$  to form the excited states.



*1.4.1.2. Example of reductive-oxidation ECL (Peroxydisulfate (persulfate) ( $Ru(bpy)_3^{2+}/S_2O_8^{2-}$ ) system)*

Persulfate is the first example of so-called “reductive-oxidation” coreactant ECL system.<sup>44</sup> Since  $Ru(bpy)_3^+$  is unstable in aqueous solutions while  $(NH_4)_2S_2O_8$  has a low solubility in acetonitrile, the reaction was carried out in acetonitrile- $H_2O$  mixed solution. Upon the application of cathodic potential,  $S_2O_8^{2-}$  is reduced directly at the electrode surface but also catalytically by  $Ru(bpy)_3^+$  forming  $S_2O_8^{\bullet 3-}$  that decomposes to strongly oxidising intermediate  $SO_4^{\bullet-}$ .<sup>45</sup> The radical then oxidises  $Ru(bpy)_3^+$  to the excited state  $Ru(bpy)_3^{2+*}$  or  $Ru(bpy)_3^{2+}$  to  $Ru(bpy)_3^{3+}$  that undergo annihilation giving  $Ru(bpy)_3^{2+*}$ .



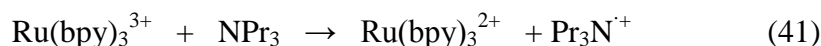
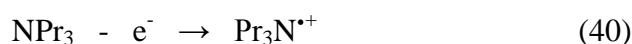
### 1.4.1.3. A model ECL systeme (Tri-n-propylamine (Ru(bpy)<sub>3</sub><sup>2+</sup>/ TPrA) system)

The first experiments of ECL with aliphatic amines date from earlies 90-s.<sup>5, 24</sup> Ru(bpy)<sub>3</sub><sup>2+</sup> or its derivatives with TPrA as coreactant exhibit the highest ECL efficiency and this system forms the basis of commercial systems for immunoassay and DNA analysis.<sup>1, 6, 45</sup> The efficiency of all other ECL systems are compared with efficiency of Ru(bpy)<sub>3</sub><sup>2+</sup>/ TPrA system thus it can be considered as an ECL standard. The ECL mechanism of this reaction is complex and it is still under investigation.<sup>5, 24, 29, 30, 46-48</sup> The first report that Ru(bpy)<sub>3</sub><sup>3+</sup> and aliphatic amines emit the light in a chemiluminescence reaction has been reported by Noffsinger and Danielson.<sup>24</sup> The reaction was explained by oxidation of aliphatic amines by Ru(bpy)<sub>3</sub><sup>3+</sup> leading to the formation of short lived radical cation which then loses a proton giving a free radical. This free radical can then reduce Ru(bpy)<sub>3</sub><sup>3+</sup> to excited state Ru(bpy)<sub>3</sub><sup>2+\*</sup>. Following this work and the idea that reactants in the presented reaction can be electrochemically generated, Leland and Powell reported a new ECL reaction based on TPrA and Ru(bpy)<sub>3</sub><sup>2+</sup>.<sup>5</sup> The experiment was carried out on a gold electrode in a buffer solution of TPrA and Ru(bpy)<sub>3</sub><sup>2+</sup>. Comparing the ECL curve and cyclic voltammogram recored simultaneously, they concluded that ECL emission tracks the current for the oxidation of TPrA. In the same work they proposed a mechanism. According to this work and some later works on the ECL mechanism, the proposed mechanism can be represented by the following reactions.<sup>5, 46-48</sup>

Acid-base equilibrium:



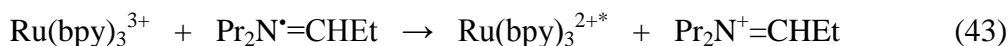
Oxidation step:



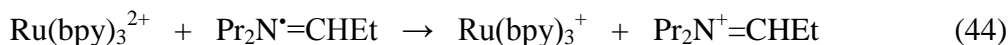
Deprotonation:



Excited state formation 1:



Excited state formation 2:



Light emission:

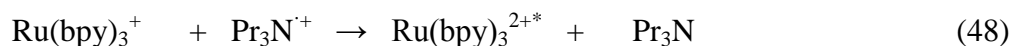
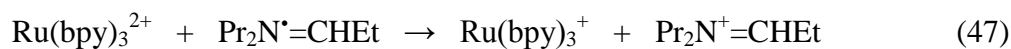


(Where Pr = CH<sub>3</sub>CH<sub>2</sub>CH<sub>2</sub>- and Et = CH<sub>3</sub>CH<sub>2</sub>-)

In anodic part of the scan, both Ru(bpy)<sub>3</sub><sup>2+</sup> and TPrA (NPr<sub>3</sub>) are oxidised (eqs 39-41). The oxidation of TPrA results in broad wave due to preceding acid-base equilibrium (eq 38) (pK<sub>a</sub> of ~10.4).<sup>48</sup> Oxidation of TPrA may occur both by direct oxidation on the electrode surface (eq 40) and by catalytic homogeneous oxidation by Ru(bpy)<sub>3</sub><sup>3+</sup> (eq 41). The relative contribution of the two routes depends on relative concentration of Ru(bpy)<sub>3</sub><sup>2+</sup> and TPrA and factors that affect the potential and rate of direct oxidation of TPrA at the electrode.<sup>46</sup> It was found that direct oxidation plays an important role in the ECL process when concentration of Ru(bpy)<sub>3</sub><sup>2+</sup> is low.<sup>46</sup> It shows a strong dependence on the electrode material. The oxidation is more efficient on the glassy carbon electrode than on gold or platinum where it is blocked by formation of surface oxides. Therefore, the enhancement of the TPrA oxidation current might lead to an increase in the ECL intensity.

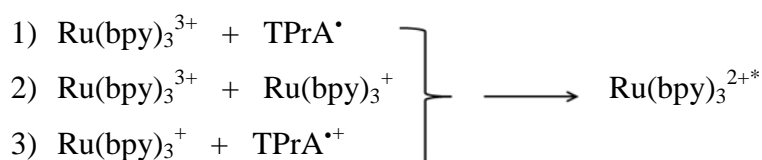
The oxidation of TPrA results in forming a short-lived intermediate radical cation (eq 42). The obtained species undergo fast deprotonation forming strong reducing free radical (eq 41) which can reduce Ru(bpy)<sub>3</sub><sup>2+</sup> to Ru(bpy)<sub>3</sub><sup>+</sup> and Ru(bpy)<sub>3</sub><sup>3+</sup> to form excited state Ru(bpy)<sub>3</sub><sup>2+\*</sup>.

When the concentration of TPrA is high and the concentration of Ru(bpy)<sub>3</sub><sup>2+</sup> is low, it was found that ECL curve shows two peaks.<sup>29, 30, 46</sup> The second peak appears at the potential which corresponds to the oxidation of Ru(bpy)<sub>3</sub><sup>2+</sup> but the first one appears earlier before its oxidation. With the previously presented mechanism that involved direct oxidation of Ru(bpy)<sub>3</sub><sup>2+</sup> these results can not be explained. Miao and Bard reported the possibility to achieve excited state with no direct oxidation of Ru(bpy)<sub>3</sub><sup>2+</sup>.<sup>29</sup> This mechanism involves reactive radical cation of TPrA.



This mechanism explains that the ECL emission appears at less positive potential than the oxidation of ruthenium centres. The intensity of this ECL emission strongly depends on the electrode material which confirms that it is based on direct oxidation of TPrA.<sup>46</sup>

To summarise, the excited state of  $\text{Ru}(\text{bpy})_3^{2+}$  may be produced via three different routes: 1)  $\text{Ru}(\text{bpy})_3^{3+}$  reduction by TPrA<sup>\*</sup>; 2) the  $\text{Ru}(\text{bpy})_3^{3+}$  and  $\text{Ru}(\text{bpy})_3^+$  annihilation reaction, and 3)  $\text{Ru}(\text{bpy})_3^+$  oxidation by TPrA<sup>\*+</sup> radical cation.



The ECL intensity of both waves depends on different conditions. The pH of the solution has an important role in the ECL generation. ECL intensity increases drastically at  $\text{pH} > 5.5$  and has a maximum at  $\text{pH} = 7.5$ . pH should be sufficiently high to promote deprotonation of TPrA<sup>\*+</sup> to TPrA<sup>\*</sup>.<sup>1</sup> However, pH value should not be higher than 9 because  $\text{Ru}(\text{bpy})_3^{3+}$  generates on the electrode surface can react with hydroxide ions and produce ECL background signal.<sup>45</sup>

Direct oxidation of TPrA strongly depends on electrode material. On glassy carbon electrode, direct oxidation is evident while on Au and Pt electrodes formation of surface oxide can block it significantly.<sup>46</sup> The electrode hydrophobicity has also an effect on direct TPrA oxidation and ECL intensity. It was found that addition of some non-ionic surfactants such as Triton X-100 significantly increases ECL intensity on Pt and Au electrodes.<sup>49-52</sup>

The ECL intensity of the first and second waves are proportional to the concentration of both  $\text{Ru}(\text{bpy})_3^{2+}$  and TPrA in a very large dynamic range<sup>5, 29, 46-48</sup> with detection limits of 0.5 pM for  $\text{Ru}(\text{bpy})_3^{2+}$ <sup>53</sup> and 10 nM TPrA.<sup>54, 55</sup> Due to these properties, the system has a wide range of analytical applications.



### 1.4.2. ECL Luminophores

In general, the luminophores that are used in ECL systems can be classified into three categories: 1) inorganic systems, which mainly contain organometallic complexes; 2) organic systems, which include polycyclic aromatic hydrocarbons (PAHs); and 3) semiconductor nanoparticle systems.

#### 1.4.2.1. Inorganic systems

Metal chelates, in particular the tris(bipyridine)ruthenium(II),  $\text{Ru}(\text{bpy})_3^{2+}$  have an important role in ECL detection. This is not surprising, considering that many metal chelates display electrochemical and spectroscopic qualities required for an ECL luminophore.<sup>56</sup>  $\text{Ru}(\text{bpy})_3^{2+}$  and its derivatives are the most used luminophores. This is for a number of reasons including strong luminescence and solubility of  $\text{Ru}(\text{bpy})_3^{2+}$  in a variety of aqueous and nonaqueous solvents at room temperature and its ability to undergo reversible one electron-transfer reactions at easily attainable potentials.<sup>2</sup>

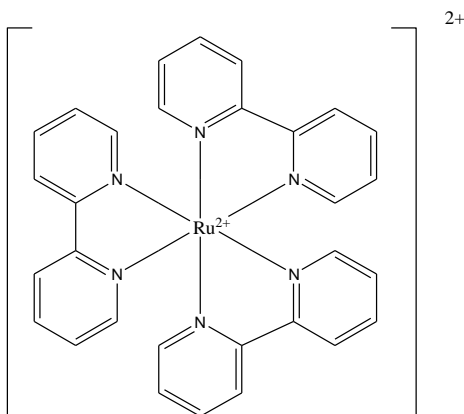


Figure 4. Structure formula of  $\text{Ru}(\text{bpy})_3^{2+}$

$\text{Ru}(\text{bpy})_3^{2+}$  is a yellow-orange coloured complex ( $\lambda_{\text{abs}}$  454 nm,  $\lambda_{\text{em}}$  607 nm).<sup>57</sup>  $\text{Ru}^{2+}$  is a  $d^6$  system with electron configuration  $[\text{Kr}] 4d^6$ . In  $\text{Ru}(\text{bpy})_3^{2+}$  it is surrounded with three bidentate polypyridine ligands that are usually colorless molecules possessing  $\sigma$ -donor orbitals localised on the nitrogen atoms and  $\pi$ -donor and  $\pi^*$ -acceptor orbitals more or less delocalised on aromatic rings.<sup>58</sup> Figure 5 shows a simplified representation of the electronic situation for a  $d^6$  complex (such as Ru(II)) in an octahedral microsymmetry ( $D_3$ ).

One electron excitation from a  $\pi_M$  metal orbital to the  $\pi_L^*$  ligand orbitals gives rise to metal-to-ligand charge transfer (MLCT) excited states, whereas promotion of an electron from  $\pi_M$  to  $\sigma_M$  orbitals gives rise to metal centered (MC) excited states. Ligand centered (LC) excited states are obtained by promoting an electron from  $\pi_L$  to  $\pi_L^*$ .<sup>58, 59</sup>

The MC excited states of  $d^6$  octahedral complexes are strongly displaced with respect to the ground state geometry along metal-ligand vibration coordinates. When the lowest excited state is MC, it undergoes fast radiationless deactivation to the ground state and/or ligand dissociation reactions. As a consequence, at room temperature, the excited state lifetime is very short and no luminescence emission is observed.<sup>58</sup> LC and MLCT excited states are usually not strongly displaced compared to the ground state geometry. Thus, when the lowest excited state is LC or MLCT it does not undergo fast radiationless decay to the ground state and luminescence can usually be observed. The exception is at high temperature when thermally activated radiationless deactivation via upper lying MC excited states can occur. The radiative deactivation rate constant is somewhat higher for  $^3\text{MLCT}$  than for  $^3\text{LC}$  because of the larger spin-orbit coupling effect. For this reason, the  $^3\text{LC}$  excited states are longer lived at low temperature in rigid matrix and the  $^3\text{MLCT}$  excited states are more likely to exhibit luminescence at room temperature in fluid solution where the lifetime of  $^3\text{LC}$  and  $^3\text{MLCT}$  is shortened by activated surface crossing to short lived MC excited states or by bimolecular quenching processes.<sup>58</sup>

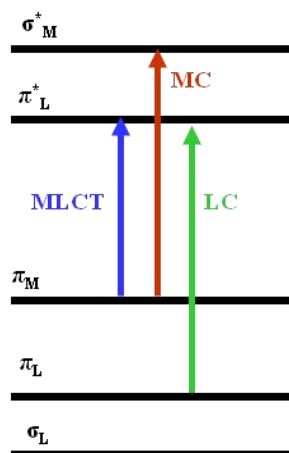


Figure 5. Simplified molecular orbital diagram for  $\text{Ru}(\text{LL})^{z+}$  complexes in octahedral symmetry showing the three types of electronic transitions occurring at low energies

$\text{Ru}(\text{bpy})_3^{2+}$  is the most use ECL luminophore thus it is involved in a wide range of applications. It can be applied in solution and more likely immobilised on the electrode surface.<sup>38, 60-64</sup> It is used for direct detection of different coreactants such as amines, oxalate, pyruvate, peroxydisulfate etc. but also for indirect detection of analytes that do not have coreactant properties.<sup>1, 2, 65</sup> Some analytes are detected after enzymatic reaction which involves transformation of  $\text{NAD}^+$  to  $\text{NADH}$  which is also a coreactant.<sup>66-69</sup>  $\text{Ru}(\text{bpy})_3^{2+}$ -based

ECL systems find application in flow systems such as high performance liquid chromatography (HPLC)<sup>70</sup>, capillary electrophoresis (CE)<sup>14, 15, 17</sup> and flow injection analysis (FIA).<sup>71</sup>

Even if  $\text{Ru}(\text{bpy})_3^{2+}$  has excellent properties as an ECL luminophore, many attempts have been made in designing or modifying the ligands of the complexes so as to improve both the light emitting and the electron transfer performances of such systems. The two main goals are to find new luminophores with higher ECL efficiencies and to modify a moiety of the emitter so that it can be used for labeling biomolecules.

To be an efficient luminophore a molecule should meet certain conditions. First of all it should be soluble in water or some other solvent depending on the potential application and should show reversible and stable electrochemistry. The pH on which the luminophore shows the most efficient emission is also very important especially for the luminophores that should be used as ECL labels for biomolecules where analyse are carried out in physiological conditions.

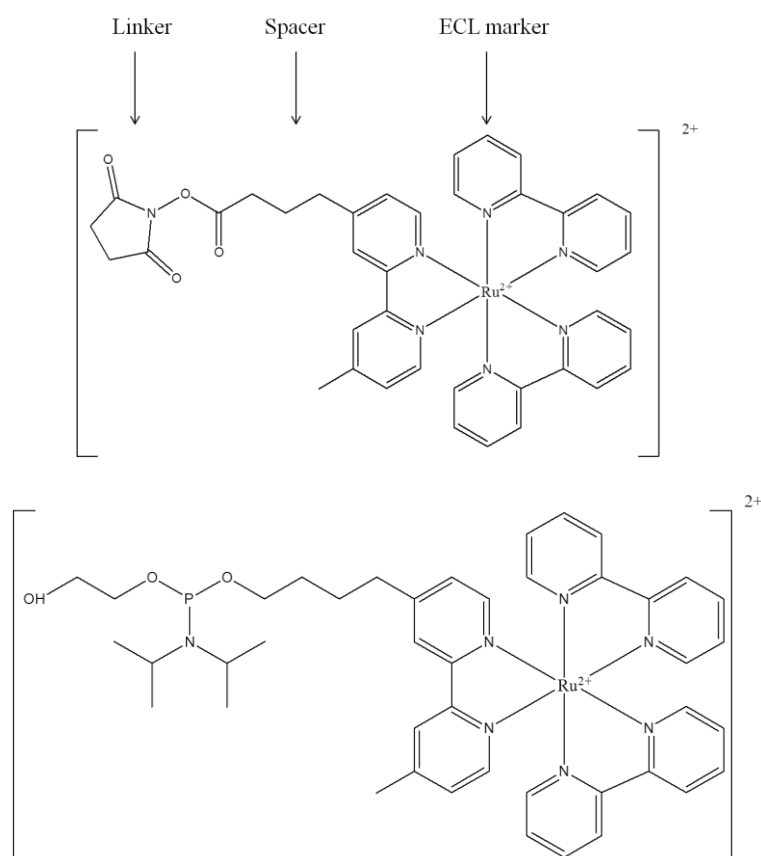


Figure 6. (Top)  $\text{Ru}(\text{bpy})_3^{2+}$ - NHS ester for ECL labelling of biological molecules, (bottom)  $\text{Ru}(\text{bpy})_3^{2+}$ - phosphoramidate linker for ECL for DNA and RNA

The increase of number of ECL systems in recent years is mainly due to different applications in immunoassays and DNA probe assays. In these systems biomolecules are labeled with an ECL luminophore. The  $\text{Ru}(\text{bpy})_3^{2+}/\text{TPrA}$  system provides extremely sensitive labeled detection at subpicomolar concentration as well as an extremely wide dynamic range, greater than six orders of magnitude. Thus, most of the ECL labels are based on  $\text{Ru}(\text{bpy})_3^{2+}$  complex and its derivatives. Figure 6 presents some ECL labels. Regarding the complex structures, the ruthenium centre is, similarly to  $\text{Ru}(\text{bpy})_3^{2+}$ , coordinated with three bipyridyl ligands thus these labels have similar ECL properties to  $\text{Ru}(\text{bpy})_3^{2+}$ . From the other hand, the bipyridyl ligands are functionalised to be able to react with other groups and to attach to biomolecules. To increase the sensitivity of the system which is especially important for ECL labelling, multimetallic ruthenium complexes have been reported.

A dendritic label for multilabelling of biomolecules at a single site has been synthesised. As advantage, the single-site multilabeling strategy enhances signal intensity with potentially minimum perturbation of the binding affinity.<sup>72</sup> A zeroth-generation dendron, succinimidyl-functionalised trinuclear ruthenium(II)tris(bipyridine) (Figure 7) was applied in protein detection.<sup>72</sup> The concept was presented by labeling the BSA as a model protein. Although the comparative ECL immunoassay with a multireporter label and a similar monoreporter label was not performed, it is concluded that using a dendritic platform bearing multiple signal generating units for multilabeling biomolecules enhances signal intensity.

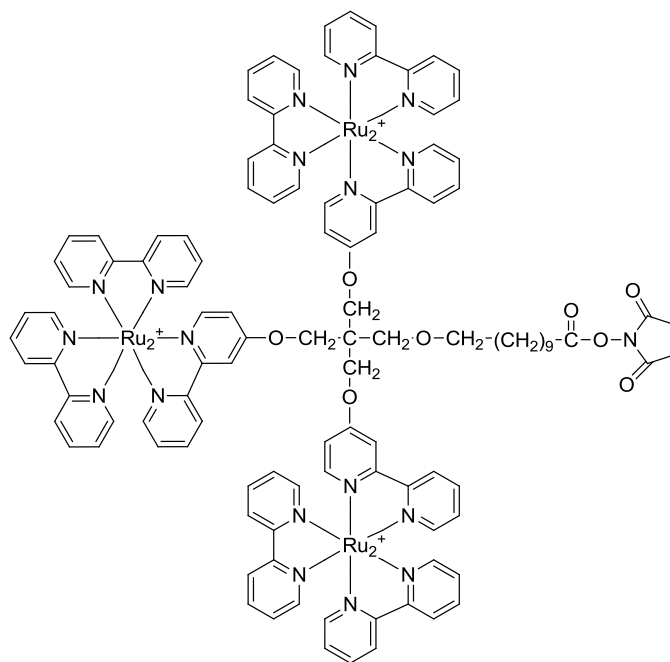


Figure 7. Structure of succinimidyl-functionalized trinuclear ruthenium(II)tris(bipyridine)

A series of bimetallic ruthenium complexes  $[(\text{bpy})_2\text{Ru}-(\text{bpy})(\text{CH}_2)_n(\text{bpy})\text{Ru}(\text{bpy})_2]^{4+}$  ( $n=3, 5, 8$ ) with a different length of carbon chain have been synthesised.<sup>73</sup> It was found that ECL intensity increases with increasing the length of carbon chain linkage. The ECL intensity of bimetallic complex with  $-(\text{CH}_2)_8-$  bridge shows ECL emission with TPrA up to 25 times stronger than that of reference  $\text{Ru}(\text{bpy})_3^{2+}$ .

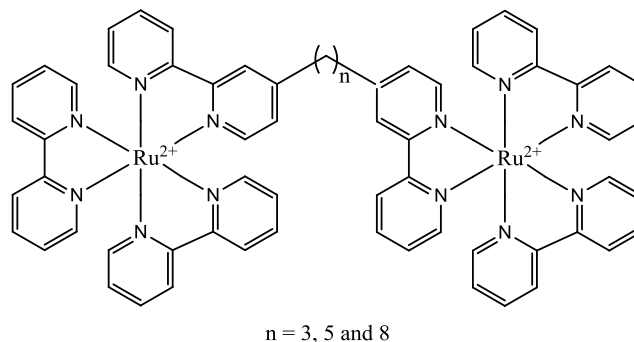


Figure 8. Structure for the bimetallic ruthenium(II) tris-bipyridyl complex

The synthesis of dendritic supramolecular structures was also performed in order to increase efficiency of ECL labels. The dendritic assembly with eight  $\text{Ru}(\text{II})\text{tris}(\text{bipyridine})$  units which structure is shown in figure 9 shows molar ECL intensity five times higher than that of the reference  $\text{Ru}(\text{bpy})_3^{2+}$ .<sup>74</sup>

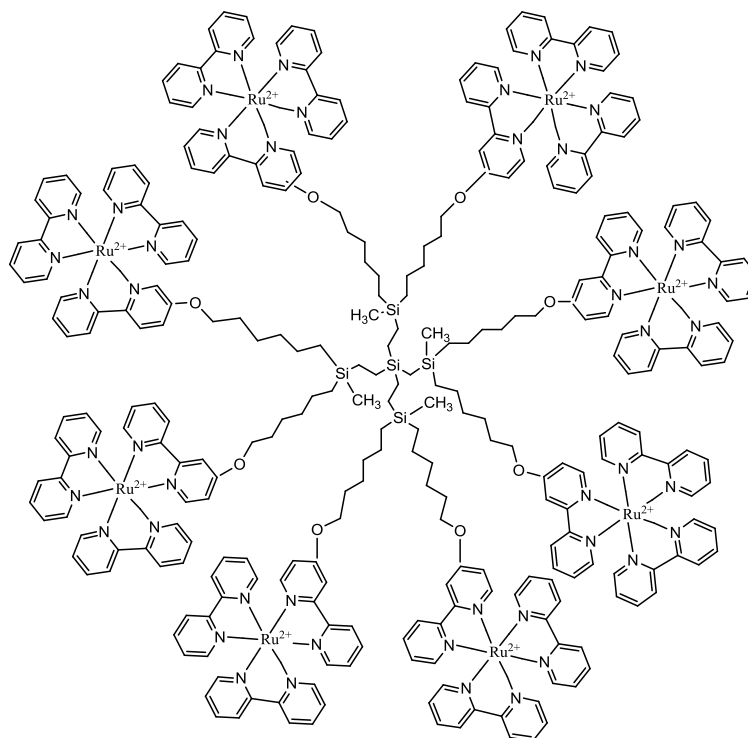


Figure 9. Structure of dendritic assembly with eight  $\text{Ru}(\text{II})\text{tris}(\text{bipyridine})$  units

Many attempts have been made in designing or modifying the ligands of ruthenium complexes to improve molecular recognition ability. For example, ruthenium complexes containing crown ether moieties covalently bonded to bipyridyl or phenanthroline ligands have been used for metal-cation sensing. These complexes may be used for clinical and environmental detection of metal ions which are not directly involved in redox reaction. When it was used of  $\text{Ru}(\text{bpy})_2(\text{CE-bpy})^{2+}$  where CE-bpy is a bipyridine ligand with crown ether (15-crown-5) moiety, it has been reported that ECL intensity of  $\text{Ru}(\text{bpy})_2(\text{CE-bpy})^{2+}$  increases in the presence of sodium ions which can be used for its detection in both aqueous and non-aqueous media.<sup>75</sup> In the same time it has been reported that electrochemical, photoluminescence (PL), and ECL properties of  $(\text{bpy})_2\text{Ru}(\text{AZA-bpy})^{2+}$  (AZA-bpy = 4-(N-aza-18-crown-6-methyl - 2,2'-bipyridine) changes when some metal cations are introduced in the solutions. The complex showed to be sensitive to  $\text{Pb}^{2+}$ ,  $\text{Hg}^{2+}$ ,  $\text{Cu}^{2+}$ ,  $\text{Ag}^+$  and  $\text{K}^+$  but it was difficult to discriminate ECL response between different cations so far.<sup>76</sup>

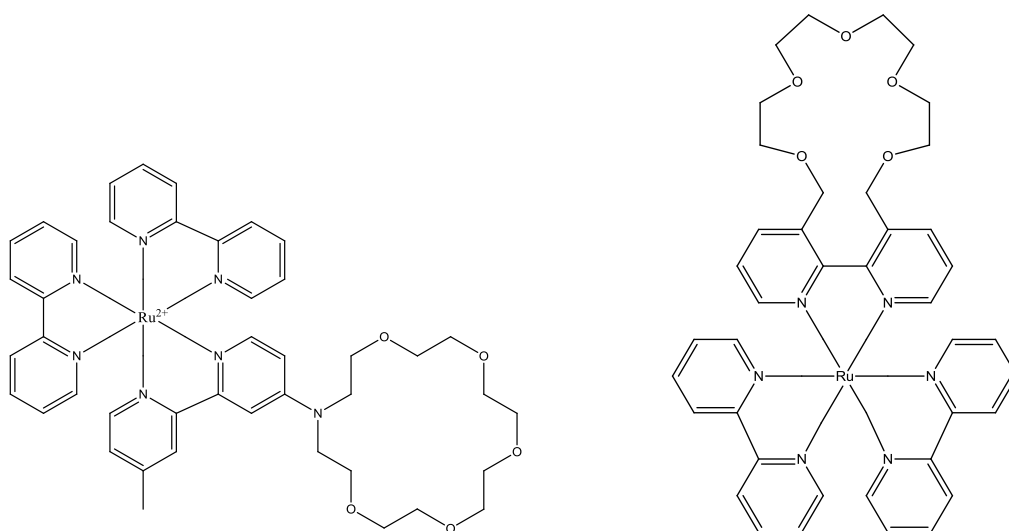


Figure 10. (Left)  $(\text{bpy})_2\text{Ru}(\text{AZA-bpy})^{2+}$ ; (right)  $\text{Ru}(\text{bpy})_2(\text{CE-bpy})^{2+}$

Based on the ruthenium complex with crown ether moieties, it has been reported “a lab on molecule”, quadruple-channel sensing for selective and quantitative multi-ion analysis.<sup>77</sup> Ruthenium complex with aza crown ethers as the receptor units were designed and four different parameters: 1) absorption; 2) emission; 3) redox properties and 4) ECL were monitored in the presence of different metal ions (Figure 11).

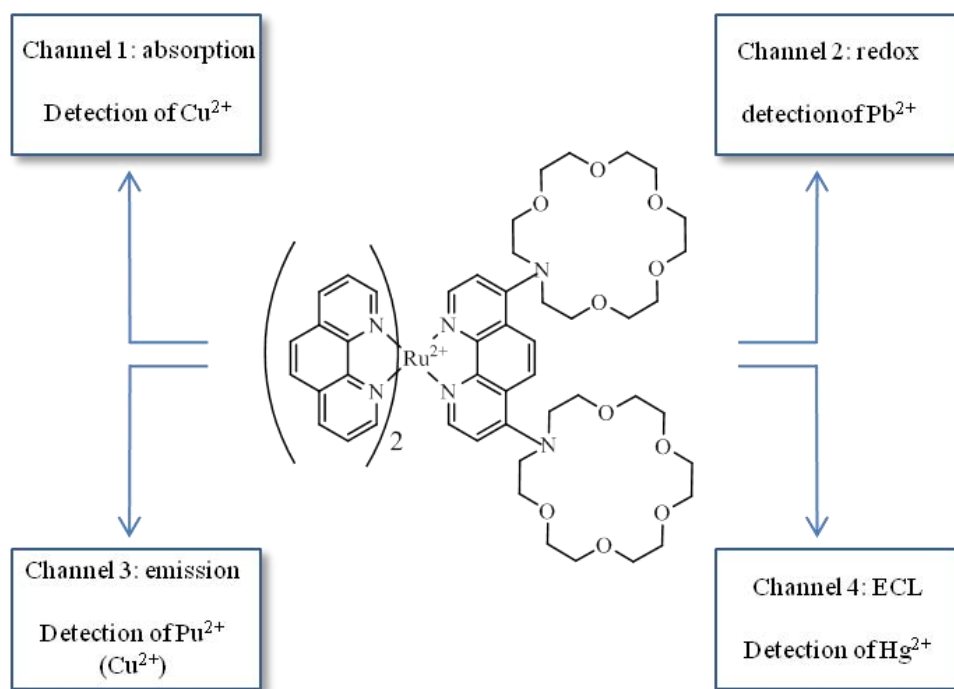


Figure 11. Quadrupole-channel sensing with ruthenium complex with aza crown ethers<sup>77</sup>

In the UV/Vis absorption of the complex in acetonitrile only  $\text{Cu}^{2+}$  ions caused a notable response on MLCT intensity (Channel 1). The complex is also an intense luminophore with an emission band at 672 nm. A survey of the photoluminescence in the presence of various metal ions in acetonitrile indicated that only the  $\text{Pb}^{2+}$  and  $\text{Cu}^{2+}$  ions induced marked changes in the emission, whereas other examined metal ions do not exhibited the emission changes almost at all (Channel 2). Cyclic voltammetry studies of the complex in acetonitrile showed that reversible wave for the  $\text{Ru}^{2+}/\text{Ru}^{3+}$  transition is shifted anodically by 180 mV upon addition of  $\text{Pb}^{2+}$  while the change is <50 mV in the presence of  $\text{Na}^+$ ,  $\text{K}^+$ ,  $\text{Mg}^{2+}$ ,  $\text{Ca}^{2+}$ ,  $\text{Zn}^{2+}$ ,  $\text{Cd}^{2+}$ ,  $\text{Ag}^+$   $\text{Hg}^{2+}$  and  $\text{Cu}^{2+}$  metal ions (Channel 3). The ECL emission in the presence of TPrA in acetonitrile showed a remarkable enhancement with addition of  $\text{Hg}^{2+}$  and negligible changes upon addition of others examined metal ions (Channel 4). Getting together all observations, the used complex presented as a “lab on a molecule” which contains only a single type of receptor site, may be used for simultaneous detection of  $\text{Pb}^{2+}$ ,  $\text{Hg}^{2+}$  and  $\text{Cu}^{2+}$  by using quadruple-channel detection (UV/Vis, PL, ECL, CV).

Recently, a new modified ruthenium(II)–bipyridyl complex for the detection of ions has been reported.<sup>78</sup> A new guanidinium 3,3′-functionalised bipyridylruthenium(II) complex has been prepared for the differential sensing of L-glutamate and dihydrogenophosphate anions depending on the luminescent detection scheme. The PL intensity was found to increase up to four-fold in the presence of L-glutamate while the increase of intensity in the presence of

dihydrogenphosphate was weaker. The ECL emission with TPrA increases only in the presence of dihydrogenophosphate allowing differential detection of L-glutamate and of dihydrogenophosphate.

As already mentioned, most of ECL applications are based on  $\text{Ru}(\text{bpy})_3^{2+}$  or its derivatives. Many metal complexes and clusters have electrochemical and spectroscopic properties required for an ECL emitter. ECL of complex or clusters containing Ag, Al, Au, Cd, Cr, Cu, Eu, Hg, Ir, Mo, W, Os, Pd, Pt, Re, Ru, Si, Tb, and Tl have been reported.<sup>2</sup>

The first reported osmium complex used in ECL was  $\text{Os}(\text{phen})_3^{2+}$ . ECL was generated in DMF with  $\text{S}_2\text{O}_8^{2-}$  as coreactant.<sup>79</sup> The development of osmium based systems would be advantageous because osmium systems are more photostable. Moreover oxidation occurs at less anodic potential than similar ruthenium systems. However, ECL application of osmium systems have been limited because of shorter excited state lifetimes and weaker emission efficiencies.<sup>80</sup>

Complexes of iridium are also able to emit ECL. Depending on the structure, some of them are extremely efficient such as  $(\text{pq})_2\text{Ir}(\text{acac})/\text{TPrA}$  (pq: 2-phenylquinoline, acac: acetylacetonate) which shows almost two orders of magnitude higher ECL efficiencies with TPrA as coreactant than  $\text{Ru}(\text{bpy})_3^{2+}$  under the same conditions.<sup>81</sup> From other hand, ECL of another iridium complex,  $\text{Ir}(\text{ppy})_3$  with TPrA shows weaker ECL emission than  $\text{Ru}(\text{bpy})_3^{2+}$  under similar conditions. However,  $\text{Ir}(\text{ppy})_3$  in acetonitrile emits green colour ( $\lambda_{\text{em}}=517$  nm).<sup>82</sup> Its maximum in comparison to emission maximum of red/orange  $\text{Ru}(\text{bpy})_3^{2+}$  is far enough and it is possible to distinguish both signals in a single ECL experiment.<sup>82</sup>

It was found that semiconductor nanoparticles (NPs) can induce ECL reaction following both annihilation and coreactant ECL pathways. Semiconductor nanoparticles NPs have excellent luminescent properties including high quantum yields, stability against photobleaching and size-controlled luminescence properties.<sup>6</sup> The ECL study of NPs was first reported for Si NPs but ECL investigation of NPs was not of important interest due to their low solubility and stability at oxidised and reduced forms. Later it was found that many semiconductors such as CdS, CdSE and CdTe can also produce ECL that can be electrically excitable in both nonaqueous<sup>83</sup> and aqueous media<sup>84</sup>. A common feature of ECL behaviour obtained from NPs is their red-shifted ECL maxima compare to their photoluminescence, suggesting that the emitting states are different.<sup>1</sup> This was explained by the fact that photoluminescence responses appears from electron transfer mainly from the interior of particles while ECL occurs at the surface where the surface chemistry has greater influence. ECL of water soluble



CdTe NPs has been recently reported, where it was shown that the size of NPs has an influence on the ECL behaviour.<sup>85</sup>

### 1.4.3. ECL Coreactants

An ECL coreactant is a reagent that after oxidation or reduction decomposes to form highly reactive reductive or oxidative species which can undergo energetic electron-transfer reaction with oxidised or reduced luminophore to generate ECL.

For an efficient ECL coreactant, a number of criteria need to be met which include solubility, stability, electrochemical properties, kinetics, quenching effect, ECL background etc.<sup>45</sup>

Some typical ECL coreactants are shown in table 1.

Table 1. Typical coreactant ECL systems

Type of coreactant ECL	Luminophore	Coreactant	Main coreactant intermediate
Oxidative reduction	$\text{Ru}(\text{bpy})_3^{2+}$	tri-(n)-propylamine	$\text{TPrA}^{+\cdot}$ , $\text{TPrA}^\bullet$
	$\text{Ru}(\text{bpy})_3^{2+}$	DBAE	$\text{DBAE}^\bullet$
	$\text{Ru}(\text{bpy})_3^{2+}$	oxalate	$\text{CO}_2^{\cdot-}$
	$\text{Ru}(\text{bpy})_3^{2+}$	pyruvate	$\text{CH}_3\text{CO}^\bullet$
Reductive-oxidation	$\text{Ru}(\text{bpy})_3^{2+}$	hydrazine	$\text{N}_2\text{H}_2$ , $\text{N}_2\text{H}_3^\bullet$
	$\text{Ru}(\text{bpy})_3^{2+}$	persulfate	$\text{SO}_4^{\cdot-}$
	aromatic hydrocarbons	benzoyl peroxide	$\text{PhCO}_2^\bullet$
	$\text{Ru}(\text{bpy})_3^{2+}$	hydrogen peroxide	$\text{OH}^\bullet$

Similarly to TPrA other amines can be also used as ECL coreactants. An important condition that should be met is that the amine should have a hydrogen atom attached to the  $\alpha$ -carbon so that upon oxidation newly formed radical can undergo reaction of deprotonation to form a strongly reducing free radical species. A lot of work has been done to correlate the coreactant ECL efficiency with the amine structure. In general it was found that ECL intensity increase in the order primary < secondary < tertiary amines.<sup>5, 24, 63, 86</sup>

Due to its excellent ECL response,  $\text{Ru}(\text{bpy})_3^{2+}/\text{TPrA}$  system is the ECL pair that is the most used in different analytical and commercial applications. Recently, a new coreactant 2-(dibutylamino)ethanol (DBAE) has been reported.<sup>87</sup> The ECL intensity of the  $\text{Ru}(\text{bpy})_3^{2+}/\text{DBAE}$  system at Au and Pt electrode was found to be almost 10 and 100 times greater than obtained with commonly used  $\text{Ru}(\text{bpy})_3^{2+}/\text{TPrA}$  system, respectively. The very strong ECL efficiency was attributed to the catalytic effect of hydroxyethyl group toward the direct oxidation of DBAE at the electrode. DBAE is less toxic, more soluble and less volatile than TPrA and it could be promising coreactant for ECL immunoassays and DNA probe assays.

A special importance in the group of amine coreactants has  $\beta$ -nicotinamide adenine dinucleotide reduced form (NADH). Namely, it was found that NADH oxidises to  $\text{NADH}^{+\bullet}$  which deprotonates forming highly reducing species  $\text{NAD}^\bullet$ . On the other hand,  $\beta$ -nicotinamide adenine dinucleotide ( $\text{NAD}^+$ ) has aromatic structure and do not undergo electrochemiluminescent reaction. For this reason, ECL is used for detection of NADH, especially in enzymatic systems where NADH is produced from  $\text{NAD}^+$ .

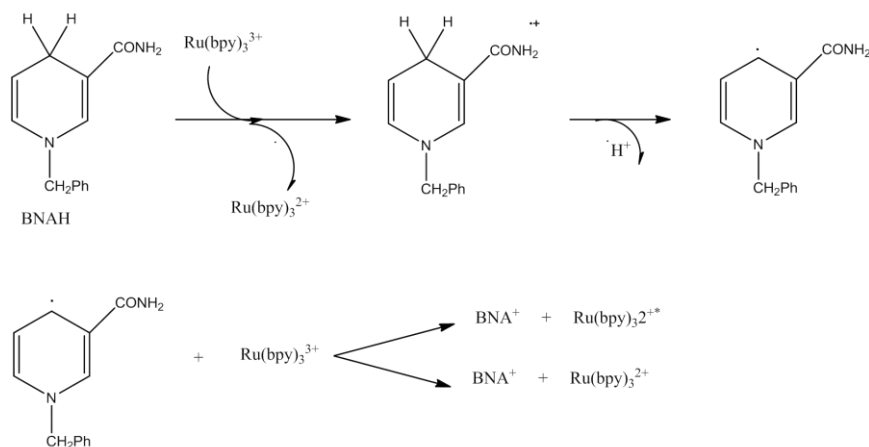


Figure 12. Chemiluminescent mechanism of BNAH with  $\text{Ru}(\text{bpy})_3^{3+}$

Chemiluminescent mechanism was studied on 1-benzyl-1,4-dihydronicotinamide (BNAH), a NADH analog in the presence of  $\text{Ru}(\text{bpy})_3^{3+}$ .<sup>88, 89</sup> In the chemiluminescent mechanism, BNAH is oxidised by  $\text{Ru}(\text{bpy})_3^{3+}$  and generates  $\text{BNAH}^{+\bullet}$  cation radical. After deprotonation, the neutral radical  $\text{BNA}^\bullet$  reacts homogeneously with  $\text{Ru}(\text{bpy})_3^{3+}$  and produce the excited state  $\text{Ru}(\text{bpy})_3^{2+*}$  (Figure 12).

### 1.5. ECL APPLICATION

Due to its advantages over the other techniques, ECL becomes a robust detection methodology.<sup>90</sup> Figure 13 summarised advantages and disadvantages of ECL as a detection technique. It is widely used in clinical diagnostics, environmental assay such as food and water testing and biowarfare agent detection. Since the  $\text{Ru}(\text{bpy})_3^{2+}$  /TPrA pair shows the most efficient ECL emission and it is suitable for work in physiological conditions, the majority of ECL detection systems involves  $\text{Ru}(\text{bpy})_3^{2+}$  or its derivatives as emitter and TPrA or other related amines as coreactant.

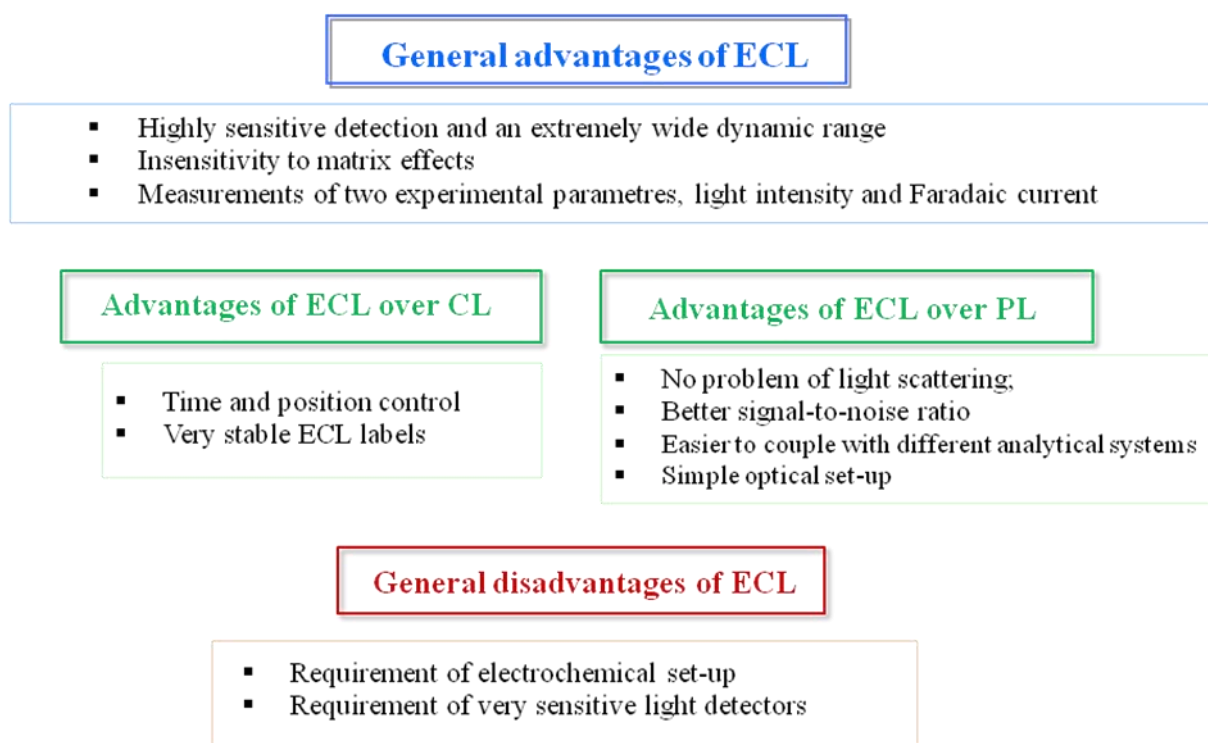


Figure 13. Advantages and disadvantages of ECL as detection technique

Analytical applications are based on the fact that ECL intensity is proportional to the concentration of the ECL luminophore or the concentration of coreactant. If ECL experiments are carried out in the presence of high and constant concentrations of coreactant, ECL intensity will linearly depend on the concentration of ECL emitter in a wide dynamic range. Alternatively, if the experiments are running in the presence of constant  $\text{Ru}(\text{bpy})_3^{2+}$  concentration, ECL signal will show dependence on coreactant concentration.

### 1.5.1. Application in CE, HPLC and FIA systems

An important feature of ECL is its easy integration with analytical systems such as capillary electrophoresis (CE), high performance liquid chromatography (HPLC) and flow injection analysis (FIA). The analytes or its derivatives should behave like an ECL coreactant which often means to have secondary or tertiary amine groups with an  $\alpha$ -carbon hydrogen so that efficient ECL can be produced in the presence of  $\text{Ru}(\text{bpy})_3^{2+}$ . Because tertiary amines can produce sensitive ECL responses, a lot of efforts have been made to introduce such groups to initially less or non-ECL sensitive analytes such as amino acids and fatty acids.<sup>70, 91</sup> Amino acids such as proline, valine and leucine can be successfully detected in CE-ECL system with detection limit in the nM -  $\mu\text{M}$  concentration range.<sup>91</sup> The group of E. Wang employed CE-ECL for different applications. For example, CE-ECL was applied for investigation of drug-protein binding.<sup>92</sup> Three basic drugs, pridinol, procyclidine and trihexyphenidyl, were successfully separated by capillary zone electrophoresis with end-column  $\text{Ru}(\text{bpy})_3^{2+}$  ECL detection. Thermodynamic and kinetic studies have been also realised using CE-ECL system. Drug-human serum albumin binding of paracetamol on prolidase activity in erythrocytes and in serum of diabetic patients was reported.<sup>68, 92, 93</sup> The same group also developed micro total analysis systems ( $\mu\text{TAS}$ ) also called "lab on a chip" for fast analysis of ofloxacin and lidocaine.<sup>17</sup>

A number of advantages are offered by CE-ECL with respect to other commonly used separation-detection methods including UV-vis or fluorescent detection. ECL-based detection methods offer very powerful resolving ability, good selectivity, high sensitivity and easy sample preparation as there is no need of sample pre-treatment.<sup>68, 94</sup> Due to large application of CE coupled with ECL, a commercialised CE-ECL analyser have been designed at the Changchun Institute of Applied Chemistry in China (Figure 14).

HPLC may be also coupled with ECL. Recently, it has been reported direct detection of ofloxacin, one of the most frequently used fluorinated quinolones antibiotics.<sup>13</sup> Applying the HPLC-ECL system ofloxacin was detected in human serum in the range of concentration from  $1.0 \times 10^{-8}$  to  $4.0 \times 10^{-6}$  g/mL, the detection limit was  $4 \times 10^{-9}$  gm/L. The detection was based on the fact that ofloxacin exhibits strong ECL at Pt electrode in  $\text{NaNO}_3$  solution.



Figure 14. MPI-A capillary electrophoresis-electrogenerated chemiluminescent analyser developed at the Changchun Institute of Applied Chemistry, Chinese Academy of Sciences, and manufactured by Xi'an Remax Electronic Co. Ltd.<sup>1</sup>

It was found that many compounds are able to quench, inhibit or enhance ECL intensity. For example phenols, ferrocene, anilines and their derivatives can significantly quench the oxidative-reduction ECL by energy or electron transfer between  $\text{Ru}(\text{bpy})_3^{2+*}$  and the electro-oxidised species of the quencher.<sup>95-97</sup> This strategy has been used in FIA-ECL system for detection of tetracycline in Chinese proprietary medicine and noradrenalin and dopamine in commercial pharmaceutical injection samples.<sup>98</sup>

### 1.5.2. Solid Phase ECL Assay

The most important commercial applications of ECL are in diagnostic assays. A large number of biomolecules such as proteins, DNAs and peptides have no coreactant functionalities or they give very poor ECL signal. Thus, their ECL detection is mainly carried out with solid phase ECL assay formats in which biomolecules are linked with ECL labels, usually  $\text{Ru}(\text{bpy})_3^{2+}$  or its derivatives. They are immobilised on a solid substrate and ECL is generated in the presence of an ECL coreactant, typically TPrA.

There is a number of methods that can be used for immobilisation of biomolecules onto a solid substrate which include avidin/biotin interactions,<sup>31, 99</sup> sol-gel,<sup>100</sup> self-assembled thiol-COOH monolayers (SAMs),<sup>101</sup> polymer films<sup>102</sup> and glyoxyl agarose.<sup>103</sup> Biomolecules may be directly adsorbed by hydrophobic or electrostatic interactions<sup>104</sup> but they are less stable and reproducible and there is more nonspecific adsorption.

Sensitive and selective detection of DNA hybridisation has a great importance in genetic disease screening. An ultrasensitive DNA hybridisation detection method based on ECL using polystyrene microspheres/beads (PSB) as the carrier of the ECL label tris(2,2'-bipyridyl)ruthenium(II) tetrakis (pentafluorophenyl)borate ( $\text{Ru}(\text{bpy})_3\text{-}[\text{B}(\text{C}_6\text{F}_5)_4]_2$ ) has been reported by Miao and Bard.<sup>31</sup> Single-stranded DNA probe (p-ssDNA) was attached to the surface of magnetic beads (MB) and hybridised with target-ssDNA (t-ssDNA) immobilised on PSB containing a large number of water insoluble  $\text{Ru}(\text{bpy})_3\text{-}[\text{B}(\text{C}_6\text{F}_5)_4]_2$  species (Figure 15). With this approach a large amplification factor of  $\text{Ru}(\text{bpy})_3\text{-}[\text{B}(\text{C}_6\text{F}_5)_4]_2$  molecules for each t-ssDNA can be achieved, when each PSB is attached to a limited number of t-ssDNA. With this approach, the ECL intensity was found to be linearly proportional to the t-ssDNA concentration in a range of 1 fM to 10 nM under optimised conditions.

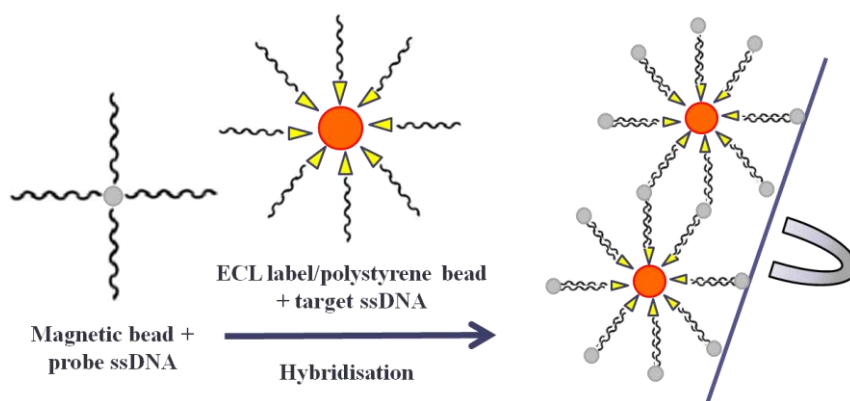


Figure 15. Schematic diagram of DNA hybridisation on a polystyrene bead as the ECL label carrier and a magnetic bead for the separation of analyte-contained ECL label/polystyrene beads.<sup>31</sup>

Another example of DNA detection is based on the role of guanine bases as ECL coreactant. Namely, guanine radical initially formed by catalytic oxidation of guanines by  $\text{Ru}^{3+}$  can react with  $\text{Ru}^{3+}$  sites in a metallopolymer ( $[\text{Ru}(\text{bpy})_2(\text{PVP})_{10}]_{2+}$ ) to produce  $\text{Ru}^{2+*}$  sites. ECL signal was sensitive to oligonucleotide hybridisation and chemical damage of DNA. ECL intensity decreases after the hybridisation and increases if the dsDNA is damaged by some harmful agent.<sup>9</sup>

One of the most important applications of ECL is its use in immunoassays. For example, anti-C-reactive protein (CRP), an acute-phase protein found in human serum was measured by a sandwich-type immunoassay which uses ECL as a readout mechanism. Biotinylated CRP species were attached to the surface of streptavidin-coated magnetic beads (MB). They were then attached to the avidin-coated polystyrene microspheres/beads (PSB) in which a large

number of ECL labels ( $\text{Ru}(\text{bpy})_3\text{-[B(C}_6\text{F}_5)_4\text{]}_2$ ) was entrapped. This results in formation of a sandwich-type binding  $\text{anti-CRP} \leftrightarrow \text{MB} \leftrightarrow \text{Ru(II)-PSB/avidin} \leftrightarrow \text{anti-CRP}$ .<sup>99</sup> The ECL intensity was found to be proportional to the analyte CRP over the range of 0.010-10  $\mu\text{g/mL}$ .

Recently, an ECL immunosensor for the detection of protein cancer biomarkers using single-wall carbon nanotube (SWCNT) forests and  $\text{Ru}(\text{bpy})_3^{2+}$ -doped silica nanoparticles (NPs) has been reported.<sup>105</sup> The sandwich format was designed by first chemically attaching capture antibodies  $\text{Ab}_1$  on SWCNT forests on pyrolytic graphite disks, and then incubating the prostatic specific antigen (PSA). After washing with non-specific binding blockers, the RuBPY-silica- $\text{Ab}_2$  NP bioconjugate was added (Figure 16). A detection limit reached by this method was 40  $\text{pg/mL}$ , which is well below the normal serum levels of PSA. The method was further developed for detection of PSA and interleukin-6 (IL-6) simultaneously.<sup>106</sup>

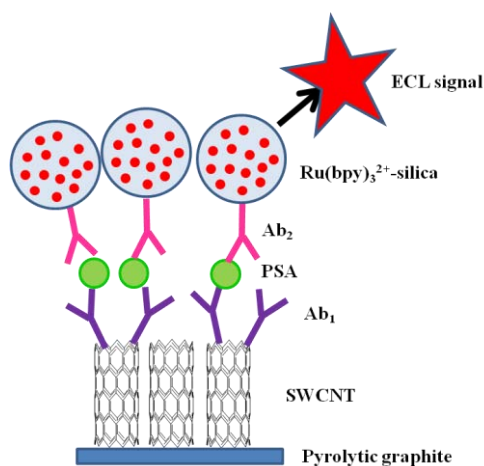


Figure 16. Representation of ECL-based SWCNT immunosensors after addition of PSA and the RuBPY-silica- $\text{Ab}_2$  nanoparticles.<sup>105</sup>

In the recent years different multiplexed assays which employ ECL have been developed. Our group reported a new class of sensing microarray based.<sup>10</sup> The approach involves attaching specific receptors to microbeads and beads immobilization in the wells of etched and gold-coated fiber optic bundles (Figure 17). ECL imaging was used as readout mechanism. The method enables multiplexed assays because all the individual sensing beads in the array are simultaneously imaged.

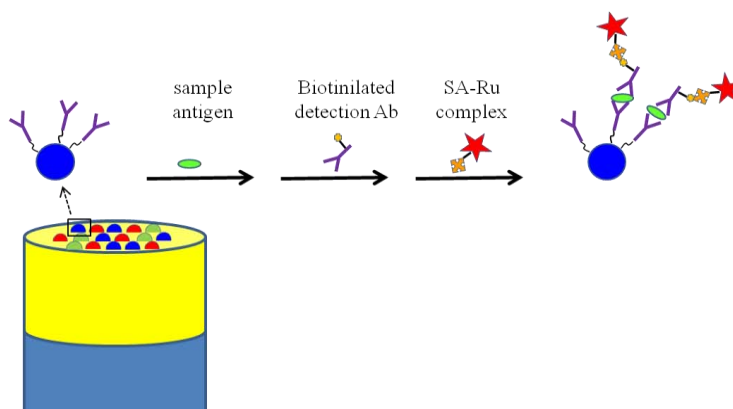
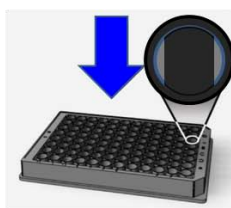


Figure 17. Scheme of multiplexed bead-based immunoassay on the fiber optic bundles<sup>10</sup>

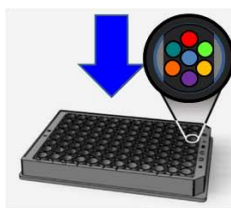
ECL detection is also widely used in commercialised systems. ECL instrumentation has been commercially available since 1994 and has been rapidly adopted for clinical, industrial and research detection.<sup>90</sup> The first instrument that applies ECL detection was the ORIGEN Analyser (IGEN International Inc.)<sup>90</sup> The ORIGEN Analyser is adapted to measure ECL labels present on the surface of magnetically responsive beads. The beads are coated with binding reagents and are used as assay supports in solid-phase binding assays. The assays are designed so that amount of label on the beads is indicative of the amount of analyte in a sample. Roche Diagnostic design three analysers based on ORIGEN technology. Analysers are made for clinical immunoassay testing for small- to medium and for medium- to large-volume laboratories depending on the type.<sup>8</sup> These systems are automated and offer over 50 immunoassay tests in the area of cardiology, thyroid function, oncology, anemia, fertility, infection diseases and osteoporosis.



SECTOR Imager 6000



**Multi-array** plates formats include 96- and 384-well plates for high throughput analysis



**Multi-spot** plates offer arrays within the well for increased throughput and assay multiplexing, are available in 24-, 96-, and 384 well formats, with up to 100 spots per well.

Figure 18. Commercial ECL imager from Meso Scale Discovery. The instrument use ultra-low noise CCD camera and it is suitable for single and multiplexed assay formats.<sup>7</sup>



Another type of commercialised ECL system is provided by Meso Scale Discovery. The detection is based on multi-array and multi-spot technology. Assays are carried out on the surfaces of screenprinted carbon ink electrodes within the wells of multiwell plates. Each well may consist of one electrode for single detection or of few electrode spots immobilised with different capture molecules for multiplexed detection. A variety of plate formats are available to suit the needs of drug discovery and biological research. Depending on the design, single and multiplexed assay kits for profiling biomarkers, cell signaling pathways and other applications are available.

## 1.6. CONCLUSION

ECL is a powerful detection method where the analytical signal is the light intensity. The method offers several advantages over other detection methods such as high sensitivity, good selectivity, insensitivity to matrix effects and high dynamic range. As the reaction is initiated and controlled by applying the adequate potential, the method offers the time and position control with a possibility of simultaneous measurements of both experimental parameters, light intensity and Faradaic current. Depending on the reaction mechanism two ECL types may be distinguished: annihilation and coreactant ECL. Though the first experiments were mainly based on annihilation ECL, the applications were limited due to experimental conditions such as wide potential window and non-aqueous media. The coreactant ECL is mainly performed in aqueous media often in physiological conditions, thus it is more appropriate for different applications including biorelated systems. Due to its excellent electrochemical and spectroscopic properties  $\text{Ru}(\text{bpy})_3^{2+}$  and its derivatives are the most used luminophore. It can be used in water or organic solutions or more likely when immobilised on the electrode surface. There are several advantages to immobilise luminophores including higher sensitivity due to concentration of emitter centres in the detection region near the electrode surface and less consumption of chemicals which has a special impact in flow systems. ECL may be coupled with CE, HPLC and FIA for different analysis in the environmental chemistry, for food and water testing and biowarfare agents detection. ECL is also used as a detection method in enzymatic biosensors, in immunoassays and DNA probe analysis where ECL label is attached to the biomolecule. ECL detection is applied in research as well as in commercialised detection systems. Different detection kits provided by Roche Diagnostic and Meso Sale Discovery offer a large number of fast, reliable and inexpensive

analyses for clinical diagnostic. ECL applications reported so far indicate the significance of ECL as a general detection method. For this reason many efforts are made to improve and to develop new ECL-based detection systems. Great importance is given to the development of new immobilisation strategies and to improvement of experimental conditions in respect to the chemistry that occur which is the aim of the work presented in the following chapters.

## REFERENCES

1. W. Miao, *Chem. Rev.*, 2008, **108**, 2506.
2. M. M. Richter, *Chem. Rev.*, 2004, **104**, 3003.
3. L. Hu and G. Xu, *Chem. Soc. Rev.*, 2010, **39**, 3275.
4. A. Bard, in *Electrogenerated Chemiluminescence*, CRC Press, 2004, pp. 1-22.
5. J. K. Leland and M. J. Powell, *J. Electrochem. Soc.*, 1990, **137**, 3127.
6. P. Bertonecello and R. J. Forster, *Biosens. Bioelectron.*, 2009, **24**, 3191.
7. [www.mesoscale.com](http://www.mesoscale.com).
8. [www.roche.com](http://www.roche.com).
9. L. Dennany, R. J. Forster and J. F. Rusling, *J. Am. Chem. Soc.*, 2003, **125**, 5213.
10. F. Deiss, C. N. LaFratta, M. Symer, T. M. Blicharz, N. Sojic and D. R. Walt, *J. Am. Chem. Soc.*, 2009, **131**, 6088.
11. Y. Shan, J.-J. Xu and H.-Y. Chen, *Chem. Commun.*, 2009, 905.
12. Y. Shan, J.-J. Xu and H.-Y. Chen, *Chem. Commun.*, 2010, **46**, 5079.
13. Y. Sun, Z. Zhang and Z. Xi, *Anal. Chim. Acta*, 2008, **623**, 96.
14. J. Wang, Z. Yang, X. Wang and N. Yang, *Talanta*, 2008, **76**, 85.
15. J. Li, Y. Xu, H. Wei, T. Huo and E. Wang, *Anal. Chem.*, 2007, **79**, 5439.
16. Y. Chi, Y. Dong and G. Chen, *Electrochem. Commun.*, 2007, **9**, 577.
17. X.-B. Yin, J. Kang, L. Fang, X. Yang and E. Wang, *J. Chromatogr. A*, 2004, **1055**, 223.
18. N. Harvey, *J. Phys. Chem.*, 1929, **33**, 1456.
19. R. T. Dufford, D. Nightingale and L. W. Gaddum, *J. Am. Chem. Soc.*, 1927, **49**, 1858.
20. R. E. Visco and E. A. Chandross, *J. Am. Chem. Soc.*, 1964, **86**, 5350.
21. K. S. V. Santhanam and A. J. Bard, *J. Am. Chem. Soc.*, 1965, **87**, 139.

22. N. E. Tokel and A. J. Bard, *J. Am. Chem. Soc.*, 1972, **94**, 2862.
23. M.-M. Chang, T. Saji and A. J. Bard, *J. Am. Chem. Soc.*, 1977, **99**, 5399.
24. J. B. Noffsinger and N. D. Danielson, *Anal. Chem.*, 1987, **59**, 865.
25. P. Innocenzi, H. Kozuka and T. Yoko, *J. Phys. Chem. B*, 1997, **101**, 2285.
26. T. N. Singh-Rachford and F. N. Castellano, *Coord. Chem.Rev.*, 2010, **254**, 2560.
27. M. Yamaguchi, H. Yoshida and H. Nohta, *J.Chromatogr. A*, 2002, **950**, 1.
28. E. H. White and M. M. Bursey, *J. Am. Chem. Soc.*, 1964, **86**, 941-942.
29. W. Miao, J.-P. Choi and A. J. Bard, *J. Am. Chem. Soc.*, 2002, **124**, 14478.
30. S. Zanarini, E. Rampazzo, L. D. Ciana, M. Marcaccio, E. Marzocchi, M. Montalti, F. Paolucci and L. Prodi, *J. Am. Chem. Soc.*, 2009, **131**, 2260.
31. W. Miao and A. J. Bard, *Anal. Chem.*, 2004, **76**, 5379.
32. W. Miao and G. Z. Cynthia, in *Handbook of Electrochemistry*, Elsevier, Amsterdam, 2007, p. 541.
33. F. E. Beideman and D. M. Hercules, *J. Phys. Chem. A*, 1979, **83**, 2203.
34. L. R. Faulkner, H. Tachikawa and A. J. Bard, *J. Am. Chem. Soc.*, 1972, **94**, 691.
35. L. R. Faulkner and A. J. Bard, *J. Am. Chem. Soc.*, 1969, **91**, 209.
36. E. L. Ritchie, P. Pastore and R. M. Wightman, *J. Am. Chem. Soc.*, 1997, **119**, 11920.
37. H. Tachikawa and A. J. Bard, *Chem. Phys. Lett.*, 1974, **26**, 246.
38. I. Rubinstein and A. J. Bard, *J. Am. Chem. Soc.*, 1981, **103**, 5007.
39. F. Kanoufi, C. Cannes, Y. Zu and A. J. Bard, *J. Phys. Chem. B*, 2001, **105**, 8951.
40. I. Rubinstein and A. J. Bard, *J. Am. Chem. Soc.*, 1981, **103**, 512.
41. I. Rubinstein, C. R. Martin and A. J. Bard, *Anal. Chem.*, 1983, **55**, 1580.
42. F. Kanoufi and A. J. Bard, *J. Phys. Chem. B*, 1999, **103**, 10469.
43. D. Ege, W. G. Becker and A. J. Bard, *Anal. Chem.*, 1984, **56**, 2413.
44. H. S. White and A. J. Bard, *J. Am. Chem. Soc.*, 1982, **104**, 6891.
45. J.-P. Choi and W. Miao, in *Electrogenerated Chemiluminescence*, CRC Press, 2004, pp. 213-271.

46. Y. Zu and A. J. Bard, *Anal. Chem.*, 2000, **72**, 3223.
47. E. M. Gross, P. Pastore and R. M. Wightman, *J. Phys. Chem. B*, 2001, **105**, 8732.
48. F. Kanoufi, Y. Zu and A. J. Bard, *J. Phys. Chem. B*, 2000, **105**, 210.
49. B. Factor, B. Muegge, S. Workman, E. Bolton, J. Bos and M. M. Richter, *Anal. Chem.*, 2001, **73**, 4621.
50. D. Bruce, J. McCall and M. M. Richter, *Analyst*, 2002, **127**, 125.
51. Y. Zu and A. J. Bard, *Anal. Chem.*, 2001, **73**, 3960.
52. S. Workman and M. M. Richter, *Anal. Chem.*, 2000, **72**, 5556.
53. A. Arora, A. J. de Mello and A. Manz, *Anal. Commun.*, 1997, **34**, 393.
54. M. Milutinovic, E. Suraniti, V. Studer, N. Mano, D. Manojlovic and N. Sojic, *Chem. Commun.*, 2011, **47**, 9125.
55. T. M. Downey and T. A. Nieman, *Anal. Chem.*, 1992, **64**, 261.
56. M. Richter, in *Electrogenerated Chemiluminescence*, CRC Press, 2004, pp. 301-358.
57. S. J. Woltman, W. R. Even and S. G. Weber, *Anal. Chem.*, 1999, **71**, 1504-1512.
58. A. Juris, V. Balzani, F. Barigelletti, S. Campagna, P. Belser and A. von Zelewsky, *Coord. Chem. Rev.*, 1988, **84**, 85-277.
59. K. K., *Coord. Chem. Rev.*, 1982, **46**, 159-244.
60. L. M. Moretto, T. Kohls, D. Badocco, P. Pastore, N. Sojic and P. Ugo, *J. Electroanal. Chem.*, 2010, **640**, 35.
61. L. M. Moretto, T. Kohls, A. Chovin, N. Sojic and P. Ugo, *Langmuir*, 2008, **24**, 6367.
62. P. Bertoncello, L. Dennany, R. J. Forster and P. R. Unwin, *Anal. Chem.*, 2007, **79**, 7549.
63. W.-Y. Lee, *Microchim. Acta*, 1997, **127**, 19.
64. I. Rubinstein and A. J. Bard, *J. Am. Chem. Soc.*, 1980, **102**, 6641.
65. H.-J. Li, S. Han, L.-Z. Hu and G.-B. Xu, *Chinese J. Anal. Chem.*, 2009, **37**, 1557.
66. F. Jameison, R. I. Sanchez, L. Dong, J. K. Leland, D. Yost and M. T. Martin, *Anal. Chem.*, 1996, **68**, 1298.
67. A. F. Martin and T. A. Nieman, *Anal. Chim. Acta*, 1993, **281**, 475.

68. J. Yuan, T. Li, X.-B. Yin, L. Guo, X. Jiang, W. Jin, X. Yang and E. Wang, *Anal. Chem.*, 2006, **78**, 2934.
69. M. Milutinovic, S. Sallard, D. Manojlovic, N. Mano and N. Sojic, *Bioelectrochem.*, 2011, **82**, 63.
70. H. Morita and M. Konishi, *Anal. Chem.*, 2003, **75**, 940.
71. J. Jin, M. Muroga, F. Takahashi and T. Nakamura, *Bioelectrochem.*, 2010, **79**, 147.
72. M. Zhou, J. Roovers, G. P. Robertson and C. P. Grover, *Anal. Chem.*, 2003, **75**, 6708-6717.
73. S. Sun, Y. Yang, F. Liu, Y. Pang, J. Fan, L. Sun and X. Peng, *Anal. Chem.*, 2009, **81**, 10227-10231.
74. M. Zhou and J. Roovers, *Macromolecules*, 2000, **34**, 244-252.
75. R. Y. Lai, M. Chiba, N. Kitamura and A. J. Bard, *Anal. Chem.*, 2001, **74**, 551.
76. B. D. Muegge and M. M. Richter, *Anal. Chem.*, 2001, **74**, 547.
77. M. Schmittel and H.-W. Lin, *Angew. Chem. Int. Edit.*, 2007, **46**, 893.
78. E. Berni, I. Gosse, D. Badocco, P. Pastore, N. Sojic and S. Pinet, *Chem. Eur. J.*, 2009, **15**, 5145.
79. F. Bolletta, A. Rossi and V. Balzani, *Inorg. Chim. Acta*, 1981, **53**, L23.
80. C. Creutz, M. Chou, T. L. Netzel, M. Okumura and N. Sutin, *J. Am. Chem. Soc.*, 1980, **102**, 1309.
81. I.-S. Shin, J. I. Kim, T.-H. Kwon, J.-I. Hong, J.-K. Lee and H. Kim, *J. Phys. Chem. C*, 2007, **111**, 2280.
82. D. Bruce and M. M. Richter, *Anal. Chem.*, 2002, **74**, 1340.
83. N. Myung, Z. Ding and A. J. Bard, *Nano Letters*, 2002, **2**, 1315.
84. B. Yoonjung and et al., *Nanotechnology*, 2006, **17**, 3791.
85. X. Liu, H. Jiang, J. Lei and H. Ju, *Anal. Chem.*, 2007, **79**, 8055.
86. A. W. Knight, *TrAC Trends Anal. Chem.*, 1999, **18**, 47.
87. X. Liu, L. Shi, W. Niu, H. Li and G. Xu, *Angew. Chem. Int. Edit.*, 2007, **46**, 421.
88. S. Fukuzumi, O. Inada and T. Suenobu, *J. Am. Chem. Soc.*, 2003, **125**, 4808.

89. J. Yuasa and S. Fukuzumi, *J. Am. Chem. Soc.*, 2006, **128**, 14281.
90. B. Sigal George, E. Glezer, J. Leland, J. Wohlstadter and J. Debad, in *Electrogenerated Chemiluminescence*, CRC Press, 2004, pp. 359-396.
91. J. Li, Q. Yan, Y. Gao and H. Ju, *Anal. Chem.*, 2006, **78**, 2694.
92. X. Zhao, T. You, J. Liu, X. Sun, J. Yan, X. Yang and E. Wang, *Electrophoresis*, 2004, **25**, 3422.
93. J. Yuan, H. Wei, W. Jin, X. Yang and E. Wang, *Electrophoresis*, 2006, **27**, 4047.
94. Y. Huang, W. Pan, M. Guo and S. Yao, *J. Chromatogr. A*, 2007, **1154**, 373.
95. H. Cui, F. Li, M.-J. Shi, Y.-Q. Pang and X.-Q. Lin, *Electroanal.*, 2005, **17**, 589.
96. W. Cao, J. P. Ferrance, J. Demas and J. P. Landers, *J. Am. Chem. Soc.*, 2006, **128**, 7572.
97. J. McCall, C. Alexander and M. M. Richter, *Anal. Chem.*, 1999, **71**, 2523.
98. F. Li, Y.-Q. Pang, X.-Q. Lin and H. Cui, *Talanta*, 2003, **59**, 627.
99. W. Miao and A. J. Bard, *Anal. Chem.*, 2004, **76**, 7109.
100. J. R. Phinney, J. F. Conroy, B. Hosticka, M. E. Power, J. P. Ferrance, J. P. Landers and P. M. Norris, *J. Non-Cryst. Solids*, 2004, **350**, 39.
101. W. Miao and A. J. Bard, *Anal. Chem.*, 2003, **75**, 5825.
102. N. C. Fawcett, R. D. Craven, P. Zhang and J. A. Evans, *Langmuir*, 2004, **20**, 6651.
103. F. López-Gallego, T. Montes, M. Fuentes, N. Alonso, V. Grazu, L. Betancor, J. M. Guisán and R. Fernández-Lafuente, *J. Biotechnol.*, 2005, **116**, 1.
104. X.-H. Xu, H. C. Yang, T. E. Mallouk and A. J. Bard, *J. Am. Chem. Soc.*, 1994, **116**, 8386.
105. N. Sardesai, S. Pan and J. Rusling, *Chem. Commun.*, 2009, 4968.
106. N. P. Sardesai, J. C. Barron and J. F. Rusling, *Anal. Chem.*, 2011, **83**, 6698.

~ ~ ~

## CHAPTER 2:

# NEW SENSING APPROACH BASED ON ELECTRODEPOSITED ECL REDOX POLYMER

~ ~ ~



The need to analyse a large number of analytes in very diverse samples leads to huge progress in the field of sensing in particular of biosensing. Sensors are widely used in clinical diagnostic, for monitoring in industrial and pharmaceutical processes, for environmental control such as food and water testing. They offer fast and reliable qualitative and/or quantitative information about a sample. Chemical sensor (here called sensor) can be defined as a device which responds to particular analyte in a selective way through a chemical reaction and can be used for the qualitative or quantitative determination of the analyte.<sup>1</sup> All sensors consist of detection element which is responsible for selective recognition of the analyte, transducer which converts an observed change (physical or chemical) into a measurable signal and a measuring device. If the recognition of analyte is based on a biochemical reaction, it is defined as a biosensor. Biosensor design is based on molecular recognition reactions including enzyme-substrate, receptor-ligand and antibody-antigen interactions.

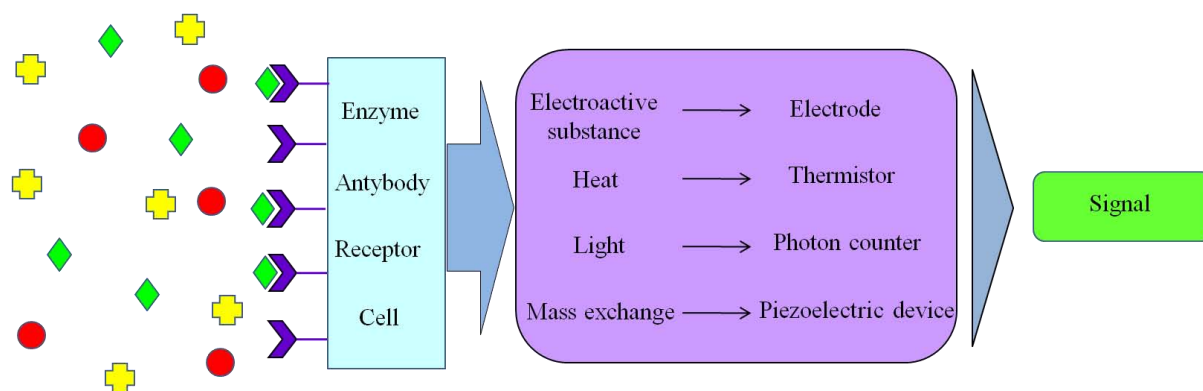


Figure 1. Principle of biosensors

ECL has an important role in the development of sensors. ECL provides high sensitivity and selectivity detection with wide linear dynamic range for numerous coreactants. For example, ruthenium polypyridyl complexes have been used to detect a wide range of analytes including oxalate,<sup>2</sup> alkylamines,<sup>3</sup> NADH,<sup>4, 5</sup> hydrazine,<sup>6, 7</sup> amino acids,<sup>8, 9</sup> biomolecules,<sup>10-12</sup> and a variety of pharmaceutical compounds.<sup>13, 14</sup>

Here we present a new sensing approach which employs ECL as readout mechanism based on an electrodeposited ECL exhibiting redox hydrogel. The approach is established on the type of enzymatic reactions in which  $\text{NAD}^+$  is transform to NADH that can be detected as an ECL coreactant.

As the immobilisation of ECL luminophore is the starting point to fabricate an ECL biosensor, in the first part of this chapter, we present already established methods for

immobilisation of a ruthenium containing hydrogel. In the second part of the chapter, electrochemical deposition of a Ru metallopolymer and its characterisation are presented. Finally, a new ECL sensing approach based on an electrodeposited redox hydrogel is reported.

## 2.1. IMMOBILISATION OF $\text{Ru}(\text{bpy})_3^{2+}$ AND ITS DERIVATIVES

As already described in Chapter 1,  $\text{Ru}(\text{bpy})_3^{2+}$  presents excellent electrochemical and luminescent properties and it is therefore the most used ECL luminophore.

There are several disadvantages to employ the ECL emitter in solution phase such as a loss of signal due to diffusion out of the detection zone and high consumption of reactants. Also the experimental design in systems such as FIA, CE and HPLC may be complex. Finally, the miniaturisation of the instrument is difficult.

To overcome these problems, a number of approaches have been reported to immobilise ruthenium complexes on the electrode surface such as immobilisation in polymer, in sol-gel films, in metallopolymer films, in Nafion Langmuir-Blodgett films, attaching to micro- or nanoparticles and covalent bonding to the substrate.

### 2.1.1. Immobilisation in cation exchange polymers

One of the first applied approaches for immobilisation of  $\text{Ru}(\text{bpy})_3^{2+}$  was the loading in the Nafion film.<sup>15, 16</sup> Nafion is perfluorinated, sulfonated ion-exchange polymer with very good chemical and mechanical stability. Therefore it was largely used for polymer modified electrodes. It shows also good ionic transport properties and selectivity for large hydrophobic cation such as  $\text{Ru}(\text{bpy})_3^{2+}$ .<sup>17</sup>  $\text{Ru}(\text{bpy})_3^{2+}$  is immobilised in Nafion by electrostatic binding.

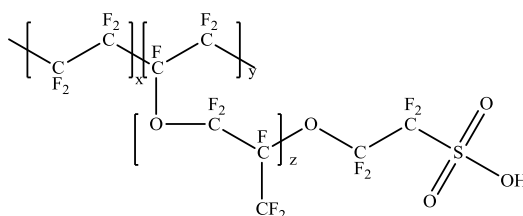


Figure 2. Nafion structure

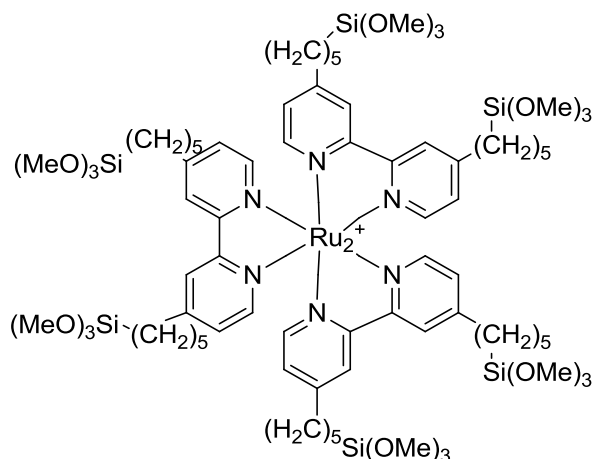
Immobilisation process may be realised either in two steps: a) forming the Nafion layer at the electrode surface and b) loading of Nafion film with  $\text{Ru}(\text{bpy})_3^{2+}$  or in a one step procedure

where Nafion and  $\text{Ru}(\text{bpy})_3^{2+}$  are both dissolved in ethanol solution and applied at the electrode. Because it was shown that films with a thickness of few micrometers have lengthy response-time due to the low diffusion constant and electron hopping, the fabrication of ultrathin Nafion films using Langmuir-Schaefer<sup>18</sup> and Langmuir-Blodgett<sup>19, 20</sup> techniques have been reported. In the last case, the homogeneity of LB films and its physico-chemical properties were studied by ECL measurements and epifluorescence imaging.  $\text{Ru}(\text{bpy})_3^{2+}$  immobilised in Nafion was applied in flow injection system for quantification of oxalate, alkyl amines and  $\text{NADH}^{21}$  and in biosensing of glucose, lactate and ethanol.<sup>22</sup>

Despite the advantages of a sensor based on immobilised  $\text{Ru}(\text{bpy})_3^{2+}$  in Nafion, its wide spread use is limited by the instability in the long term. When it is stored over night in buffer the ECL intensity decreases likely due to the result of  $\text{Ru}(\text{bpy})_3^{2+}$  partitioning into hydrophobic regions of Nafion.<sup>17</sup> Therefore,  $\text{Ru}(\text{bpy})_3^{2+}$  sensors should be prepared daily.

### 2.1.2. Immobilisation in Silica Sol-Gel films

In order to improve stability of  $\text{Ru}(\text{bpy})_3^{2+}$  based sensors, other approaches of  $\text{Ru}(\text{bpy})_3^{2+}$  immobilisation have been developed such as immobilisation in silica sol-gel films. Typically, silica sol-gels are prepared via the acid-catalysed hydrolysis of tetramethoxysilane (TMOS) or tetraethoxysilane (TEOS) in the presence of  $\text{Ru}(\text{bpy})_3^{2+}$  which is entrapped in the matrix after the gelation.  $\text{Ru}(\text{bpy})_3^{2+}$  and TPrA were trapped in porous silicate host matrix providing high optical quality, good photochemical and electrochemical stability.<sup>23</sup> An important requirement is that the ECL gel-entrapped chemiluminescent precursors are able to diffuse and react in the gel on the local scale. Depending on the procedure the thickness of silica film can be extremely thin (~200 nm) which allows rapid diffusion of the complex molecule towards and from the electrode surface together with a rapid permeation of the analyte from the external solution.  $\text{Ru}(\text{bpy})_3^{2+}$  can be also covalently incorporated in the silica. For example, functionalised  $\text{Ru}(\text{bpy}')_3^{2+}$  has been reported with polymerisable trimethoxysilyl end groups -  $\text{Si}(\text{OMe})_3$  on each bipyridine ligand. When the solution of this complex in the mixed solvent isopropanol-methanol (1:1) was spin-coated at the surface of ITO electrode, the gelation was initiated at ambient temperature and completed after curing at 170°C. This leads to the formation of  $\text{Ru}(\text{bpy}')_3^{2+}$  gel film which was used to develop stable and sensitive ECL sensors.<sup>24</sup>

Figure 3.  $\text{Ru}(\text{bpy}')_3\text{Cl}_2$  structure

### 2.1.3. Immobilisation in nanoparticle composite film

The system for immobilisation of  $\text{Ru}(\text{bpy})_3^{2+}$  in nanoparticle composite films usually consists of polymers which present a carrier in the system and nanoparticles that can play different roles. For example,  $\text{Ru}(\text{bpy})_3^{2+}$ -doped silica nanoparticles present the carrier of ECL luminophore and it can be selectively immobilised on the electrode surface by electrodeposition of chitosan.<sup>25</sup> Chitosan is an amine-rich polysaccharide derived by deacetylation of chitin. In a solution with a pH value lower than its pKa, most of the amino groups are protonated and positively charged making chitosan soluble in aqueous solutions. At pH higher than pKa the amine groups becomes deprotonated and uncharged thus making chitosan insoluble in water. Therefore, when protons are consumed at cathode electrode, pH near the electrode surface increases leading to the precipitation of the chitosan on the electrode surface. Thus,  $\text{Ru}(\text{bpy})_3^{2+}$ -doped silica nanoparticles which bound with chitosan by H-bonding interaction is immobilised on the electrode along with it. ECL sensors based on this composite film modified electrode show excellent reproducibility, stability and sensitivity for the detection of TPrA.<sup>25</sup> In another example, partially sulfonated polystyrene (PSP) was used as ion-exchange polymer for immobilisation of  $\text{Ru}(\text{bpy})_3^{2+}$  with introduction of carbon nanotubes (CNTs).<sup>26</sup> In this case CNTs has a double role, as conducting pathway to accelerate the electron transfer and as a proper matrix to immobilise  $\text{Ru}(\text{bpy})_3^{2+}$  on the electrode by hydrophobic interactions.

#### 2.1.4. Immobilisation in self assembled monolayer

ECL generated by a monolayer of emitter molecules confined to the surface of electrode has also been reported.<sup>27-29</sup> Self-assembly of a monolayer involves the spontaneous coordinated action of independent building blocks to create a superstructure. Dennany et al. reported the monolayer formation of  $[\text{Ru}(\text{bpy})_2\text{dcb}]\text{Cl}_2$  (dcb: 4,40-dicarboxy-2,20-bipyridine) on ITO electrode.<sup>27</sup> The ability of such a complex to form stable monolayers enables its utilisation for the detection of oxalate and several amino acids, producing significant ECL. Interestingly, proline and hydroxy-proline were the most efficient species for generating ECL. The ECL intensity varied linearly in the range 0.2-1 nM and 1–10 nM for proline and hydroxy-proline, respectively.

The well-known affinity of thiols for metals such as gold, platinum, silver and mercury allowed strong chemisorption of this complex giving as a result a stable modified electrode. Bertoncello et al. reported the synthesis of a new surface-active Ru(II) complex,  $[\text{Ru}(\text{bpy})_2(\text{bpySH})]^{2+}$ , denoted RuBpySH.<sup>30</sup> Stable monolayers of RuBpySH, have been formed on micro and macro platinum electrodes by spontaneous adsorption.

Metallopolymer films were also immobilised by adsorption on electrode surface. Dennany, Forster and Rusling reported direct ECL detection of DNA in 10 nm-thick films of cationic polymer  $[\text{Ru}(\text{bpy})_2(\text{PVP})_{10}]^{2+}$  assembled layer-by-layer with DNA.<sup>31</sup> This metallopolymer was applied for detection of DNA hybridization or DNA damage. The same ruthenium metallopolymer was previously used for detection of oxalate in flow injection analysis system.<sup>32</sup>

The same group of researchers also reported that ECL can be obtained directly from the reaction of oxidised guanines in DNA in thin films with the catalytic metallopolymer  $[\text{Os}(\text{bpy})_2(\text{PVP})_{10}]^{2+}$ .<sup>33</sup>

The combination of ruthenium  $[\text{Ru}(\text{bpy})_2(\text{PVP})_{10}]^{2+}$  and osmium  $[\text{Os}(\text{bpy})_2(\text{PVP})_{10}]^{2+}$  metallopolymers in the films can allow applications to the simultaneous detection of chemical and oxidative DNA damage.<sup>33</sup>

#### 2.1.5. Covalent attachment of the luminophore

One convenient way to immobilise an ECL complex is the covalent attachment to the electrode surface. Namely, the new revisited route of ECL mechanism was studied in a (SECM)-ECL experiment where ruthenium centers were covalently immobilized on the substrate.<sup>34</sup> The ITO electrode was first functionalized with  $(\text{CH}_3\text{O})_3\text{-Si}(\text{CH}_2)_3\text{NH}_2$  by

formation of ITO/O-Si(CH<sub>2</sub>)<sub>3</sub>-NH<sub>2</sub> bonds and then incubated with Ru(bpy)<sub>2</sub>[bpy(COOH)<sub>2</sub>]<sup>2+</sup>. By this treatment, a layer of Ru(bpy)<sub>2</sub>[bpy(COOH)<sub>2</sub>]<sup>2+</sup> was covalently attached to the aminosilane formed previously on the ITO.<sup>34</sup> The similar process has been reported for Ru(bpy)<sub>3</sub><sup>2+</sup> attachment to the microspheres thanks to the reaction between carboxylate beads and Ru(bpy)<sub>3</sub><sup>2+</sup>-NH<sub>2</sub>.<sup>35</sup>

## 2.2. ELECTRODEPOSITION OF [POLY(4-VINYLPYRIDINE)-RU(2,2'-BIPYRIDINE)<sub>2</sub>Cl]<sup>+2+</sup>

The main advantage of using a metallopolymer over a lot of other immobilisation methods is that luminescent ruthenium complex is covalently attached to the preformed polymer backbone. This leads to stable films over a wide range of solution compositions and in flowing streams. Since the ruthenium complexes are covalently attached they cannot leak out of the assembly.

In our case we were using a ruthenium containing metallopolymer [poly(4-vinylpyridine)-Ru(2,2'-bipyridine)<sub>2</sub>Cl]<sup>+2+</sup> denoted PVP-Ru(bpy)<sub>2</sub><sup>2+</sup>.

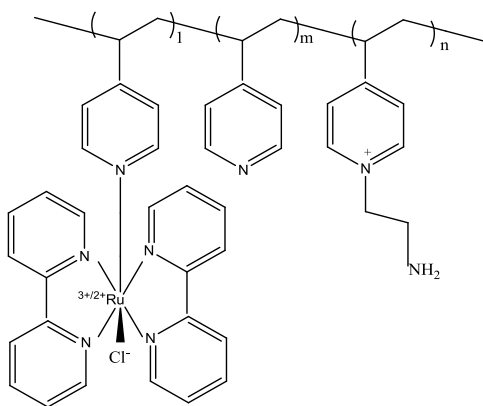


Figure 4. [poly(4-vinylpyridine)-Ru(2,2'-bipyridine)<sub>2</sub>Cl]<sup>+2+</sup> (PVP-Ru(bpy)<sub>2</sub><sup>2+</sup>)

The synthesis and electrodeposition of this metallopolymer was chosen regarding the properties of similar redox hydrogels. Namely, Gao et al. reported the synthesis of a series of osmium metallopolymers.<sup>36</sup> The osmium centres were surrounded with two bipyridyl ligands, different polymer backbones coordinated to the osmium centre and one chloro-ligand, similarly to the structure of PVP-Ru(bpy)<sub>2</sub><sup>2+</sup>. The electrodeposition of the metallopolymers was performed by cycling the polymer solution between -150 and +150 mV vs. the polymer's redox potential. Transition metal ions exchange ligands when electroreduced and/or electrooxidised, thus chloride, a weakly coordinating anionic ligand, is exchanged when Os<sup>3+</sup>

is electroreduced to  $\text{Os}^{2+}$ . Consequently, initially reversibly adsorbed water-soluble redox polymers were electrodeposited forming crosslinked irreversibly immobilized redox hydrogel. Redox hydrogels are electron-conducting. Although, in theory, electrons could also propagate by hopping between fixed position-redox centres, hopping from trap to trap is rarely seen in the hydrogels. If hopping is dominant, hydration and swelling, which increases the distance between the redox centers, will decrease the electronic conductivity. In hydrogels, the swelling enhances the electronic conductivity, because it free segments of the dehydrated redox polymer to move short, but finite, distances. Such a movement allows electron transferring collisions between segments that in the rigid, dehydrated matrix are too far apart for the electrons to traverse by tunneling.<sup>37</sup> The benefit of electron-conducting in redox hydrogel is to electrically connect the redox centers of enzymes to electrodes. It was reported that  $\text{Ru}^{2+}$  complexes containing labile ligands are readily bound to proteins by exchanging their labile ligand with a protein-bound histidine. Also, it was shown that  $\text{Os}^{2+}$  complexes can be coordinated with histidine, lysine, and arginine functions. Thus, enzymes can be co-electrodeposited with redox polymer. In our case we switched the metal center from  $\text{Os}^{2+}$  to  $\text{Ru}^{2+}$  to obtain a redox polymer for enzyme based detection which employs ECL as readout mechanism. The synthesis of  $\text{PVP-Ru}(\text{bpy})_2^{2+}$  has already been reported.<sup>38</sup> The electrodeposited ruthenium-containing redox hydrogel shows electrochemical and ECL properties required for sensing elements. The ECL intensity showed linear dependence on TPrA concentration in the range between 100 nM to 100  $\mu\text{M}$ . The aim of this work was to develop a new sensing approach based on electrodeposited  $\text{PVP-Ru}(\text{bpy})_2^{2+}$ .

### **2.2.1. Electrochemical immobilisation of $\text{PVP-Ru}(\text{bpy})_2^{2+}$ on the electrode surface**

The electrode modification was carried out in a three-electrode electrochemical cell with glassy carbon or home-made graphite electrode as working electrode.  $\text{Ag/AgCl/KCl}$  3 M saturated electrode and a platinum wire were used as reference and counter electrodes, respectively. Both types of electrodes were plasma pre-oxidised (oxygen or air, 0.5 Torr, 10 min). This treatment leads to structural and surface chemistry modification of carbon surface, creating microporosity of the surface and addition of carboxyl and phenolate functions<sup>39-41</sup> which allows better electrodeposition of  $\text{PVP-Ru}(\text{bpy})_2^{2+}$  at the electrode surface. Because of small amount of synthesised  $\text{PVP-Ru}(\text{bpy})_2^{2+}$  the whole process was realised in a drop.

PBS solution containing 0.95 mg/mL of PVP-Ru(bpy)<sub>2</sub><sup>2+</sup> were cycled between +0.2 V and +1.1 V vs. Ag/AgCl/KCl. The electrodeposition of PVP-Ru(bpy)<sub>2</sub><sup>2+</sup> is based on ligand exchange. It is known that transition metal ions exchange ligands during electroreduction or electrooxidation.<sup>5, 36</sup> PVP-Ru(bpy)<sub>2</sub><sup>2+</sup> contains un-coordinated backbone pyridines partially quaternised with bromoethylamine for solubility in water and for swelling to a hydrogel after cross-linking. The polymer is electroadsorbed in anodic half of the potential cycle when chloride, a weakly coordinated ligand is exchanged by primary amines or by pyridines of neighbouring polymer chains causing coordinative cross-linking and leading to irreversible electrodeposition of the hydrated redox polymer.

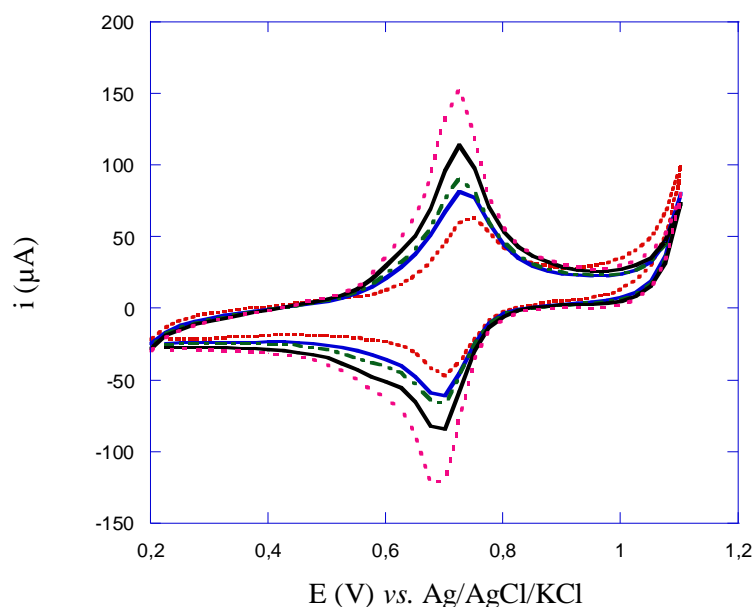


Figure 5. Sequential cyclic voltammograms recorded during the electrodeposition of the hydrogel film at a GC electrode after 10, 100, 200, 300, and 400 scans. (Scan rate = 100 mV/s) The is composed of 0.95 mg/mL of PVP-Ru(bpy)<sub>2</sub><sup>2+</sup> in 10 mM phosphate buffer.

The advantage of electrodeposition of the metalopolymer over the simple adsorption<sup>31, 32</sup> is that thickness of polymer film and thus the amount of luminescent ruthenium centres can be controlled by changing the number of scans. On figure 5 are presented voltammetric curves during the electrodeposition. Intensity of current response increases with number of scans which indicates an increasing amount of Ru centres on the electrode surface. ECL response of the films immobilised during different number of scans from 100 to 500 was compared. Figure 6 presents overlapped ECL curves obtained for hydrogel electrodeposited during 200, 400 and



500 scans in the presence of NADH as ECL coreactant. With increasing the number of scans, the ECL response of the hydrogel film increases up to 400 scans while with further increase of scan numbers the ECL response decreases. This may be explained by two aspects. From one side, with the increasing of scan number the thickness of the hydrogel film increases. Even if the hydrogel is permeable to water soluble compounds, the diffusion of the coreactant can be limited and further increase of film thickness may reduce the coreactant penetration. On other hand, thicker films on the electrode surface increase the amount of ruthenium centres which can cause self-quenching and thus a decrease of ECL signal. As the highest ECL signal is obtained for the film obtained after 400 cycles, the same number of scans was used for electrode modification in further experiments.

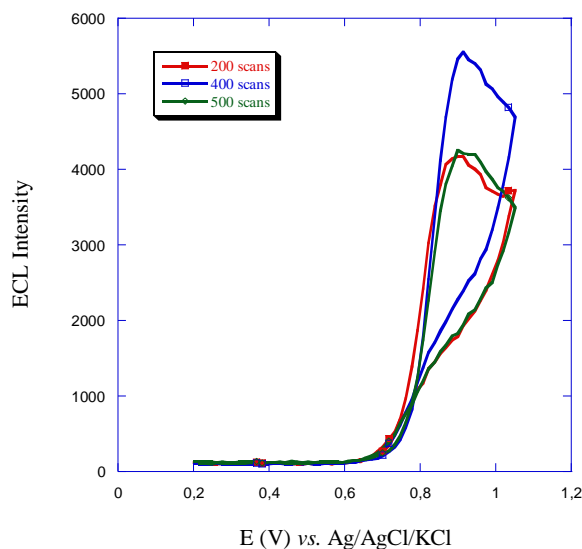


Figure 6. ECL response of electrodeposited polymer films obtained by 200, 400 and 500 cyclic voltammetry scans in 10 mM NADH in 100 mM phosphate buffer, scan rate 30 mV/s

### 2.2.2. Characterisation of the electrodeposited redox hydrogel

The electrode surface modified with hydrogel film was characterised by SEM. It is observed that the electrodeposited hydrogel forms a uniform film over the entire electrode surface (Figure 7). The SEM pictures were recorded with the film in dried state which explains the cracks observed in Figure 7. At higher magnification (Figure 7B) the thickness of the film is clearly visible. The film presented in Figure 7 was electrodeposited by applying 400 scans and its thickness is 14  $\mu\text{m}$ . It is important to emphasize that both the structure and the thickness of the film are different in a swelling state in aqueous solution.

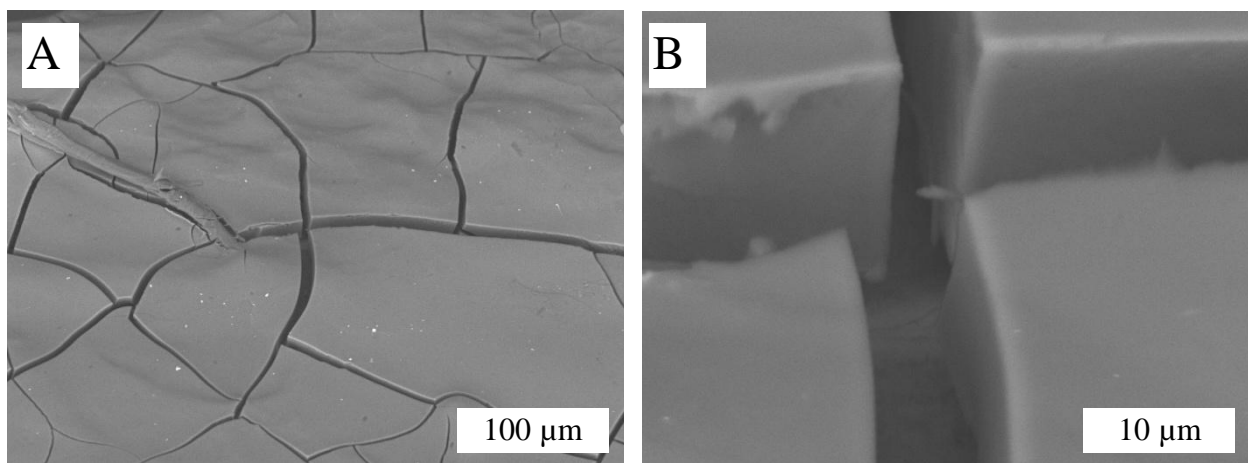


Figure 7. SEM images of the hydrogel film in the dried state on the electrode surface at different magnification. At higher magnification (B) one can observe the thickness of the hydrogel film.

Once the redox polymer is electrodeposited on the electrode surface it is necessary to test the electrochemical and ECL properties of immobilised film. Cyclic voltammetry is the most used method for electrochemical studies of the system. It can give the “electrochemical spectrum” which can indicate oxidation or reduction potential of the species, the presence of homogeneous reactions in the final electrochemical process, adsorption of electrochemically reactive species and similar information about the system.<sup>42</sup> Electrochemical characterisation of immobilised hydrogel was performed by cycling between +0.2 V and +1.05 V with a scan rate of 10 mV/s in PBS. Figure 8A (solid line) shows the electrochemical characterization of the hydrogel. The peak current in anodic half of cycle corresponds to oxidation of hydrogel's  $\text{Ru}^{2+}$  centres while the reversible peak in cathodic half corresponds to its reduction from  $\text{Ru}^{3+}$  state. The midpoint potential observed at +0.72 V vs. Ag/AgCl/KCl is similar to previously report value.<sup>38</sup> It is important to notice that oxidation of the immobilised  $\text{PVP-Ru}(\text{bpy})_2^{2+}$  occurs at much less anodic potential than  $\text{Ru}(\text{bpy})_3^{2+}$ <sup>43, 44</sup> which can be advantageous for use in biorelated systems. The shape of the cyclic voltammogram and the small separation between oxidation and reduction peaks ( $\Delta E_p \sim 20$  mV) indicates that the polymer is surface-confined.

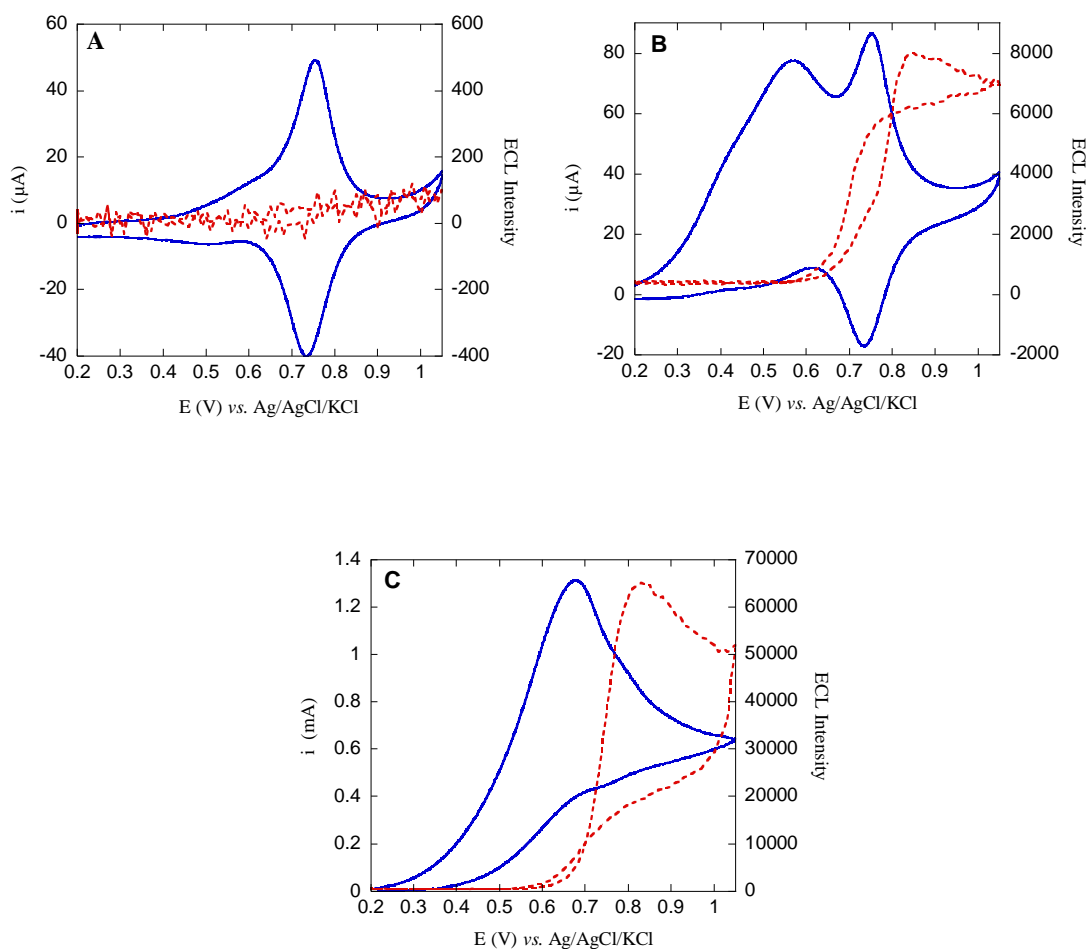


Figure 8. Cyclic voltammograms (blue line) and ECL curves (red dashed line) of the electrodeposited film in PBS solution (pH = 7.4) containing various concentrations of NADH: A) 0 mM NADH; B) 2 mM and C) 50 mM. Scan rate  $\nu = 10$  mV/s

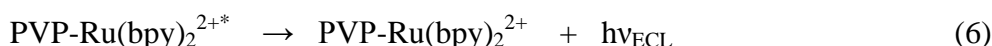
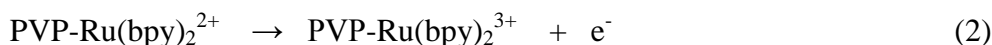
The enzymatic sensing approach described here is based on the enzymatic reaction in which  $\text{NAD}^+$  is transformed to NADH. For this reason, the ECL response of immobilised hydrogel was studied using NADH like coreactant.

Figure 8 presents the overlap of cyclic voltammograms with ECL curves obtained in the same experiment. In the absence of NADH (Figure 8A; red line) no light is emitted. When NADH is added to the PBS solution (Figures 8B and 8C) both voltammetric signal (blue line) and the ECL intensity (red dashed line) change progressively. Another irreversible oxidation wave appears before the redox wave of the ruthenium hydrogel which is still present. This wave peaking at 0.6 V vs. Ag/AgCl/KCl increases progressively with the NADH concentration as expected.<sup>45</sup> Both waves are well-separated up to a 2 mM concentration of NADH. At higher concentration the measured current corresponds to a convolution of both depending on the

respective concentration of the bulk and surface confined species. The first wave was assigned to the irreversible oxidation of NADH.<sup>45,46</sup>

An ECL signal is observed by adding NADH to PBS solution (Figure 8B-C) where it can be seen that ECL intensity increases with increasing the NADH concentration. It is important to notice that no ECL emission occurs at potential where only oxidation of NADH occurs ( $< 0.6 - 0.7$  V vs. Ag/AgCl/KCl). ECL is generated only at sufficiently anodic potentials where hydrogel's Ru<sup>2+</sup> centres are oxidised. So it means that a similar "revisited route" as for tri-n-propylamine does not occur for the NADH ECL.<sup>34</sup> In the present case, ECL clearly involves reaction between both intermediate species<sup>5</sup> formed upon oxidation of NADH (1<sup>st</sup> oxidative wave) and hydrogel's Ru<sup>3+</sup> centres (2<sup>nd</sup> wave).

Based on the electrochemical and ECL results that we obtained, we describe the ECL process by the following reaction scheme where an oxidative-reductive sequence occurs.<sup>47</sup>



NADH and PVP-Ru(bpy)<sub>2</sub><sup>2+</sup> are oxidised at their respective potentials. NADH can also be oxidised catalytically by PVP-Ru(bpy)<sub>2</sub><sup>3+</sup>, even if this step is not very efficient on the basis of the cyclic voltammograms (Figure 8). Then the radical cation NADH<sup>•+</sup> deprotonates to form a highly reducing species NAD<sup>•</sup> (reaction 4). This reaction scheme is similar to the deprotonation of the cation radical when tri-n-propylamine is the coreactant.<sup>48</sup>

The reaction with PVP-Ru(bpy)<sub>2</sub><sup>3+</sup> leads to the excited state. The homogeneous electron-transfer reaction between PVP-Ru(bpy)<sub>2</sub><sup>3+</sup> and NAD<sup>•</sup> (reaction 5) is exergonic enough to generate excited state of the hydrogel's Ru<sup>2+\*</sup> centres. Eventually PVP-Ru(bpy)<sub>2</sub><sup>2+\*</sup> returns to the ground state emitting a photon.

The ECL emission spectrum of the hydrogel was investigated in the presence of TPrA as coreactant. As the emission wavelength depends only on luminophore and not on the used coreactant, the spectrum is the same with NADH. The TPrA was chosen because it gives higher ECL intensity which improves the quality of the spectrum. The experimental setup was similar as for ECL experiments except that photomultiplier tube was replaced by optical fibre input of the spectrograph. The spectra were recorded by applying constant step potential of 1.2 V vs. Ag/AgCl/KCl during the acquisition.

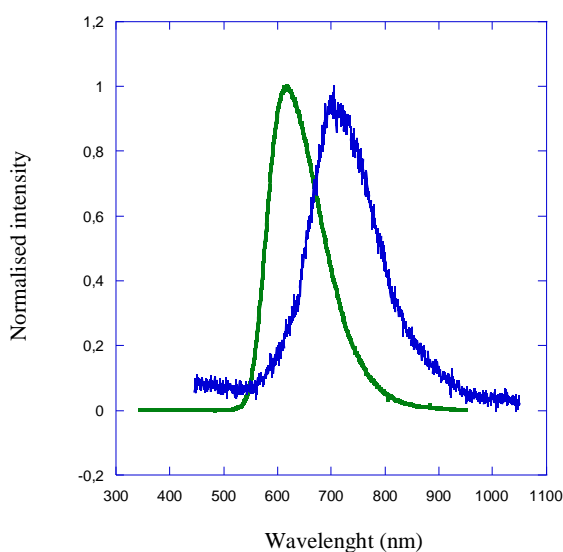


Figure.9. ECL spectra of dissolved  $\text{Ru}(\text{bpy})_3^{2+}$  (green line) and electrodeposited PVP- $\text{Ru}(\text{bpy})_2^{2+}$  hydrogel (blue line), GC electrode in 10 mM TPrA, potential step +1.2 V vs. Ag/AgCl/KCl

On figure 9 the ECL spectra of PVP- $\text{Ru}(\text{bpy})_2^{2+}$  and  $\text{Ru}(\text{bpy})_3^{2+}$  are compared. The PVP- $\text{Ru}(\text{bpy})_2^{2+}$  was electrodeposited on the surface of GC electrode and spectrum was obtained with 10 mM TPrA. The  $\text{Ru}(\text{bpy})_3^{2+}$  was in solution in the presence of TPrA and the spectrum was obtained using bare GC electrode. It can be noticed that ECL spectrum of PVP- $\text{Ru}(\text{bpy})_2^{2+}$  peaking at 700 nm is red shifted comparing to the spectrum of  $\text{Ru}(\text{bpy})_3^{2+}$ . This is in agreement with lower MLCT transition state in PVP- $\text{Ru}(\text{bpy})_2^{2+}$  due to presence of one chloro ligand instead of pyridine. Namely, the initial structure of the metallopolymer contains five pyridine and one chloro ligand. During the electrodeposition chloride ligand has been exchanged by more strongly coordinating primary amines or by pyridines of neighbouring polymer chains changing the MLCT of the complex. Even the ligand exchange occurs

allowing immobilisation of the polymer on the electrode surface, for some similar complexes it was estimated that only 5 - 10 % of the label  $\text{Cl}^-$  ions of the Ru complex were exchanged by primary amines or by pyridines ligands.<sup>36</sup> Thus the ECL spectrum of immobilised hydrogel has higher contribution of non ligand-exchanged  $\text{PVP-Ru}(\text{bpy})_2^{2+}$  emission than of exchanged  $\text{PVP-Ru}(\text{bpy})_2^{2+}$ .

To test the sensitivity of this system, a calibration curve has been constructed. Figure 10 displays the dependence of the ECL intensity on the NADH concentration in the 100 nM to 50 mM range. The detection limit is 100 nM. The intensity increases linearly with the NADH concentration and the correlation coefficient is 0.999 in a linear plot.

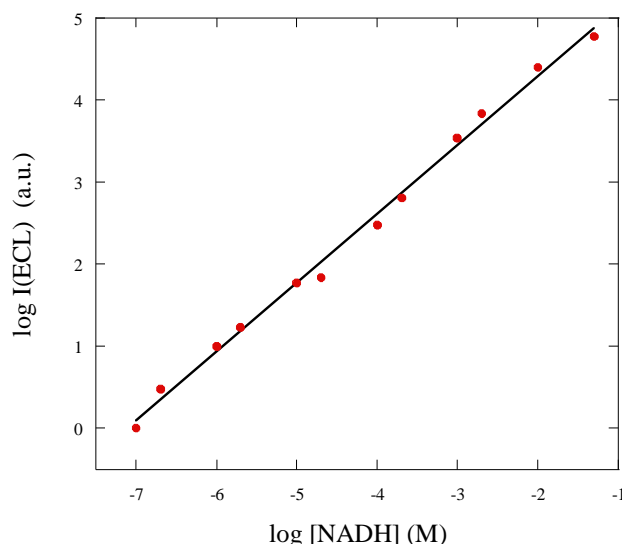


Figure 10. Dependence of the ECL intensity (a.u.) on the NADH concentration (M)

Considering the obtained calibration curve, the linear dependence of ECL signal on the concentration of NADH and the wide dynamic range of detection with very low detection limit, we conclude that immobilized hydrogel possesses all properties to be applied in a detection system.

### 2.3. GLUCOSE SENSING

The use of enzymes as the biological recognition element was very popular in the development of biosensors due to their commercial availability or ease of isolation and purification from different sources.<sup>49</sup> Because of its simplified set-up, low background signal,

and high sensitivity, ECL has received considerable attention in enzyme sensor design. The time and position control present a unique advantage of ECL because the light emission can be delayed until enzyme-catalysed reactions have taken place.<sup>43</sup> Although various ECL enzyme biosensors have been developed, many analytes are commonly quantified by coupling them to enzyme systems that either utilized  $\beta$ -nicotinamide adenine co-factors or produced  $\text{H}_2\text{O}_2$ . The developed enzyme based biosensors can be classified in different types. The luminol-based enzymes ECL systems are mainly based on the detection of hydrogen peroxide (Figure 11).

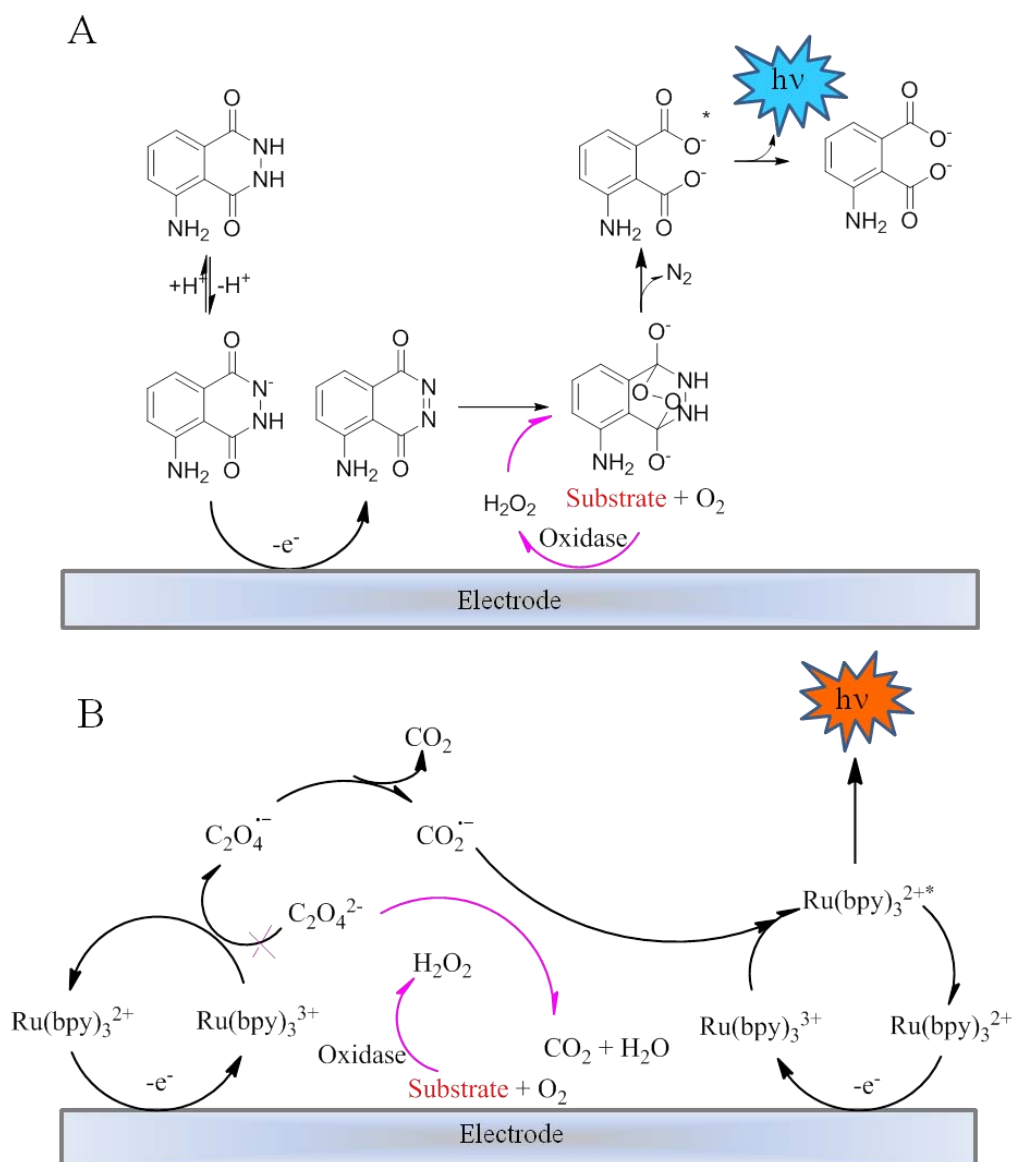


Figure 11. A) Luminol-based ECL reaction mechanism; B)  $\text{Ru}(\text{bpy})_3^{2+}/\text{oxalate}$  -based ECL mechanism for detection  $\text{H}_2\text{O}_2$  generating oxidase substrates

In an alkaline or neutral medium, luminol is electrochemically oxidized. In the presence of hydrogen peroxide ( $\text{H}_2\text{O}_2$ ), the diazo compound undergoes further oxidation to produce the

excited state of 3-aminophthalate. The excited state then goes back to its ground state and gives the emission at 425 nm.  $\text{H}_2\text{O}_2$  participates in this ECL reaction in the form of the peroxide anion  $\text{HOO}^-$  or an electrochemically formed superoxide radical  $\text{O}_2^{\cdot-}$ . Because many enzymes can produce  $\text{H}_2\text{O}_2$  during their substrate-specific enzymatic reaction, ECL enzymatic biosensors are made possible by coupling the luminol light-emitting reaction with enzyme-catalyzed reactions generating  $\text{H}_2\text{O}_2$ .<sup>49</sup> Hydrogen peroxide can be detected also by enzyme ECL biosensor based on  $\text{Ru}(\text{bpy})_3^{2+}$ /oxalate system.<sup>49</sup> The reaction between oxalate and  $\text{H}_2\text{O}_2$  lead to the production of  $\text{H}_2\text{O}$  and  $\text{CO}_2$  which decreases of ECL emission.<sup>2</sup>

The principle of a biosensor for the detection of NADH is presented in figure 12. Both NADH and  $\text{Ru}(\text{bpy})_3^{2+}$  are oxidised on the electrode surface. The radical cation  $\text{NADH}^{\cdot+}$  loses a proton forming highly reductive agent  $\text{NAD}^{\cdot}$ , which reduces  $\text{Ru}(\text{bpy})_3^{3+}$  to form the excited state. Most of the  $\text{Ru}(\text{bpy})_3^{2+}$ /NADH systems in enzyme-based biosensors involve dehydrogenase-type enzymes. In dehydrogenase-type enzyme-catalyzed reactions, the addition of  $\text{NAD}^+$  is required as a cofactor for the enzymatic reaction. Under substrate oxidation,  $\text{NAD}^+$  is simultaneously reduced to NADH. Numerous examples of dehydrogenase-based ECL detection have been reported such systems based on alcohol dehydrogenase<sup>50-53</sup> and glucose dehydrogenase.<sup>22, 54</sup>

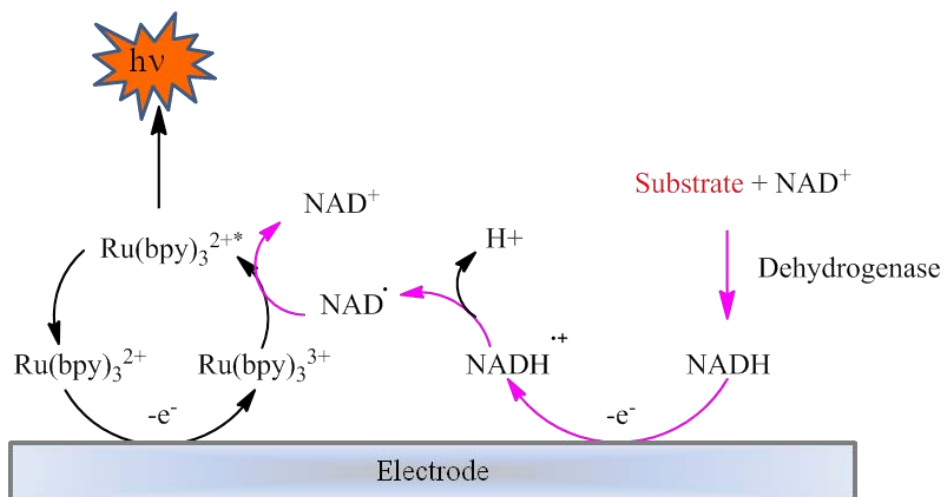


Figure 12.  $\text{Ru}(\text{bpy})_3^{2+}$ -based ECL mechanism for detection of  $\text{NAD}^+$ -dehydrogenase substrates

Here we present a new sensing approach based on ECL in an electrodeposited redox hydrogel using glucose dehydrogenase (GDH) as a model system.



The solution was consisting of GDH and  $\text{NAD}^+$  in PBS. Without glucose no ECL signal is detectable.

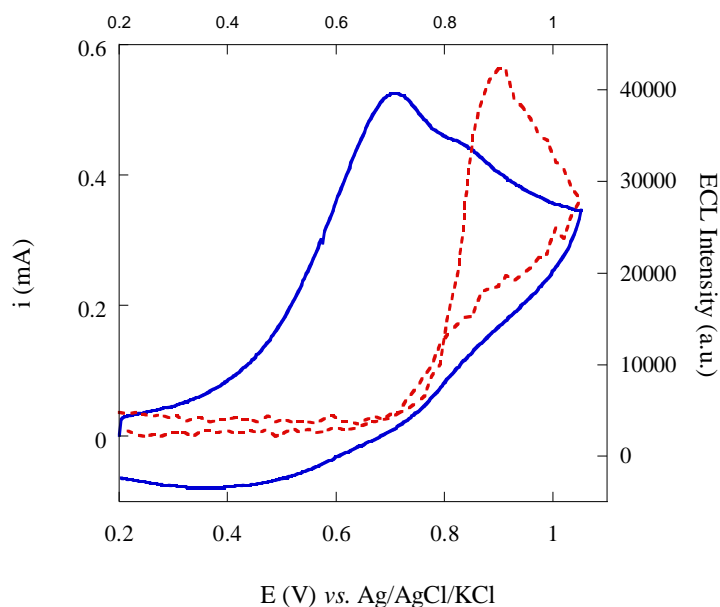


Figure 13. Cyclic voltammogram (blue line) and ECL emission (red dashed line) of the film electrodeposited for 400 scans. The solution consists of GDH, 10 mM  $\text{NAD}^+$  and 10 mM glucose in PBS. (Scan rate  $\nu = 30$  mV/s)

Figure 13 shows the voltammetric response and the ECL signal of the modified electrode when coupled to the GDH enzymatic reaction. When  $\text{NAD}^+$  is in solution, no ECL is generated until glucose is added. Then GDH oxidizes its substrate and reduces  $\text{NAD}^+$  to NADH. The enzymatically generated NADH is oxidized at the electrode surface and reacts with hydrogel's  $\text{Ru}^{2+}$  centers. This leads to the ECL emission in the hydrogel film. ECL light is therefore electrocatalytically generated in presence of the enzyme and of the substrate. It is interesting to notice that classically the luminophore is regenerated during the ECL process, whereas the coreactant is consumed by the electrochemical reactions. But using NADH as a coreactant, the ECL-active form of the coreactant is regenerated by the enzymatic reaction.

In order to optimise working conditions, the influence of the pH has been studied. It was found that ECL intensity is highly dependent on the pH. From pH 6 to 7, the ECL signal increases linearly and the highest intensity is recorded at pH 7.5. At more alkaline pH, the response decreases rapidly. This behavior may be attributed to the degradation of  $\text{NAD}^+$  known to be unstable in alkaline solution<sup>50</sup> but also to a decrease of the enzyme activity out of optimal pH range. Therefore pH 7.5 was used in all further experiments.

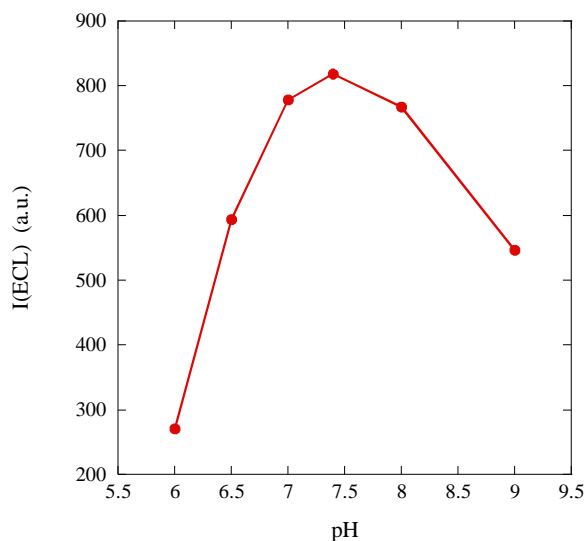


Figure 14. Effect of pH on ECL intensity in PBS solution of GDH, 10 mM  $\text{NAD}^+$  and 30 mM glucose. Scan rate  $v = 30$  mV/s.

The thickness of the immobilised film is an important parameter. Immobilised hydrogel undergoes water swelling and it is permeable to water soluble chemical and biochemicals. By increasing the film thickness, the amount of Ru centres confined to electrode surface increases but also electron transfer and mass transfer may be slower. The convenience of electrodeposition is that by varying the number of scans the thickness of electrodeposited hydrogel can be controlled. It is important to emphasize that the film thickness was measured by SEM so the hydrogel films were in a dry state. When applying 50 scans, the film thickness was  $0.9 \mu\text{m}$ . After 200 and 400 scans, it increases to  $2 \mu\text{m}$  and  $14 \mu\text{m}$ , respectively. But with 500 scans, we measured also a film thickness of  $14 \mu\text{m}$ . Since the highest ECL signal was measured with the films prepared after 400 scans, we selected such parameter for all further experiments.

The capability to use the immobilised hydrogel for ECL detection of glucose was verified for different glucose concentrations.

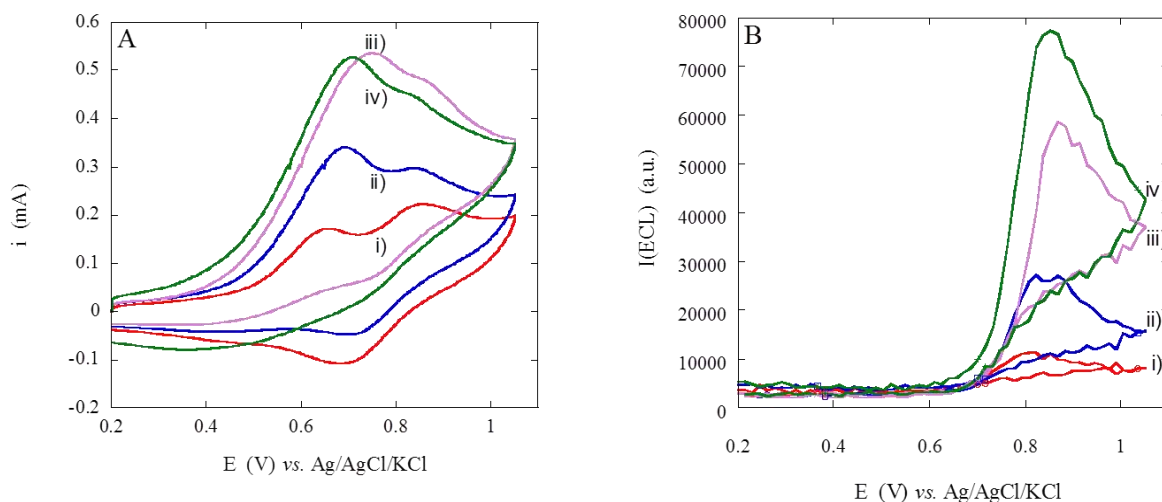


Figure 15. Cyclic voltammograms A) and ECL signals B) of the electrodeposited film in PBS solution of GDH, 10 mM  $\text{NAD}^+$  and different glucose concentrations: i) 1, ii) 5, iii) 20 and iv) 30 mM. pH 7.5. Scan rate  $v = 30$  mV/s.

Figure 15A shows the cyclic voltammograms in presence of increasing glucose concentration on an electrode modified with the hydrogel film by applying 400 scans. We observed a similar electrochemical behavior in comparison to Figure 8B-C. At low glucose concentrations, two oxidation waves appeared. Then they were progressively convoluted to a single wave corresponding to the oxidation of NADH and of  $\text{PVP-Ru}(\text{bpy})_2^{2+}$  centers.

In the same experimental configuration, ECL signals were recorded on the modified electrode. The results are presented on Figure 15B. The onset of ECL occurred near 0.7 V. There was a slight shift of the ECL wave when increasing the glucose concentration. This is probably related to the coupled enzymatic process between glucose and  $\text{NAD}^+$  with ECL reaction. The peak of the ECL intensity is located at 0.85 V for the glucose detection. It is a much lower anodic potential compared to the model  $\text{Ru}(\text{bpy})_3^{2+}$  complex immobilized on different substrates.<sup>51, 52</sup> In this later case for enzymatic measurements, ECL is generated at 1.1-1.2 V so it requires a higher anodic potential.<sup>51, 52</sup> This is an important advantage since the measurements performed with the ECL hydrogel would be less sensitive to interfering species in real samples.

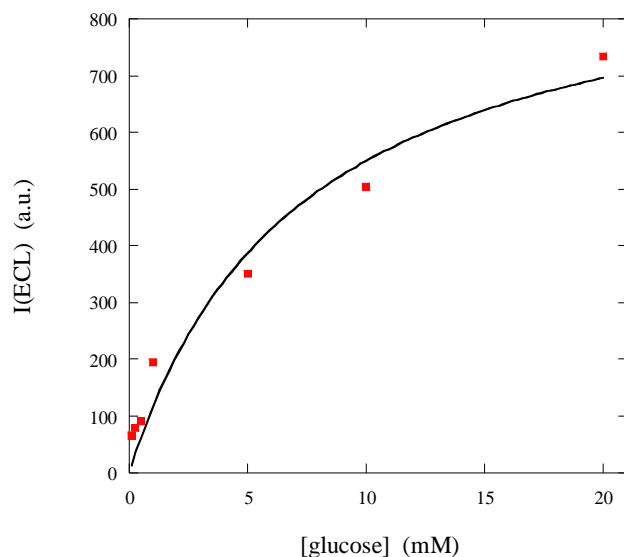


Figure 16. Dependence of the ECL signal on the glucose concentration. Experimental data (squares) were fitted with the classical Michaelis-Menten equation (solid line). pH 7.4.

The ECL intensity increased with the addition of glucose. It is thus possible to detect glucose by ECL of NADH; this latter results from the catalyzed reaction between glucose and  $\text{NAD}^+$  by GDH. Glucose was quantified by ECL using GDH to generate NADH as shown in reactions (1-6). Figure 16 shows the dependence of the ECL emission on the glucose concentration in the 100  $\mu\text{M}$  to 20 mM range. The ECL signals were measured during the application of a potential pulse from 0 to 0.9 V. For concentrations up to 2 mM, the ECL signal increases linearly with the glucose concentration. But for higher concentrations, the slope is less important and the ECL intensity tends progressively to a saturation value. The detection limit was 100  $\mu\text{M}$ . On Figure 16 (solid line), we fitted the experimental data with the classical Michaelis-Menten equation.<sup>55</sup> The apparent Michaelis-Menten constant ( $K'_M$ ) was estimated to be 7.2 mM and it is consistent with reported values.<sup>56</sup>

#### 2.4. CONCLUSION

We presented here the ECL detection of NADH based on electrodeposited redox hydrogel. This approach was applied to glucose detection using glucose dehydrogenase. The ruthenium metallopolymer was immobilised by cyclic voltammetry which allows deposition in rapid, reproducible and well-controlled one-step procedure. The redox hydrogel which contains

$\text{Ru}(\text{bpy})_3^{2+}$  units showed reversible, surface confined electrochemistry. In the presence of NADH, the hydrogel film shows intense ECL emission. It was found that ECL intensity linearly depends on the concentration of NADH in range from 100 nM to 50 mM.  $\text{NAD}^+$  is a cofactor in enzymatic reaction and it is transformed to NADH when the substrate is transformed to the product. Therefore, the detection of enzymatically formed NADH allows indirect quantification of the substrate. The concept was used in combination with glucose dehydrogenase as a sensor model system. By adding the glucose in the solution of GDH and  $\text{NAD}^+$ , the ECL signal is recorded. The signal increases with glucose concentration, which demonstrates the spectrum of applications of this system for substrate detection. The detection is demonstrated at much lower anodic potential than with the model  $\text{Ru}(\text{bpy})_3^{2+}$  complex. It is interesting to notice that the immobilised luminophore in the hydrogel is regenerated during the ECL process and that the coreactant is also regenerated by the enzymatic reaction. This approach can be applied for all  $\text{NAD}^+$  depended enzymes which include group of dehydrogenase.

To develop a biosensor design, some preliminary experiments were dedicated to the immobilization of GDH along with redox polymer. It was reported that weak ligands which coordinate ruthenium and osmium complexes may be exchanged with histidine, lysine, and arginine functions. Thus the co-electrodeposition was performed with no use of any cross-linker. So far no ECL was detected in the system but the experiments are in progress in order to optimise condition for successful fabrication of redox polymer based ECL biosensor.

## REFERENCES

1. B. R. Eggins, in *Analytical Techniques in the Sciences*, John Wiley & Sons, Ltd., 2007, p. 1.
2. I. Rubinstein, C. R. Martin and A. J. Bard, *Anal. Chem.*, 1983, **55**, 1580.
3. J. B. Noffsinger and N. D. Danielson, *Anal. Chem.*, 1987, **59**, 865.
4. K. Yokoyama, S. Sasaki, K. Ikebukuro, T. Takeuchi, I. Karube, Y. Tokitsu and Y. Masuda, *Talanta*, 1994, **41**, 1035.
5. J. Ludvík and J. Volke, *Anal. Chim. Acta*, 1988, **209**, 69.
6. G. M. Cruise, D. S. Scharp and J. A. Hubbell, *Biomaterials*, 1998, **19**, 1287.
7. A. Venkatanarayanan, B. S. O'Connell, K. A. D. Tia E and R. J. Forster, *Electrochem. Commun.*, 2011, **13**, 396.
8. S. N. Brune and D. R. Bobbitt, *Anal. Chem.*, 1992, **64**, 166.
9. W. A. Jackson and D. R. Bobbitt, *Anal. Chim. Acta*, 1994, **285**, 309.
10. G. F. Blackburn, H. P. Shah, J. H. Kenten, J. Leland, R. A. Kamin, J. Link, J. Peterman, M. J. Powell, A. Shah and D. B. Talley, *Clin Chem*, 1991, **37**, 1534-1539.
11. J. H. Kenten, S. Gudibande, J. Link, J. J. Willey, B. Curfman, E. O. Major and R. J. Massey, *Clin Chem*, 1992, **38**, 873-879.
12. Y. T. Hsueh, R. L. Smith and M. A. Northrup, *Sensor. Actuat. B: Chem*, 1996, **33**, 110.
13. M. S. Hahn, L. J. Taite, J. J. Moon, M. C. Rowland, K. A. Ruffino and J. L. West, *Biomaterials*, 2006, **27**, 2519.
14. X. Liu, L. Shi, W. Niu, H. Li and G. Xu, *Angew. Chem. Int. Edit.*, 2007, **46**, 421.
15. I. Rubinstein and A. J. Bard, *J. Am. Chem. Soc.*, 1980, **102**, 6641.
16. I. Rubinstein and A. J. Bard, *J. Am. Chem. Soc.*, 1981, **103**, 5007.
17. W.-Y. Lee, *Microchim. Acta*, 1997, **127**, 19.
18. P. Bertocello, L. Dennany, R. J. Forster and P. R. Unwin, *Anal. Chem.*, 2007, **79**, 7549.
19. L. M. Moretto, T. Kohls, D. Badocco, P. Pastore, N. Sojic and P. Ugo, *J. Electroanal. Chem.*, 2010, **640**, 35.
20. L. M. Moretto, T. Kohls, A. Chovin, N. Sojic and P. Ugo, *Langmuir*, 2008, **24**, 6367.
21. T. M. Downey and T. A. Nieman, *Anal. Chem.*, 1992, **64**, 261.
22. A. F. Martin and T. A. Nieman, *Biosens. Bioelectron.*, 1997, **12**, 479.

23. M. M. Collinson, J. Taussig and S. A. Martin, *Chem. Mater.*, 1999, **11**, 2594.
24. J.-K. Lee, S.-H. Lee, M. Kim, H. Kim, D.-H. Kim and W.-Y. Lee, *Chem. Commun.*, 2003, 1602.
25. W. Yun, P. Dong, Y. Xu, L. Yang, P. He and Y. Fang, *Sens. Actuat. B Chem.* 2009, **141**, 244.
26. J. Li, Y. Xu, H. Wei, T. Huo and E. Wang, *Anal. Chem.*, 2007, **79**, 5439.
27. L. Dennany, E. J. O'Reilly, T. E. Keyes and R. J. Forster, *Electrochem. Commun.*, 2006, **8**, 1588.
28. Y. S. Obeng and A. J. Bard, *Langmuir*, 1991, **7**, 195.
29. X. Zhang and A. J. Bard, *J. Phys. Chem.*, 1988, **92**, 5566.
30. P. Bertoncello, E. T. Kefalas, Z. Pikramenou, P. R. Unwin and R. J. Forster, *J. Phys. Chem. B*, 2006, **110**, 10063.
31. L. Dennany, R. J. Forster and J. F. Rusling, *J. Am. Chem. Soc.*, 2003, **125**, 5213.
32. R. J. Forster and C. F. Hogan, *Anal. Chem.*, 2000, **72**, 5576.
33. L. Dennany, R. J. Forster, B. White, M. Smyth and J. F. Rusling, *J. Am. Chem. Soc.*, 2004, **126**, 8835.
34. W. Miao, J.-P. Choi and A. J. Bard, *J. Am. Chem. Soc.*, 2002, **124**, 14478.
35. L. S. Dolci, S. Zanarini, L. D. Ciana, F. Paolucci and A. Roda, *Anal. Chem.*, 2009, **81**, 6234.
36. Z. Gao, G. Binyamin, H.-H. Kim, S. C. Barton, Y. Zhang and A. Heller, *Angew. Chem. Int. Edit.*, 2002, **41**, 810.
37. A. Heller, *Curr. Opin. Chem. Biol.*, 2006, **10**, 664.
38. S. Sallard, J. Patole, V. Soukharev, A. Heller, N. Mano and N. Sojic, *Electrochem. Commun.*, 2009, **11**, 599.
39. M. Domingo-García, F. J. López-Garzón and M. Pérez-Mendoza, *Carbon*, 2000, **38**, 555.
40. A. B. Dongil, B. Bachiller-Baeza, A. Guerrero-Ruiz, I. Rodríguez-Ramos, A. Martínez-Alonso and J. M. D. Tascón, *J Colloid Interf Sci*, 2011, **355**, 179.
41. M. Pérez-Mendoza, M. Domingo-García and F. J. López-Garzón, *Carbon*, 1999, **37**, 1463.
42. D. Manojlovic, J. Mutic and D. Segan, *Osnove elektroanaliticke hemije*, Hemijski fakultet Univerziteta u Beogradu, 2010.
43. W. Miao, *Chem. Rev.*, 2008, **108**, 2506.
44. M. M. Richter, *Chem. Rev.*, 2004, **104**, 3003.

45. J. Moiroux and P. J. Elving, *Anal. Chem.*, 1979, **51**, 346.
46. P. Hapiot, J. Moiroux and J. M. Saveant, *J. Am. Chem. Soc.*, 1990, **112**, 1337.
47. F. Jameison, R. I. Sanchez, L. Dong, J. K. Leland, D. Yost and M. T. Martin, *Anal. Chem.*, 1996, **68**, 1298.
48. F. Kanoufi, C. Cannes, Y. Zu and A. J. Bard, *J. Phys. Chem. B*, 2001, **105**, 8951.
49. X.-m. Chen, B.-y. Su, X.-h. Song, Q.-a. Chen, X. Chen and X.-r. Wang, *TrAC Trend. Anal. Chem.*, 2011, **30**, 665.
50. Z. Xu, Z. Guo and S. Dong, *Biosens. Bioelectron.*, 2005, **21**, 455.
51. L. Zhang, Z. Xu, X. Sun and S. Dong, *Biosens. Bioelectron.*, 2007, **22**, 1097.
52. T.-t. Jia, Z.-m. Cai, X.-m. Chen, Z.-j. Lin, X.-l. Huang, X. Chen and G.-n. Chen, *Biosens. Bioelectron.*, 2009, **25**, 263.
53. L. Zhang, Z. Xu and S. Dong, *Anal. Chim. Acta*, 2006, **575**, 52.
54. A. F. Martin and T. A. Nieman, *Anal. Chim. Acta*, 1993, **281**, 475.
55. L. D. Mell and J. T. Maloy, *Anal. Chem.*, 1975, **47**, 299.
56. Z. Wang, S. Liu, P. Wu and C. Cai, *Anal. Chem.*, 2009, **81**, 1638.



~ ~ ~

## CHAPTER 3:

# PHOTODEPOSITION AND PHOTOPATTERNING OF ULTRATHIN ELECTROCHEMILUMINESCENT REDOX HYDROGEL FILMS

~ ~ ~

The need to analyse complex biological samples and to measure multiple analytes simultaneously has led to the development of new analytical strategies. Multiplexed assays are solid-phase-based assays in which different kinds of capture molecules are immobilised at distinct locations allowing the simultaneous measurement of several analytes on a single sample.<sup>1</sup> In the traditional way the sample has to be divided in several aliquots and each analysed separately on the single analyte. Multiplexed assays offer much faster analyses requiring less quantity of sample. Due to its high sensitivity, a lot of reported multiplexed assays employed ECL like detection system. An important advantage of ECL is that only labels bound near the electrode surface can be detected which enables assay with no washing step.<sup>2</sup> Here we present a photodeposition and photopatterning process allowing efficient and rapid immobilisation of an ECL luminophore. In comparison with already reported methods where the entire electrode surface is usually covered by uniform layer, this approach allows immobilisation of ECL luminophore in the form of photopatterns which may find application in multiplexed bioassays. First part of this chapter deals with principles of multiplexed assays that have been already reported. The second part is dedicated to photodeposition as a novel method for immobilisation of an ECL luminophore. The third part of the chapter introduces photopatterning as a new approach for fabrication of ECL microspot arrays.

### **3.1. MULTIPLEXED ASSAYS**

Multiplexed assays represent a key technology which allows simple, fast and reliable detection giving large amount of information obtained from a single experiment. They are usually based on biosensors where biological recognition element is required. Two types of recognition are distinguished.<sup>3</sup> In catalytic recognition such as in enzymatic biosensors, the recognised (bio)chemical species is transformed into a product through a chemical reaction. The second type, affinity recognition, is based on specific capabilities of an analyte to bind a recognition element such as a group of immunosensors (which rely on specific interactions between an antibody and an antigen) or nucleic acid biosensors (which makes use of the affinity between complementary oligonucleotides). A multiplexed platform can be presented as an array of miniaturised biosensors assembled together which, in the same conditions, at the same time and for the same quantity of sample, can give the results about several analytes simultaneously. In order to work with the smallest amount of sample, the platform should

have small dimensions, which requires the miniaturisation of individual sensors. They are usually of micrometric size uniformly organised at the platform surface.

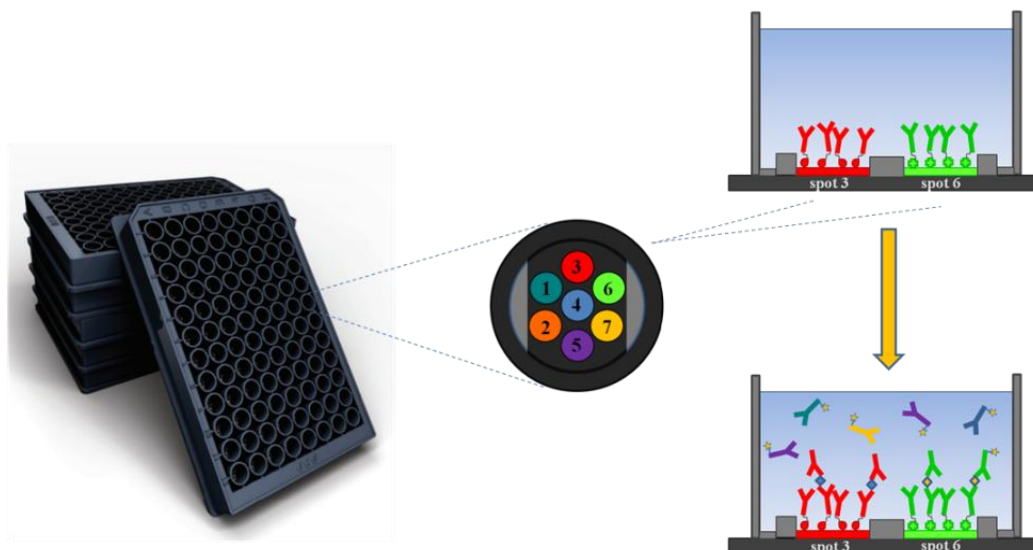


Figure 1. An example of multi-array platform provided by Meso Scale Discovery. (The platform consists of 96 separate wells. In each well 4, 7 or 10 analytes are detected simultaneously)

Basically, there are two types of multiplexed platforms based on microarray and bead-based technology.<sup>4</sup> Microarray technology includes immobilisation of capture element in the form of microspots or microwells uniformly organised at the solid support. In immunoassays for example, different capture antibodies are immobilised in separated wells, or even on the different microspots in the same well, depending on the design. Then the platform is incubated with tested antigen attached to the optical label or it is incubated first with antigen and then with secondary labelled antibody in the case of so called sandwich immunoassay. On the other hand, bead-based assays systems employ microspheres as solid support for the capture molecules. The principle for the detection may be similar as for microarray technology but here the recognition reaction occurs at the surface of microbeads. To be distinguished, the beads with different capture molecules are loaded with different dyes or with a dye in different concentrations.<sup>1, 5-7 3</sup> The detection in multiplexed systems is mainly based on using optical labels and probes of various kind. This requires the biomolecule to be covalently labelled to allow the detection of target molecule using fluorescence, chemiluminescence or some other spectroscopic technique. When the ECL detection is used the biomolecule is attached to the target that may be involved on an ECL reaction. Usually, this is a derivate of  $\text{Ru}(\text{bpy})_3^{2+}$  complex while the coreactant is present in the solution. Due to

advantages over the other spectroscopic techniques such as improved signal-to-noise ratio<sup>8</sup> and no problems of light scattering and fluorescent impurities<sup>8,9</sup> ECL starts to be more often use in different kinds of biosensors and multiplexed assays. To illustrate the design and fields of application, here are given some examples of multiplexed assays which employ ECL as readout mechanism.

### 3.1.1 Microarray-based assays

Microarray technology is so far the most represented technique for multiplexed assays. The design can be based on microspots or microwells organised on a flat platform. The group of James F. Rusling recently presented ECL array platform for metabolic toxicity screening.<sup>10,11</sup> The platform consists of arrays of spots on the pyrolytic graphite chip obtained by pipetting 0.5  $\mu\text{L}$  drop of mixture of ds-DNA, RuPVP (ruthenium(II)polyvinylpyridine polymer) and human or rat liver microsomes as natural source of cytochrome P450 enzyme. The incubations were done on arrays with incubating solutions containing test chemicals and enzyme cofactors. The toxicity examination was based on the concept that reactive metabolic products of xenobiotic chemicals which are produced in the enzymatic reaction can damage DNA. The dissociation of ds-DNA can be detected by ECL. Namely, it was found that guanine bases presented in DNA react as an ECL coreactant. ECL intensity is higher for ss-DNA than for ds-DNA and increases with chemical damage of ds-DNA.<sup>12,13</sup> The ECL light emitted from the spots at which DNA damage occurs gives higher intensity than the light from control spot which was not in contact with sample. These ECL arrays can find application in agricultural, cosmetic and pharmaceutical industry for early toxicity screening of new chemicals and drug candidates.

The same research group very recently reported an ECL immunosensor array for detection of cancer biomarker proteins.<sup>14</sup> This array consists of 10  $\mu\text{L}$  wells organised on a conductive support with a forest of single-wall carbon nanotubes (SWCNT) incorporated inside microwells. SWCNTs were decorated with different capture antibodies and then incubated sequentially with antigens and secondary antibodies previously attached to  $\text{Ru}(\text{bpy})_3^{2+}$ -modified silica nanoparticles. The ECL image of the array with captured analytes was recorded in the presence of TPrA as a coreactant. The concept is presented for the detection of prostate specific antigen (PSA) and interleukin-6 (IL-6) with the final goal to enable the detection of up to 10 proteins simultaneously.

By comparison with other detection methods that are used in multiplexed assays, the ECL offers several advantages. ECL offers minimal background and high signal to background ratio allowing simultaneous measurement of electrical and light signal. Further, labels are stable, non-radioactive and conveniently conjugated to biological molecules. Each label can have multiple excitation cycles which lead to the amplification of the signal and improvement of sensitivity. Thus ECL is also applied for the detection in commercial multiplexed assays. Meso Scale Discovery offers over 200 multiple analyte kits for different kinds of immunoassays based on ECL technology detection.<sup>2</sup> The available kits are based on multi-array and multi-spot feature. The platforms consist of 96 or 384 wells and each well contains 4, 7 or 10 spot electrodes. Each electrode contains different capture molecules able to simultaneously measure multiple analytes in the same well while high density arrays allow high throughput assay (Figure 1). Such platforms offer rapid and reproducible assays in different fields of clinical analysis such as immunology, toxicology, inflammation, metabolic disorders, etc.

### 3.1.2. Bead-based assays

Bead-based assay systems present different approaches toward the array technology. It employs microspheres as solid support for the capture molecules instead of planar substrate, which is conventionally used for microarray assays. The group of David R. Walt developed different sensor arrays for immunoassay and DNA-assay based on bead arrays technology.<sup>1, 5,</sup>

<sup>6</sup> The addressable beads randomly ordered on the top of etched fibre optic bundle form high optical density arrays. This approach for array fabrication exploits both the high information density potential of an optical imaging fibre and rapid signal processing.<sup>6</sup>

Our group reported a new class of bead-based sensing microarray that uses ECL as a readout mechanism.<sup>7</sup> To encode the beads which will bear different capture antibodies, the populations of the beads were loaded with different concentration of europium dye. Then, the beads were incubated with different capture antibodies and loaded into the wells of etched and gold coated fibre optic bundle. The fibre optic bundle was used as beads support and working electrode in the same time. The fluorescence image of beads array was recorded in order to decode which beads bear with captured antibodies. The array is then sequentially incubated with sample containing antigens, then with solution containing biotinylated antibody and finally with a solution of streptavidin-modified  $\text{Ru}(\text{bpy})_3^{2+}$  complex to obtain ECL labelled sandwich immunoassay. Finally, an ECL image was recorded in the presence of TPrA. By

comparison of ECL image with fluorescence image it was resolved which antigens were present in the sample. This system was used for the detection of Interleukine-8 (IL-8), Vascular Endothelial Growth Factor (VEGF) and Tissue Inhibitor of Metalloproteinases-1 (TIMP-1) simultaneously.

### 3.2. PHOTODEPOSITION

The first step in the way to create a multiplexed assay is to fabricate an array of microspots which can be used for detection of different analytes at the same time. In the case of multiplexed assays where ECL is employed as readout mechanism, the reactive spots should be immobilised on the electrode surface. The methods of immobilisation of an ECL luminophore that are already reported (see paragraph 2.1) can provide the immobilisation on the whole surface of electrode but no microspots can be obtained. On the other hand, photodeposition offer the control over the position. It can be applied like a photolithography technique and provide the immobilisation in the form of patterns. For this reason, we studied the possibility of photodeposition of thin films of ruthenium containing polymer [poly(4-vinylpyridine)-Ru(2,2'-bipyridine)<sub>2</sub>Cl]<sup>+2+</sup> (PVP-Ru(bpy)<sub>2</sub><sup>2+</sup>).

#### 3.2.1 Photopolymerisation of PEGDA

Photopolymerisation is process where free radical polymerisation is initiated by UV light radiation. Basically, when a photoinitiator is exposed to the UV light, free radicals of photoinitiator are created and they initiate the reaction of polymerisation of monomer. Usually, monomers are polymer chains which are able to polymerise further resulting in linear and cross-linked structures capable for entrapping of species such as the ruthenium derivatives.

The immobilisation of the ruthenium containing polymer, PVP-Ru(bpy)<sub>2</sub><sup>2+</sup>, was achieved in matrix of poly(ethylene glycol) (PEG) hydrogel. PEG is transparent, non-degradable, hydrophilic polymer that can be cross-linked into hydrogel through various chemistries.<sup>15</sup> PEG hydrogel shows to be biocompatible and intrinsically resistant to protein adsorption and cell adhesion.<sup>16</sup> For this reason it has been used for development of drug delivery systems, in tissue engineering and for coating of implanted sensors in order to improve its biocompatibility. The group of Pishko has reported the use of PEG hydrogel in different biorelated systems.<sup>15, 17-20</sup> They have reported the fabrication of highly cross-linked hydrogel

spheres that may be used for drug delivery of protein and polynucleotide drugs.<sup>20</sup> The spheres were fabricated using UV photopolymerisation of poly(ethylene glycol) diacrylate (PEGDA) and pentaerythritol triacrylate (PETA) as macromers and 2,2-dimethoxy-2-phenylacetophenone (DMPA) as photoinitiator. The sphere fabrication was performed with and without acrylic acid, acrylamide or allylamine as cross-linking agent. The delivery simulation was performed with incorporated bovine serum albumin as a model protein drug. The same group has described a photolithographic method for the fabrication of PEG hydrogel microstructures on silicon or glass substrates.<sup>15</sup> The hydrogel patterns were prepared from poly(ethylene glycol) diacrylate (PEGDA), dimethacrylate (PEGDMA) and tetraacrylate (PEGTA) in the presence of DMPA. Silicon or glass surfaces were first acrylated with trichlorosilane self-assembled monolayer to ensure covalent attachment of the PEG and improve hydrogel adhesion to the substrate. To prepare microstructures, the precursor solution was spin-coated on the substrate surface, covered with a photomask and exposed to 365 nm UV light. The potential application of PEG-based microstructure in optical sensors was demonstrated by incorporation on SNAFL-1 labeled protein, a pH-sensitive dye which exhibits both intensity and emission wavelength changes with changing pH. The photolithography of PEG was further used for encapsulation of viable mammalian cells in microstructured hydrogel for fabrication of cell-based biosensing devices.<sup>18</sup>

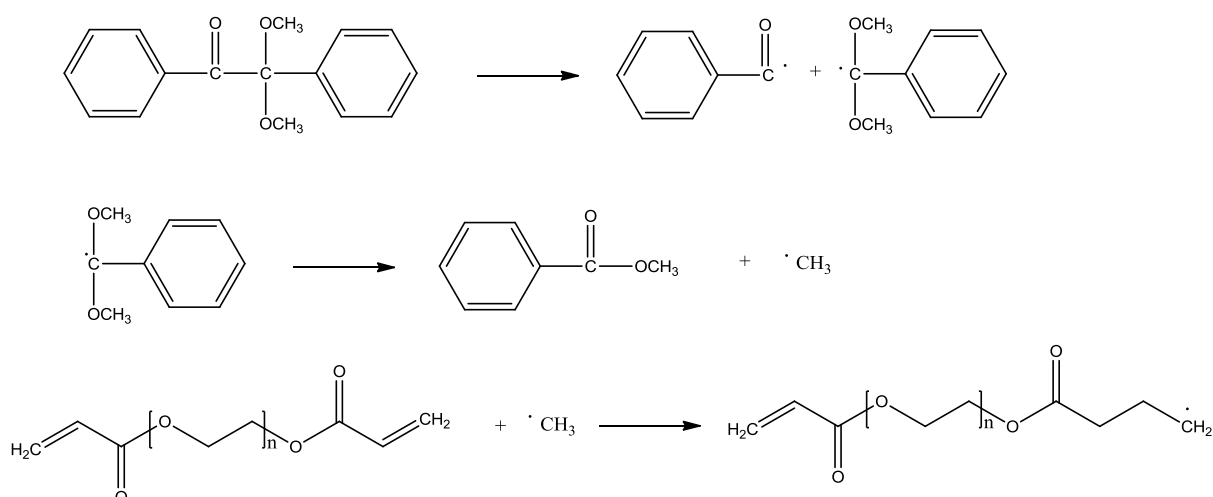
Thanks to its hydrogel structure, PEG network can entrap bigger molecules on one hand and can swell and be permeable for smaller water soluble compounds on another hand. Thus, PEG has been widely used in the design of biosensors, for example, for immobilisation of enzymes on the electrode surface.<sup>17, 21</sup> In the field of electrochemical biosensing, Pishko et al. developed an amperometric biosensor based on the immobilisation of oxidoreductases along with redox polymer in the matrix.<sup>17</sup> The glucose oxidase was mixed with polymer hydrogel precursor solution composed of PEGDA, DMPA and redox polymer vinylferrocene. The mixture was photopolymerised on the surface of gold electrodes by illumination with UV light. In a similar way, a microsensor array has been developed by immobilisation of the glucose oxidase with a redox hydrogel on the surface of microelectrode array.<sup>19</sup> Very recently, Suraniti et al. reported a new method for fast and easy enzyme immobilisation in hydrogel formed of PEGDA with DAROCUR as photoinitiator.<sup>21</sup> In the presented two-set procedure, mixture of the enzyme and the redox hydrogel is first deposited on a glassy carbon electrode. After the curing at room temperature, the electrode surface was covered with mixture of PEGDA and DAROCUR and illuminated with UV light to perform photopolymerisation.

Instead of typical chemical cross-linking, in this case, the bioelectrocatalyst was covered by an outer layer of PEGDA hydrogel. This protocol is of particular interest for label enzymes, bilirubin oxidase being used as model system.

In our case we decided to take advantages of hydrogel structure of PEG to use it for immobilisation of an ECL luminophore. The PEG hydrogel were formed by polymerisation of poly(ethylene glycol) diacrylate (PEGDA) which is a derivate of PEG with two acrylate groups at both ends of PEG molecule. These acrylate groups allow to the molecule to participate in a free radical polymerisation. Like photoinitiator was used 2,2'-dimethoxy-2-phenylacetophenone (DMPA). DMPA is a photoclivable precursor. When the mixture of PEGDA and DMPA is exposed to the UV light, the reaction of free radical polymerisation occurs. The first step is the initiation phase. Due to UV light radiation, DMPA undergoes photofragmentation forming  $\text{CH}_3^\bullet$  radicals.<sup>17</sup> These radicals attack carbon-carbon double bonds present in acrylate end groups of PEGDA forming new radicals. When first PEGDA radicals are formed, reaction propagates in cross-linking with constant forming of new radicals. This reaction takes place until all carbon-carbon double bonds are converted or most likely until the free radicals are presented. When the photopolymerisation is finished, the final product is a transparent, non-degradable hydrogel film.

Here is presented the mechanism of photoinitiated PEGDA polymerisation proposed by Pishko et al.<sup>17, 20</sup>

Initiation step:





Propagation step:

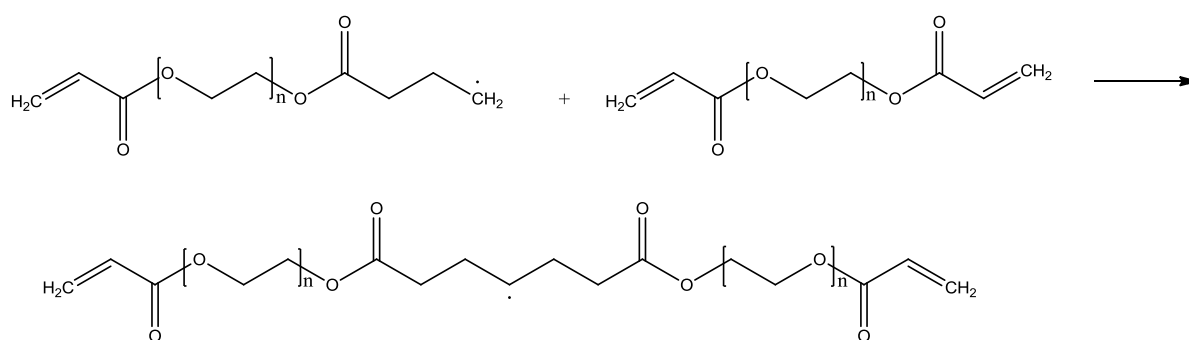
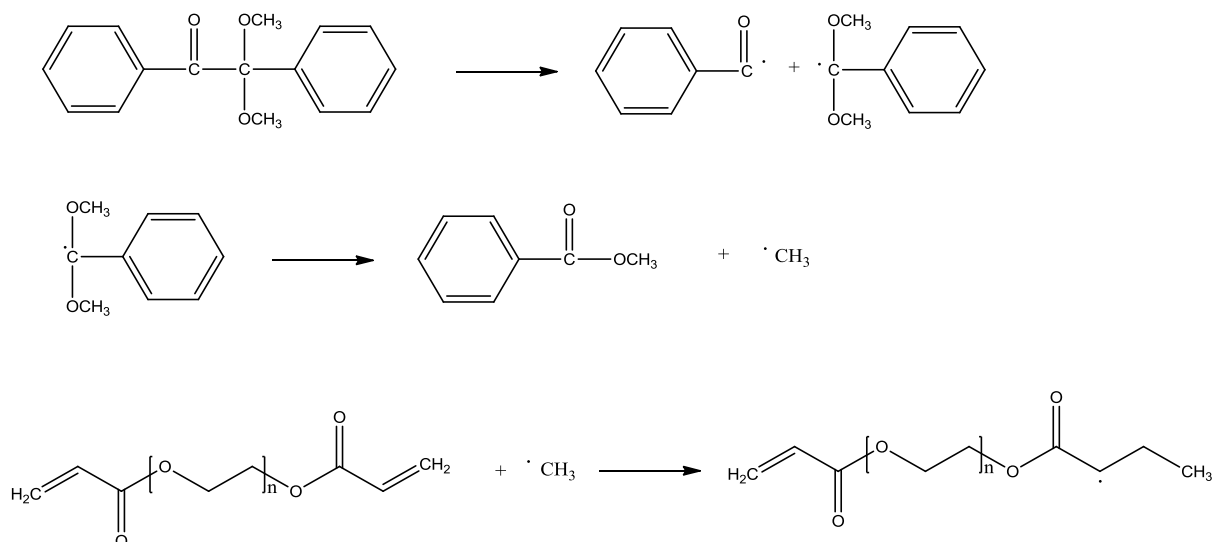


Figure 2. Mechanism of photopolymerisation of PEGDA with DMPA as photoinitiator (by forming the primary free alkyl radical)

We proposed a slightly different mechanism. Instead of forming the primary free radical, upon to reaction of methyl free radical with PEGDA it maybe formed a secondary free radical which is more stable than primary ones. The stabilisation of secondary free radical comes from electron delocalisation between neighbouring  $sp^3$  hybrid orbitals of carbon atoms and partially filled p orbital characteristic of a radical centre. This phenomenon is called hyperconjugation and explains the stability of alkyl radicals in the trend  $CH_3 \cdot < \text{primary} < \text{secondary} < \text{tertiary free alkyl radical}$ .

Initiation step:



Propagation step:

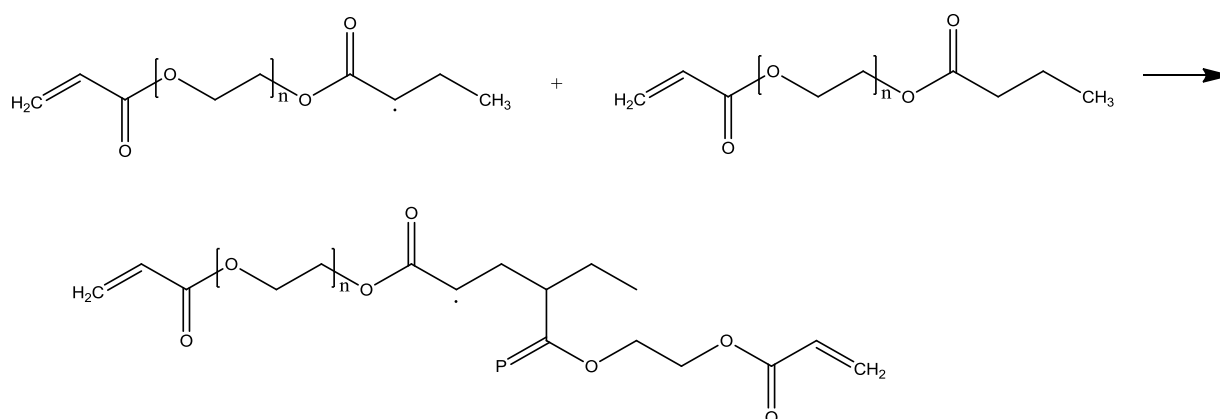


Figure 3. Mechanism of photopolymerisation of PEGDA with DMPA as photoinitiator (by forming the secondary free alkyl radical)

The same mechanism has been proposed by other authors which have studied the PEGDA polymerisation within a multicomponent semi-interpenetrating polymer network system.<sup>22</sup>

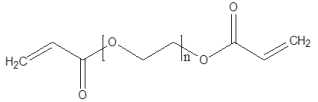
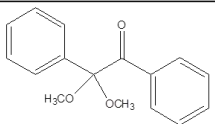
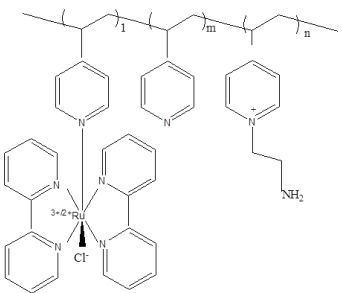
### 3.2.2. Photodeposition of PVP-Ru(bpy)<sub>2</sub><sup>2+</sup>

The immobilisation of an ECL luminophore is an important step in the fabrication of ECL based sensors. An important condition that should be met when the ECL luminophore is incorporated in a film is to ensure no leaking of the luminophore from the film. For the photodeposition of an ruthenium based ECL luminophore, we used the same ruthenium containing polymer PVP-Ru(bpy)<sub>2</sub><sup>2+</sup> that was electrodeposited in chapter 2. The first reason is that it shows both good electrochemical and ECL responses and it can be applied in enzymatic system detection. The second reason is that the ruthenium centres are covalently bonded to the polymer backbone. When this polymer is incorporated in the structure of the hydrogel it will stay entrapped inside. Thus, ruthenium complexes will be immobilised on the electrode surface with no problem of leaking from the hydrogel film.

The entrapment of the ruthenium containing polymer was realised by simple mixing of it with PEGDA and DMPA in the desired ratio. The mixture was spin coated on the electrode surface in order to form a thin polymer layer, and immediately illuminated by UV light. This induce PEGDA polymerisation on the electrode surface forming a hydrogel network in which PVP-Ru(bpy)<sub>2</sub><sup>2+</sup> complex is entrapped. As the properties of obtained film depend on the experimental parameters such as PVP-Ru(bpy)<sub>2</sub><sup>2+</sup>/PEGDA/DMPA ratio, rotational speed, duration of spin-coating and the time of UV exposure, the first experiments were dedicated to

optimise the conditions of photodeposition. The experiments were performed with solutions containing PEGDA/DMPA in ratios 15:1, 20:1, 50:1, 100:1 and 200:1. These solutions were then mixed with 5 mg/mL PVP-Ru(bpy)<sub>2</sub><sup>2+</sup> usually in ratio 1:1. The rotation time was varied from 2000 to 10000 rpm. The illumination was applied for 1, 5, 10 and 15s. A good compromise was obtained for conditions in which it was used precursor solution of PEGDA/DMPA/ PVP-Ru(bpy)<sub>2</sub><sup>2+</sup> in ratio 1:0.01:1. The spin-coating was performed for 20s at rotational speed of 4000 rpm except in the experiment where the films of different thickness were fabricated. The polymer mixture was illuminated for 5s to provide complete polymerisation.

Table 1. Structural formula and mass ratio of compounds in the polymer mixture

Role in the precursor solution	Formula	Mass ratio
PEGDA, comonomer		1
DMPA, photoinitiator		0.01
Ruthenium containing polymer		1 (of water solution concentration 5 mg/mL)

### 3.2.3. Electrochemical characterisation of photodeposited redox hydrogel

Electrochemical characterisation of photodeposited film was performed by cyclic voltammetry. Figure 4A shows a typical cyclic voltammogram obtained for an ultrathin photodeposited polymer film obtained by spin-coating the polymer mixture on the glassy carbon electrode. The voltammogram shows the reversible oxidation of ruthenium centres where anodic and cathodic current peaks correspond to oxidation of Ru<sup>2+</sup> to Ru<sup>3+</sup> and back reduction of electrogenerated Ru<sup>3+</sup> to Ru<sup>2+</sup>, respectively. Oxidation occurs at + 0.77 V. This

value is comparable with the oxidation peak of the same polymer electrodeposited on the electrode surface (+ 0.75 V). The separation between oxidation and reduction peak is ~20 mV indicating that redox centres are surface-confined. For comparison, figure 4B shows a cyclic voltammogram obtained of a thicker photodeposited film obtained by drop coating of the electrode surface with the polymer mixture. The oxidation potential of + 0.76 V is comparable with the previous case but the separation between peaks is ~100 mV. This can be explained by the distribution of redox centres in the thick hydrogel film. Even the ruthenium centres are immobilised in the hydrogel film, the film thickness has thus an influence on its electrochemical behaviour. In this case the oxidation peak corresponds not only to oxidation of redox centres present directly on the electrode surface but also of redox centres present in the peripheral part of the film. For this reason the peak separation is larger and the thick films behave like diffusion systems.

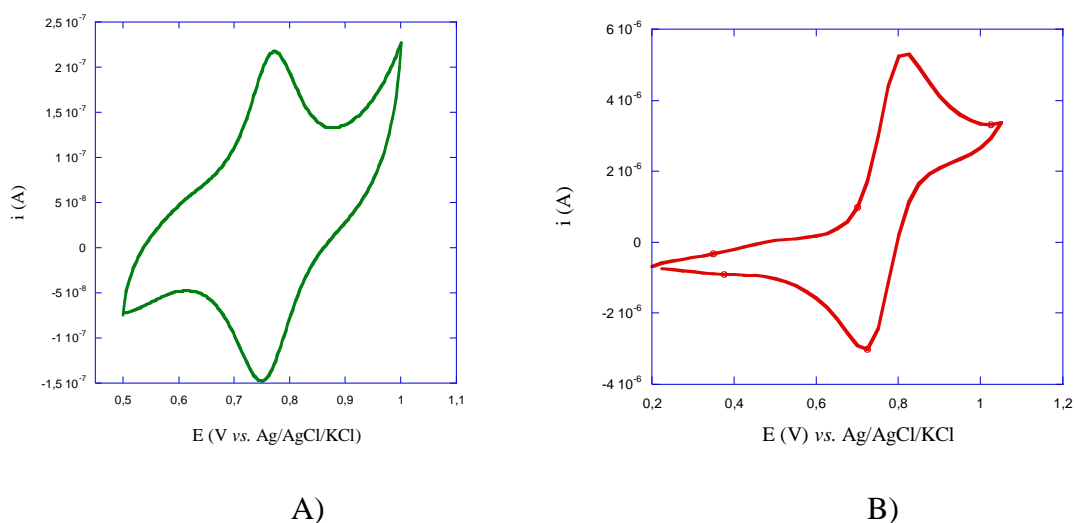


Figure 4. Cyclic voltammograms of A) spin coated and B) drop coated photodeposited films on glassy carbon electrodes in 100 mM PBS, scan rate is 50 mV/s

### 3.2.4 ECL characterisation of the photodeposited redox hydrogel

The ECL experiments were performed with TPrA.

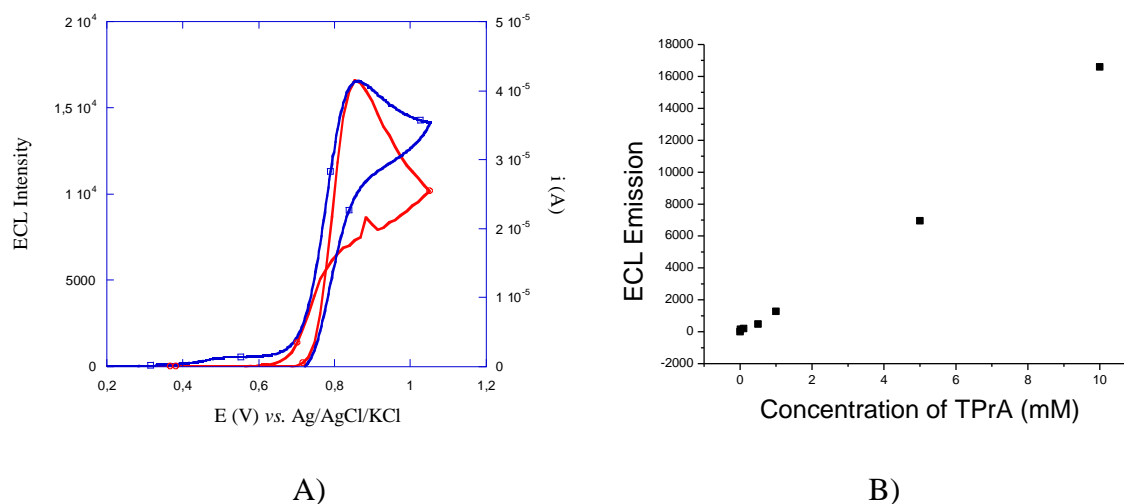


Figure 5. A) Cyclic voltammogram (blue) and ECL emission (red) of a photodeposited film on GC electrode in 10 mM TPrA, scan rate 30 mV/s; B) Dependence of ECL intensity on the concentration of TPrA

Figure 5A presents cyclic voltammetry analysis and ECL response of the film. Anodic peak on the voltammogram corresponds to oxidation of TPrA which appears at the same potential as the oxidation of  $\text{Ru}^{2+}$ . Although the oxidation of TPrA can occur directly at the electrode surface, it may also occur via a catalytic route. This route includes oxidation of  $\text{Ru}^{2+}$  to  $\text{Ru}^{3+}$  and then oxidations of TPrA by  $\text{Ru}^{3+}$ . The ECL intensity was measured in the solution with different concentrations of TPrA (figure 5B). The ECL response of photodeposited polymer shows linear dependence on the concentration of the coreactant in wide dynamic range from 10 nM to 10 mM. The very low detection limit enables this system to be used for very sensitive detection.

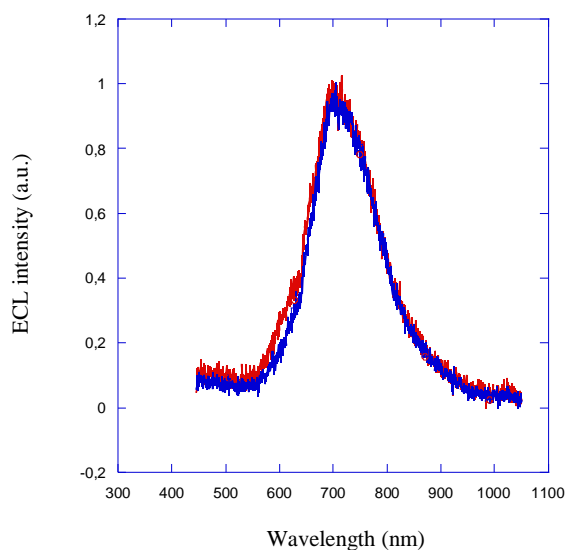


Figure 6. ECL spectra of photodeposited redox polymer (red) and electrodeposited polymer (blue) recorded at 1.2 V vs. Ag/AgCl/KCl in 10 mM TPrA.

The ECL spectrum of the photodeposited hydrogel film was recorded. The ECL emission displays a maximum of the wavelength at 700 nm. The spectrum was compared with the spectrum obtained for the same polymer immobilised by electrodeposition (Figure 6). It can be observed that the spectra are identical indicating that there is no change in the structure of the ruthenium complex and in excited state due to entrapment in PEGDA hydrogel or to the UV light illumination. Otherwise, any change in the structure of the ruthenium complex will induce a difference in MLCT energy which will result in the shift of emission maximum (see paragraph 1.4.2).

### 3.3. PHOTOPATTERNING

The main goal of this project was to photopattern the ECL hydrogel film. Photopatterning is based on classic photolithography. The general means of photolithography is replicating a predetermined master pattern on a substrate.<sup>23, 24</sup> It is a dominant manufacturing technique for electronic and optoelectronic devices due to its high speed, parallel patterning capability and high resolution.<sup>25, 26</sup> In general, photopatterning process starts by coating a substrate with a material which properties are changed by exposure to the light. Patterned exposure is most commonly achieved by passing light through a rigid mask. The mask can be positioned on the

substrate in contact mode, proximity mode or projection mode. In the contact mode, the mask is in direct contact with photosensitive material (photoresist). This approach offers high resolution but there is a risk of contamination and damage of the mask. With proximity mode, these problems can be avoided but the obtained resolution is lower. In projection mode, imaging optics can magnify and demagnify the mask image projecting the image in high resolution and with no need of contact with the substrate.<sup>26</sup> Due to the light exposure through a photomask, chemical changes occur in the exposed region. We can distinguish two types of photoresist: positive and negative. For the positive type, the solubility of the photoresist in the exposed region increases through the chemical and photochemical decomposition. Thus after the rinsing step with a developer the photoresist from the region that was exposed will be removed from the substrate surface (Figure 7A). In contrast, in negative photoresists, the photochemical reaction results in cross-linking of the polymer, rendering the films less soluble in the developer in the exposed region. Thus, the exposed regions of photoresist will be immobilised on the substrate surface while the rest of photoresist will be rinsed off (Figure 7B).<sup>24</sup> In the process of fabrication of electronic devices, remaining photopatterns are being used as a contact masks and further lithographic processing like etching, growth, deposition etc. are used to complete the device.

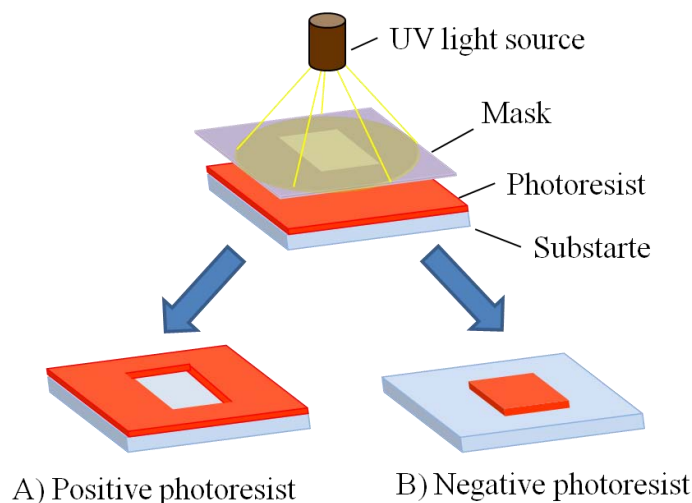


Figure 7. Scheme of the patterns obtained from positive and negative photoresists

### 3.3.1. Fabrication of ultrathin ECL photopatterns

Photolithographic techniques were used for photodeposition of an ECL luminophore. PEGDA could be used as a negative photoresist in the presence of a photoinitiator. In this case we were using proximity mode of photopatterning. First, the electrode surface was spin-coated with the mixture of PEGDA, DMPA and ruthenium polymer under the same ratio (1:0.01:1) as

for photodeposition. Then the mask was placed at a distance of  $\sim 1$  mm from the electrode surface. It is essential that the same distance between the mask and electrode surface being kept in all experiments to generate reproducible patterns. When the electrode is exposed to the UV source, light is able to pass only through the transparent parts of the mask initiating the formation of  $\text{CH}_3^{\bullet}$  radicals from DMPA. These radicals attack the molecules of PEGDA forming new radicals ready to react further. The reaction of polymerisation once initiated propagates further with neighbouring molecules even in the regions where the light was not able to pass through. The polymerisation is much faster in the exposed regions where concentration of radicals is higher giving a possibility for the formation of figures on the electrode surface. Thus, the parameters such as PEGDA/DMPA ratio, dilution factor and illumination time should be optimised in order to achieve complete polymerisation in exposed region and in the same time avoid the polymerisation between the spots. Immediately after exposure, the surface of the electrode was abundantly rinsed with water to remove non-polymerised rest of polymer mixture leaving immobilised patterns on the electrode surface.

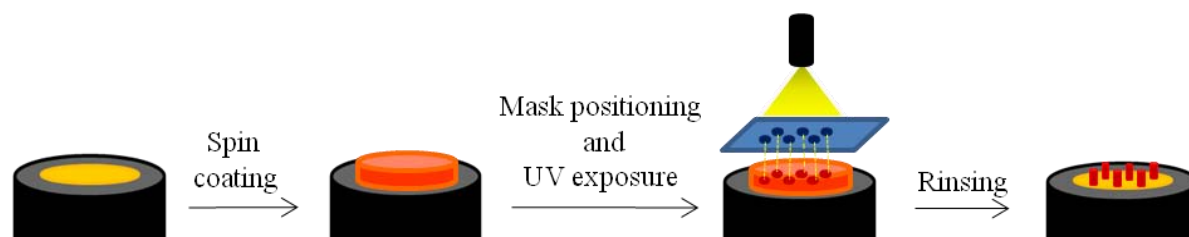


Figure 8. Scheme presenting the process of photopatterning of ultrathin hydrogel ECL films

Figure 8 presents the scheme of the photopatterning process. It is important to emphasize that the whole process is very simple and rapid. After spin-coating polymer solution for 20 s, the mask is placed above the electrode surface and exposed for 5 s. The electrode surface is then immediately rinsed and the photopattern is let to dry in the air. As the process of polymerisation is initiated with UV light ( $\sim 365$  nm),<sup>16, 17, 19</sup> the experiments were carried out in the laboratory with no restriction of the white light but whole experiments were done rapidly to avoid any possibility of non-specific photopolymerisation.

### 3.3.2. ECL imaging

The obtained photopatterns contain  $\text{Ru}^{2+}$  complex which has photoluminescent properties and take part in an ECL reaction. Thus the obtained photopatterns were characterised using PL and ECL imaging. PL imaging was done with epifluorescence microscope where the surface of electrode with the immobilised patterns was placed in an electrochemical cell with a



transparent window (see experimental part). The set-up was ready for PL and ECL imaging subsequently. Using the mercury lamp with excitation filter at 485 nm and collecting the emission light at 605 nm the PL images were recorded by CCD camera. Figure 9A presents a PL image of a photopattern. It can be seen that photopatterns are immobilised on the electrode surface but probably due to the very thin layer and low amount of  $\text{Ru}^{2+}$  centres in the patterns, the image can not be obtained with high contrast.

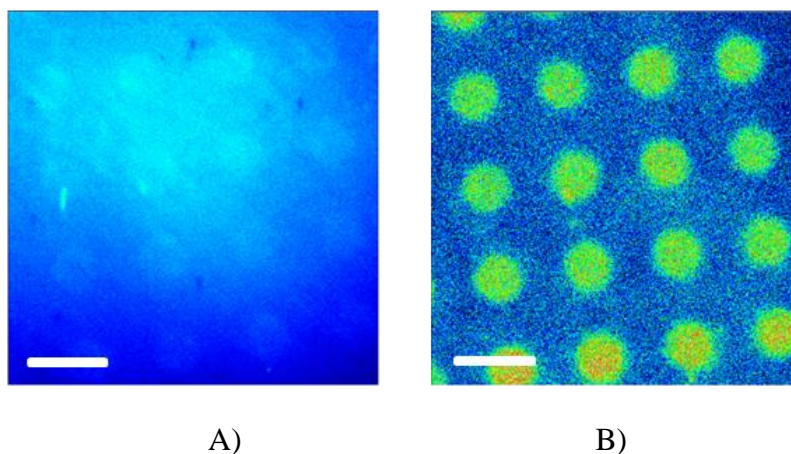


Figure 9. A) PL and B) ECL images of the same photopattern obtained on glassy carbon electrode, white bar 300  $\mu\text{m}$  (Imgaing conditions: A) Excitation filter 485 nm, dicroic filter cut off 540 nm, emission filter 605 nm, exposure time 5s, normal mode CCD, B) no light illumination, no emission filter, exposure time 20 s, EM-CCD mode)

PL and ECL images are recorded with the same electrode without moving it. For ECL imaging, there is no need to illuminate the sample with the excitation light. The ECL reaction is initiated by applying the adequate potential in a solution containing TPrA. Figure 9B presents an ECL image of the same photopattern. Here it can be observed that photopatterns are obtained in regular shape and distribution. The contrast of the image is much better than in previous case showing the advantages of ECL imaging over PL imaging.

As the patterns result from a mask projection, the shape and size of deposited patterns depend on the mask. Figure 10 demonstrates the possibility to fabricate patterns of different shapes in micrometric range. Using the same photolithography approach, smaller patterns with higher density could be easily fabricated with adequate mask dimension.

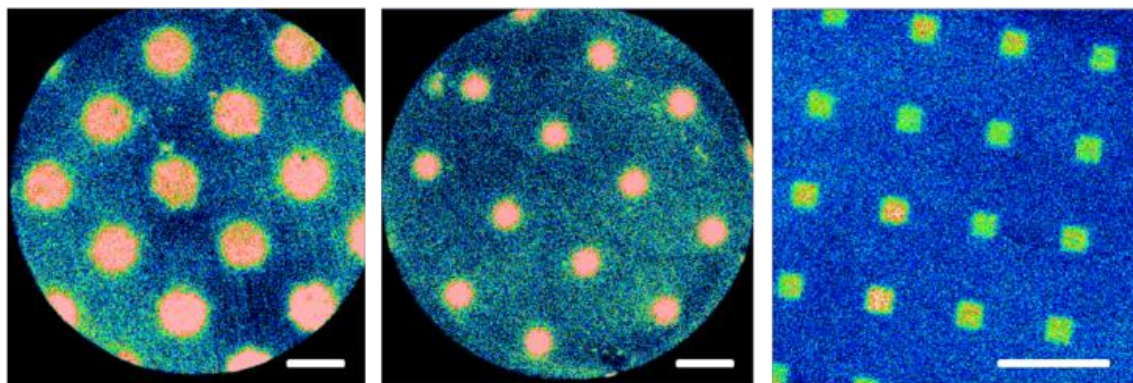


Figure 10. ECL images of different patterns obtained on gold electrode. From left to right: arrays of disks with radius of 100  $\mu\text{m}$  and 50  $\mu\text{m}$  and array of 30  $\mu\text{m}$  wide squares. White bar: 200  $\mu\text{m}$ .

### 3.3.3. Effect of the film thickness

The thickness of the photodeposited patterns is an important parameter because it governs its electrochemical and ECL behaviour. It has been reported that ultrathin films ( $<100$  nm) show better electroactivity and faster response time than thicker ones which have lower constant of diffusion and electron hopping.<sup>27, 28</sup>

Thus a lot work has been focused on the immobilisation of ultrathin films. For example Bertonecello et al. have reported the fabrication of Nafion monolayers at the air/water interface and the deposition of ultrathin Nafion films with incorporated  $\text{Ru}(\text{bpy})_3^{2+}$  using Langmuir–Schaefer (LS) technique.<sup>27, 29, 30</sup> It was found that LS ultrathin nafion films show faster responses to changes in their chemical environment concerning ion-exchange and electrochemical properties. The study of ECL dependence on the film thickness shows that thick films ( $> 90$  nm) show low ECL response because electron hopping between oxidised and reduced ruthenium centres, which generates  $\text{Ru}(\text{bpy})_3^{3+}$  at the film/solution interface is limiting. In this case the ECL intensity decreases with the increase of the film thickness, which represents the diffusion length. For thinner films, the generation of the ECL reagent occurs rapidly and the limitation factor becomes diffusion in solution.<sup>29</sup>

Similar results were obtained by Moretto et al. who reported the study of  $\text{Ru}(\text{bpy})_3^{2+}$  loading by Langmuir-Blodgett (LB) technique. The film characteristic was investigated by electrochemical, epifluorescence and ECL measurements. Since the oxidation of  $\text{Ru}(\text{bpy})_3^{2+}$  to  $\text{Ru}(\text{bpy})_3^{3+}$  decreases the intensity of luminescence of the film, the electrochemical switching of epifluorescence was used for studying the response time and ratio between PL and electroactive probes in the film. It was found that electrochemical response of LB films

was very fast for films obtained up to 30 LB layers.<sup>28</sup> The dependence of ECL measurement with  $\text{Ru}(\text{bpy})_3^{2+}$  in the solution as a function of TPrA concentration was studied with nafion film of different LB layers. The evidence that the ECL intensity did not change with nafion film thickness, indicated that the emission occurs mainly at the film/solution interface. Besides, in the study of ECL dependence on the number of LB layers of the  $\text{Ru}(\text{bpy})_3^{2+}$  loaded nafion films, it was observed that ECL emission increases with the number of layers up to reaching a particular constant value for thicker films.<sup>31</sup>

Forster and Rusling reported the application of ultrathin films of a ruthenium-containing metallopolymer.<sup>32, 33</sup> The electrochemical response of thin film layers of  $[\text{Ru}(\text{bpy})_2\text{PVP}_{10}](\text{ClO}_4)_2$  was studied using cyclic voltammetry in 0.1 M  $\text{H}_2\text{SO}_4$ . It has been reported that peak current varies linearly with scan rate up to 30 mV/s, indicating that the response is controlled by finite charge transport diffusion at these long experimental time scale. At shorter experimental time scales, (scan rates are above 100 mV/s), the thickness of depletion layer is smaller than the film thickness and the peak current varies linearly with the square root of the scan rate. These results indicate that voltammetric behaviour of these thin polymer films in sulphuric acid is close to ideal.<sup>32</sup> The application of these metallopolymer films was demonstrated on the ECL detection of oxalate as a model system using flow injection analysis system.<sup>32, 33</sup> The same metallopolymer was used for in the design of 10 nm film assembled layer-by-layer with DNA for direct detection of DNA hybridisation and damage of DNA.<sup>13</sup>

In the same manner, the direct ECL involving oxidised DNA was demonstrated in ultrathin films of  $[\text{Os}(\text{bpy})_2(\text{PVP})_{10}]^{2+}$ . DNA,  $[\text{Ru}(\text{bpy})_2(\text{PVP})_{10}]^{2+}$  and  $[\text{Os}(\text{bpy})_2(\text{PVP})_{10}]^{2+}$  were also incorporated together in films with DNA. Alternate layer-by-layer electrostatic assembly was formed ultrathin metallopolymer film for detection of both DNA oxidation and chemical DNA damage.<sup>12</sup>

The physical diffusion in the deposited film is of great importance for the ECL response of the film. To perform an ECL reaction it is necessary that the coreactant can penetrate in the hydrogel to be oxidised and to react with ruthenium centres. This is possible even with thicker hydrogel films if the level of cross-linking is not too high and the hydrogel is permeable enough. In photopatterning process, the polymerisation in the exposure regions should be fast and completed before rinsing step to stay as a pattern at the electrode surface. Thus the level of cross-linking is higher and obtained hydrogel films are compact with limited diffusion rate. Figure 11 illustrates the ECL response of two photopatterns with hydrogel films of different thickness. Image A) present the case when hydrogel is immobilised in nanometric size (~30

nm) layer and the image B) where hydrogel is immobilised in a layer of micrometric size ( $\sim 20 \mu\text{m}$ ).

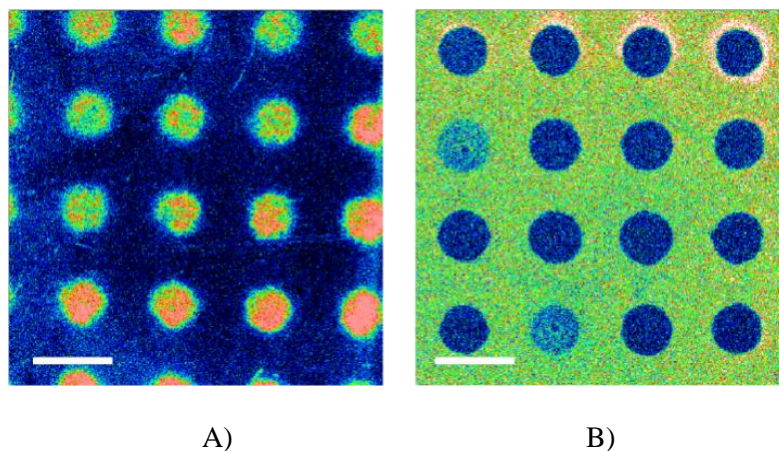


Figure 11. ECL images of photopattern with hydrogel film thickness. A) nanometric and B) micrometric size, white bar  $300 \mu\text{m}$  (automatic intensity scale).

It can be observed that ultrathin photopattern show efficient ECL emission (Figure 11A). On the other hand, the diffusion of coreactant in the micrometric thick pattern is obviously limiting factor. Moreover, the image 11B displays as an image opposite to image 11A with background brighter than photopattern itself. Namely, when immobilised hydrogel is thick the TPrA can not penetrate deep enough neither to be directly oxidised on the electrode surface nor to be oxidised via catalytic route by oxidised ruthenium centres. Thus in the area of photopatterns ECL reaction does not occur. Beside, the small amount of ruthenium complex that remains after the rinsing step on electrode surface reacts with TPrA in the solution emitting the light. The same amount of ruthenium complex probably remains on the electrode surface in all cases but when ultrathin photopatterns shows good ECL response (Figure 11A) the background light emitted from electrode surface becomes negligible.

The thickness of the photodeposited patterns can be analysed using scanning electron microscopy (SEM) only in the case where layer thickness is in micrometric size. For patterns such as presented on the figure 11B the thickness was found to be  $\sim 20 \mu\text{m}$ . The thickness of photopatterns which provide an efficient response and give expected ECL images was under the detection limit of our scanning electron microscope. The thickness of photopatterns in this case was determined using atomic force microscopy (AFM) measurements. Figure 12 shows AFM images obtained with peak force tapping mode of both bare gold and gold surface with the photodeposited film. One can observe that photodeposited films have homogenous surface with thickness of  $30 \text{ nm}$  found out by depth analysis. Since the diameter of the patterns was

up to 200  $\mu\text{m}$ , it was not possible to obtain the AFM image of whole patterns. AFM is sensitive technique thus the maximum distance that can be scanned was 20  $\mu\text{m}$ . For thickness measurement, the image of the edge of the patterns will be the most reliable. However, it was observed that the patterns consist of nanometric peaks of polymer film which frequencies decrease gradually. Thus, no clearly edge was observed. For this reason, the AFM images were recorded on the different parts of a pattern and analysed by depth analysis. The obtained results for the same pattern were in correlation. The roughness was found to be  $\sim 6$  nm.

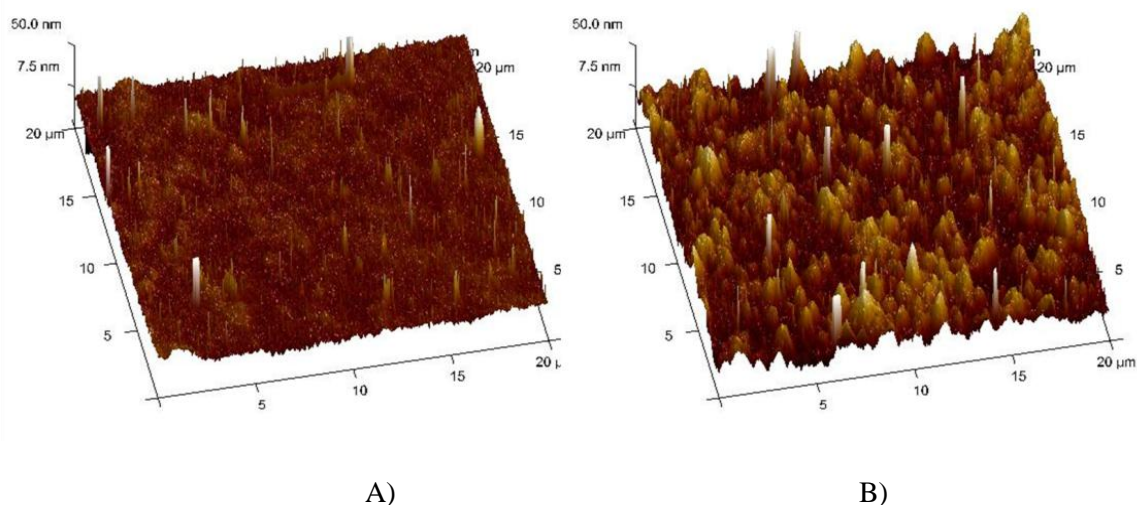


Figure 12. AFM observations of (A) bare gold surface and (B) ultrathin redox polymer film on gold electrode.

The thickness of spin-coated films depends on different parameters including the viscosity of the precursor solution, rotational speed and spin-coating time.<sup>15</sup> In order to control thickness of photopatterns different rotational speeds for the spin-coating step were tested, ranging from 2000 to 10000 rpm. The thickness of the corresponding films could be tuned thus from 30 nm to 100 nm by decreasing the rotational speed.

Thus, it was interesting to study the correlation between the film thickness and ECL intensity. Figure 13 shows the dependence of the ECL intensity on the thickness of the patterns. Regarding the obtained results, the ECL emission increases with pattern thickness up to  $\sim 60$  nm and then decreases rapidly. The possible explanation can be found in limited permeability of photodeposited pattern due to fast and highly cross-linked polymerisation. Even if the structure of the ultrathin film consists of numerous tips (Figure 12B), it should be considered

that AFM image of the pattern is obtained in dry state. When the pattern is in the solution the hydrogel swells and tips probably get in contact so the surface has more uniform shape.

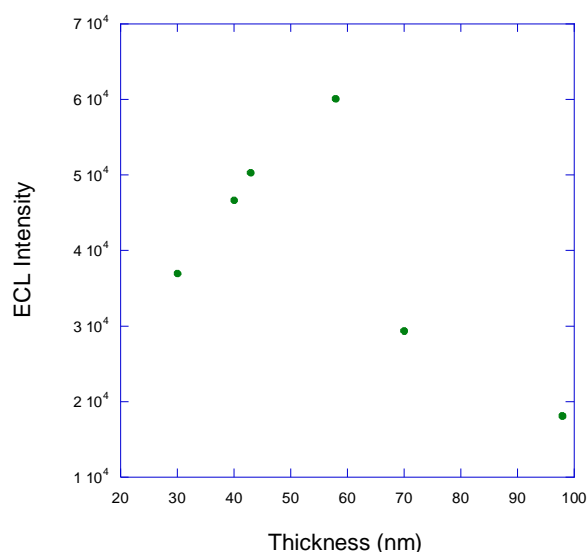


Figure 13. Dependence of the ECL intensity on the thickness of obtained patterns

The ECL reaction can occur if TPrA can be oxidised, in this case more likely via a catalytical route and react with oxidised  $\text{Ru}^{3+}$  centres. The  $\text{Ru}^{2+}$  centres can be electrochemically oxidised only on the electrode surface and in the layer where electron hopping occurs thus the ECL reaction be realised only if the TPrA molecules can reach this layer. In the very thin polymer layer, TPrA obviously react with generated  $\text{Ru}^{3+}$  centres either because the electron hopping occurs in whole polymer layer or because the TPrA can still penetrate in the hydrogel up to certain distance. Therefore, the increase of the thickness has a positive effect on the ECL intensity due to increasing amount of ECL luminophore. With further increase TPrA molecules limited by diffusion in the compact hydrogel can no more rich  $\text{Ru}^{3+}$  centres and ECL intensity decreases very rapidly.

### 3.4. CONCLUSION

Here we presented the photopatterning as a novel method for the immobilisation of ECL films. The method is simple and rapid providing ultrathin films. Moreover, it requires cheap equipment for photolithography. Such a photochemical method allows creating photopatterns of ECL films down to the micrometre scale which have not been reported so far to the best of

our knowledge. The size, shape and thickness of obtained photopatterns can be modulated depending on the fabrication parameters.

Electrochemical characterisation of obtained patterns showed good properties of immobilised films. In the presence of TPrA, photopatterns emit ECL which intensity depend linearly on the TPrA concentration. The relatively fast diffusion in ultrathin hydrogel films and their spatial structuration are important characteristics for the development of new ECL materials and for multiplexed ECL detection. As the photopatterns show strong ECL response, they can be used for ECL imaging and may find application in fabrication of multiplex bioassays with ECL as a readout mechanism.

## REFERENCES

1. L. Song, S. Ahn and D. R. Walt, *Anal. Chem.*, 2006, **78**, 1023.
2. [www.mesoscale.com](http://www.mesoscale.com).
3. S. M. Borisov and O. S. Wolfbeis, *Chem. Rev.*, 2008, **108**, 423.
4. T. O. Joos, D. Stoll and M. F. Templin, *Curr. Opin. Chem. Biol.*, 2002, **6**, 76.
5. T. M. Blicharz, W. L. Siqueira, E. J. Helmerhorst, F. G. Oppenheim, P. J. Wexler, F. Little and D. R. Walt, *Anal. Chem.*, 2009, **81**, 2106.
6. K. L. Michael, L. C. Taylor, S. L. Schultz and D. R. Walt, *Anal. Chem.*, 1998, **70**, 1242.
7. F. Deiss, C. N. LaFratta, M. Symer, T. M. Blicharz, N. Sojic and D. R. Walt, *J. Am. Chem. Soc.*, 2009, **131**, 6088.
8. P. Bertoncello and R. J. Forster, *Biosens. Bioelectron.*, 2009, **24**, 3191.
9. W. Miao, *Chem. Rev.*, 2008, **108**, 2506.
10. S. Krishnan, E. G. Hvastkovs, B. Bajrami, D. Choudhary, J. B. Schenkman and J. F. Rusling, *Anal. Chem.*, 2008, **80**, 5279.
11. S. Pan, L. Zhao, J. B. Schenkman and J. F. Rusling, *Anal. Chem.*, 2011, **83**, 2754.
12. L. Dennany, R. J. Forster, B. White, M. Smyth and J. F. Rusling, *J. Am. Chem. Soc.*, 2004, **126**, 8835.
13. L. Dennany, R. J. Forster and J. F. Rusling, *J. Am. Chem. Soc.*, 2003, **125**, 5213.
14. N. P. Sardesai, J. C. Barron and J. F. Rusling, *Anal. Chem.*, 2011, **83**, 6698.
15. A. Revzin, R. J. Russell, V. K. Yadavalli, W.-G. Koh, C. Deister, D. D. Hile, M. B. Mellott and M. V. Pishko, *Langmuir*, 2001, **17**, 5440.
16. M. S. Hahn, L. J. Taite, J. J. Moon, M. C. Rowland, K. A. Ruffino and J. L. West, *Biomaterials*, 2006, **27**, 2519.
17. K. Sirkar and M. V. Pishko, *Anal. Chem.*, 1998, **70**, 2888.
18. W. G. Koh, A. Revzin and M. V. Pishko, *Langmuir*, 2002, **18**, 2459.
19. A. Mugweru, B. L. Clark and M. V. Pishko, *Electroanal.*, 2007, **19**, 453.
20. M. B. Mellott, K. Searcy and M. V. Pishko, *Biomaterials*, 2001, **22**, 929.
21. E. Suraniti, V. Studer, N. Sojic and N. Mano, *Anal. Chem.*, 2011, **83**, 2824.
22. R. P. Witte, A. J. Blake, C. Palmer and W. J. Kao, *J. Biomed. Mater. Res. Part A*, 2004, **71A**, 508-518.
23. G. M. Wallraff and W. D. Hinsberg, *Chem. Rev.*, 1999, **99**, 1801.



24. T. C. DeVore, B. H. Augustine, A. M. Christenson and G. W. Corder, *J. Chem. Educ.*, 2003, **80**, 183.
25. Y. Wen, Y. Liu, Y. Guo, G. Yu and W. Hu, *Chem. Rev.*, 2011, **111**, 3358.
26. E. Menard, M. A. Meitl, Y. Sun, J.-U. Park, D. J.-L. Shir, Y.-S. Nam, S. Jeon and J. A. Rogers, *Chem. Rev.*, 2007, **107**, 1117.
27. P. Bertoncello, N. R. Wilson and P. R. Unwin, *Soft Matter*, 2007, **3**, 1300.
28. L. M. Moretto, T. Kohls, A. Chovin, N. Sojic and P. Ugo, *Langmuir*, 2008, **24**, 6367.
29. P. Bertoncello, L. Dennany, R. J. Forster and P. R. Unwin, *Anal. Chem.*, 2007, **79**, 7549.
30. P. Bertoncello, M. K. Ram, A. Notargiacomo, P. Ugo and C. Nicolini, *Phys. Chem. Chem. Phys.*, 2002, **4**, 4036.
31. L. M. Moretto, T. Kohls, D. Badocco, P. Pastore, N. Sojic and P. Ugo, *J. Electroanal. Chem.*, 2010, **640**, 35.
32. R. J. Forster and C. F. Hogan, *Anal. Chem.*, 2000, **72**, 5576.
33. C. F. Hogan and R. J. Forster, *Anal. Chim. Acta*, 1999, **396**, 13.

~ ~ ~

## CHAPTER 4:

### ECL IMAGING AT THE SINGLE BEAD LEVEL

~ ~ ~

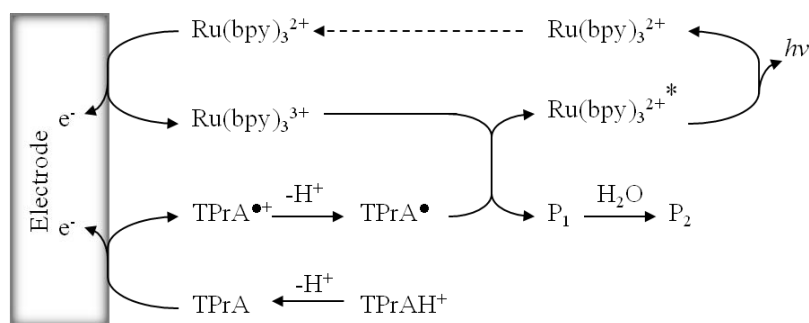
Discovery of coreactant ECL represents a revolutionary step in the applications of ECL. Indeed, the previously used annihilation reaction scheme was achieved almost only in non-aqueous media.<sup>1-3</sup> Thus the analytical applications were very limited. The discovery of coreactant ECL where the reaction occurs between the ECL luminophore and an ECL coreactant in aqueous solutions opened up the possibility for sensitive detection of numerous analytes. By using the  $\text{Ru}(\text{bpy})_3^{2+}$  complex or its derivatives various analytes such as oxalate,<sup>4, 5</sup> NADH,<sup>6</sup> glucose,<sup>7, 8</sup> amines,<sup>9, 10</sup> and amino acids<sup>11</sup> have been detected. It has been found that reaction of  $\text{Ru}(\text{bpy})_3^{2+}$  exhibits the highest ECL efficiency in the presence of tri-n-propylamine (TPrA).<sup>2</sup> Recently, 2-(dibutylamino)ethanol (DBAE) has been reported as more efficient, less toxic, more soluble and less volatile coreactant than TPrA.<sup>12</sup> Despite that, the  $\text{Ru}(\text{bpy})_3^{2+}$ /TPrA system stays the model ECL pair and presents the base of numerous applications such as immunoassays<sup>13-15</sup> and DNA analyses.<sup>15-20</sup> The understanding of the mechanism of the ECL generation is important in designing and selecting new coreactants and in improving the sensitivity and reproducibility of the ECL system. The practical interest lays in commercialised systems that employ ECL as readout mechanism. For example, ORIGEN analyser by Roche Diagnostic provides numerous clinical assays based on functionalised magnetic microbeads. The ECL emission from the beads surfaces and thus the efficiency of the system strongly depends on the mechanistic routes. Since the first ECL reaction between  $\text{Ru}(\text{bpy})_3^{2+}$  and TPrA has been reported,<sup>9</sup> a lot of work was dedicated to decipher the mechanism of this system.<sup>9, 10, 21-26</sup> It has been reported that the mechanism is complex and that it consists mainly on three different routes. The first two routes involve the oxidation of  $\text{Ru}(\text{bpy})_3^{2+}$  at the electrode surface which reacts further with other species and forms an excited state. The third route proposes the possibility to obtain an excited state without the direct oxidation of the complex at the electrode. The excited state is achieved due to presence of free radical and very reactive radical cation of TPrA. As the radical cation is very reactive and short living, different investigations have been done in order to confirm the suggested mechanism. The reported studies are mainly based on detection of the radical cation using different detection methods.<sup>23, 27</sup> In this work we propose single bead imaging as approach to visualise the contribution of the last proposed mechanistic pathway in the  $\text{Ru}(\text{bpy})_3^{2+}$ /TPrA ECL system.

The first part of this chapter deals with already reported studies of reaction mechanism of  $\text{Ru}(\text{bpy})_3^{2+}$ /TPrA system. The second part presents PL and ECL imaging at the single bead level as a new approach to investigate the ECL generation on functionalised beads.

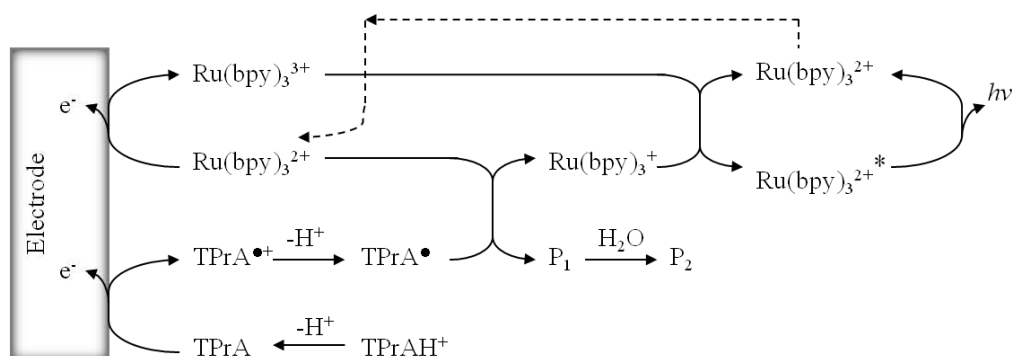
#### 4.1 REPORTED MECHANISMS OF $\text{Ru}(\text{bpy})_3^{2+}$ /TPrA ECL PAIR

The ECL reaction between  $\text{Ru}(\text{bpy})_3^{2+}$  and TPrA was reported for the first time by Leland and Powell.<sup>9</sup> According to this study and other investigations that followed, several mechanisms have been proposed.<sup>9, 21, 22, 25</sup> The mechanisms involve oxidation of both  $\text{Ru}(\text{bpy})_3^{2+}$  and TPrA.  $\text{Ru}(\text{bpy})_3^{2+}$  is oxidised to  $\text{Ru}(\text{bpy})_3^{3+}$  and TPrA is oxidised to reactive radical cation  $\text{TPrA}^{\bullet+}$  that fastly undergoes reaction of deprotonation forming a highly reducing agent  $\text{TPrA}^\bullet$ . This radical is then able to reduce  $\text{Ru}(\text{bpy})_3^{3+}$  to form excited state  $\text{Ru}(\text{bpy})_3^{2+*}$  (Scheme 1). Another reaction that may occur is that highly reducing agent can also reduce  $\text{Ru}(\text{bpy})_3^{2+}$  to  $\text{Ru}(\text{bpy})_3^+$ .  $\text{Ru}(\text{bpy})_3^{3+}$  and  $\text{Ru}(\text{bpy})_3^+$  then react in an annihilation reaction forming an excited state (Scheme 2). The mechanisms are presented in more details in Chapter 1 of this thesis.

Scheme 1:

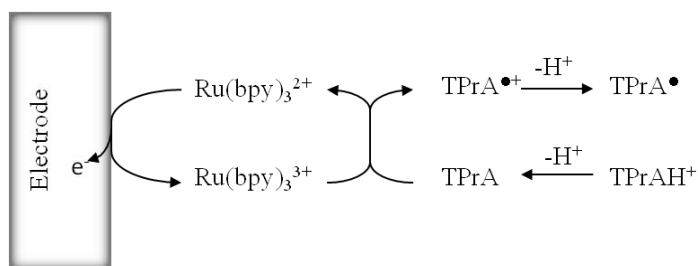


Scheme 2:



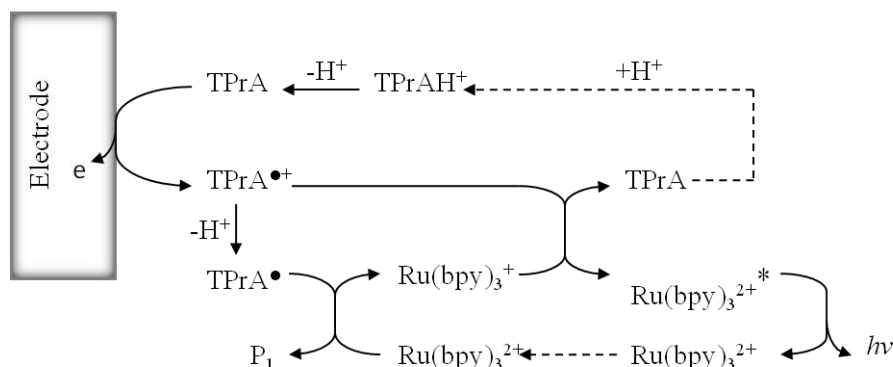
It has been reported that TPrA can be oxidised directly at the electrode surface, but also via catalytic homogeneous reaction with  $\text{Ru}(\text{bpy})_3^{3+}$  (Scheme 3).<sup>21, 22</sup>

Scheme 3:



The homogeneous oxidation has an important contribution to overall ECL reaction when the concentration of  $\text{Ru}(\text{bpy})_3^{2+}$  is relatively high. Otherwise, direct oxidation may be dominant. Zu and Bard have investigated the role of direct coreactant oxidation on the glassy carbon, gold and platinum electrode.<sup>21</sup> In the experiments performed on the glassy carbon electrode in the  $\mu\text{M}$  range of  $\text{Ru}(\text{bpy})_3^{2+}$  concentration, the ECL curve showed two peaks. The first ECL peak appeared at a potential less positive than the oxidation potential of  $\text{Ru}(\text{bpy})_3^{2+}$  while the second ECL peak appeared along with peak current of  $\text{Ru}(\text{bpy})_3^{2+}$  oxidation. The ECL emission observed at a potential less positive than the oxidation potential of  $\text{Ru}(\text{bpy})_3^{2+}$  was not possible to be explained by the presented mechanisms which are based on previous oxidation of ruthenium complex. The first peak showed dependence on the electrode material and it was not recorded at Au and Pt electrode. This led to the conclusion that the first ECL peak strongly depends on direct oxidation of TPrA since the TPrA oxidation is blocked on Au and Pt electrode due to formation of surface oxides.<sup>21</sup> Further, the ECL spectrum obtained at potential of the first peak shows that the emitted light was the emission of  $\text{Ru}(\text{bpy})_3^{2+*}$ .<sup>23</sup> Because the direct oxidation of TPrA leads to the formation of reducing radicals  $\text{TPrA}^\bullet$  that could react with  $\text{Ru}(\text{bpy})_3^{2+}$  to generate  $\text{Ru}(\text{bpy})_3^+$ , authors suggested that one possible way to produce  $\text{Ru}(\text{bpy})_3^{2+*}$  could be electron transfer from  $\text{Ru}(\text{bpy})_3^+$  to some oxidative species.<sup>21</sup> Two years later Miao and Bard reported a new revisited mechanistic route involving  $\text{TPrA}^{\bullet+}$  cation radicals.<sup>23</sup> The mechanism is based on the assumption that  $\text{TPrA}^{\bullet+}$  which is a very reactive intermediate, has a life-time long enough to react itself before it undergoes deprotonation. Namely, TPrA is oxidised at the electrode surface forming very reactive  $\text{TPrA}^{\bullet+}$  cation radicals which loses one proton forming highly reducing agent  $\text{TPrA}^\bullet$ . This radical is then able to reduce present  $\text{Ru}(\text{bpy})_3^{2+}$  to  $\text{Ru}(\text{bpy})_3^+$ . In the same time produced  $\text{TPrA}^{\bullet+}$  behaves like strong oxidant and it oxidises  $\text{Ru}(\text{bpy})_3^+$  to form an excited state (Scheme 4).<sup>23</sup>

Scheme 4.



To verify this assumption, several experiments were performed. To check whether the light emission occurs without direct oxidation of  $\text{Ru}(\text{bpy})_3^{2+}$  scanning electrochemical microscopy SECM-ECL experiments have been realised.<sup>23</sup> In this experiment,  $\text{Ru}(\text{bpy})_2[\text{bpy}(\text{COOH})_2]^{2+}$ , whose ECL behaviour is very similar to  $\text{Ru}(\text{bpy})_3^{2+}$  in the presence of TPrA, was covalently immobilised on an ITO electrode to serve as the substrate. To avoid the direct oxidation of  $\text{Ru}(\text{bpy})_2[\text{bpy}(\text{COOH})_2]^{2+}$ , during the course of SECM-ECL experiment, the modified ITO electrode was at an open circuit potential. The tip (working electrode) was 1.5 mm diameter hemispherical Au tip. The reaction medium was a buffer solution with TPrA. The tip was withdrawn from the surface to the certain distance and current and ECL signal were monitored during voltammetric cycle between 0 and 1.0 V vs. Ag/AgCl/KCl. It was detected that upon oxidation of TPrA at  $\sim 0.80$  V vs. Ag/AgCl/KCl the ECL signal appears and tracks the tip current during potential cycling. It was found that ECL signal could be detected only within very short distance ( $\sim 5\text{-}6$   $\mu\text{m}$ ) and that it decreases almost exponentially with increasing the distance. This experiment clearly demonstrates that, by simple oxidising TPrA, intermediates are formed that generate ECL emission of  $\text{Ru}(\text{bpy})_3^{2+}$ .

Since the maximum distance at which light was observed was  $\sim 6$   $\mu\text{m}$ , it represents the distance that  $\text{TPrA}^{\bullet+}$  can diffuse before deprotonation. The half-life of the cation radical was estimated at  $\sim 0.2$  ms taking the typical diffusion coefficient of  $5 \times 10^{-6}$   $\text{cm}^2/\text{s}$ .

The same group reported the detection of  $\text{TPrA}^{\bullet+}$  by using electron spin resonance (ESR).<sup>23</sup> The investigation was based on the previous studies which have shown that trimethylamine radical cation has a similar lifetime as that estimated for  $\text{TPrA}^{\bullet+}$ . The ESR spectrum showed good correlation with simulated spectrum indicating the direct evidence for  $\text{TPrA}^{\bullet+}$ .

The effect of the revisited mechanism on the overall ECL signal was reported by Zanarini et al.<sup>28</sup> In this work they used silica nanoparticles size around 18 nm covalently doped with

$\text{Ru}(\text{bpy})_3^{2+}$ . Self-assembled monolayer (SAM) of covalently doped silica nanoparticles (DSNP) that can be considered as model systems for probe-target assays was prepared on a gold working electrode. The gold electrodes functionalised with DSNP-SH SAM were characterised by CV. It was reported that oxidation of  $\text{Ru}(\text{bpy})_3^{2+}$  units was not visible and that the voltammetric curve was governed by two different phenomena: stripping of the DSNP-SH SAM and formation and reduction of Au oxides on the substrate.

The ECL intensity was measured in PBS with 30 mM TPrA during cyclic voltammetric scans and results obtained in the first two cycles were compared. The ECL profile showed two peaks located at +0.91 and +1.23 V vs. Ag/AgCl/KCl, compatible with known mechanism. Such peaks were observed in both cycles. However, while the intensity of the peak at 1.23 V remained almost unchanged, the first peak decreased by factor of 10 after the first scan. It becomes almost negligible compared with the second one. These results were explained with respect to direct oxidation of TPrA. Namely, in the first scan, the Au electrode was covered with hydrophobic SAM which prevents the formation of surface oxides and allows direct oxidation of TPrA and to produce high concentration of  $\text{TPrA}^{\bullet+}$ . These species can diffuse into the porous silica particles and generate excited state. In the following scans, detachment of the SAM occurs and direct oxidation of TPrA becomes less efficient thus the ECL profile shows dependence only on direct oxidation of  $\text{Ru}(\text{bpy})_3^{2+}$  confined only at ~1-2 nm from the electrode.<sup>28</sup> The overall decrease of ECL intensity clearly indicates the importance of the ECL emission with no direct oxidation of  $\text{Ru}(\text{bpy})_3^{2+}$  on the sensitivity of bead based assays.

Another example that indicates the contribution of the revisited mechanism to ECL emission has been reported by Li et al.<sup>29</sup> They synthesised multifunctional nanoparticles (NPs) that consist of silica-coated magnetic cores and luminescent ruthenium(II) polypyridine complexes. Multifunctional core-shell magnetic silica nanocomposites consisted of  $\text{Fe}_3\text{O}_4$  core coated with a silica shell, to which luminescent ruthenium(II) complexes  $[\text{Ru}(\text{bpy})_2(\text{phen-Si})]^{2+}$  were covalently attached and further encapsulated with an additional layer of silica shell. The first layer of silica coating serves to isolate the ruthenium(II) polypyridine luminophore from the magnetic core to avoid luminescence quenching and to provide silanol groups for the covalent immobilization of the ruthenium(II) complexes. The thin layer of silica shell at the surface of the nanoparticles serves to avoid the direct contact of the ruthenium(II) complexes with the electrode surface to prevent their direct oxidation on the electrode surface. The size of these luminomagnetic NPs was 18 nm where silica shell thickness was about 7 nm. The electrochemical characterization of obtained luminomagnetic NPs was performed on gold electrode in PBS. NPs were magnetically deposited on the

electrode surface. Cyclic voltammogram, of the luminomagnetic NPs coated gold electrode exhibited characteristic redox waves similar to those of the bare gold electrode, except that the active surface area was slightly smaller. The redox wave corresponding to the  $\text{Ru}^{3+/2+}$  couple was not observed, indicating that most of the  $[\text{Ru}(\text{bpy})_2(\text{phen-Si})]^{2+}$  species were out of the electron tunneling distance from the electrode and could not be oxidised directly. The ECL experiments were performed in 1 mM TPrA solution before and after the addition of fluorosurfactant (FSO) species. In the absence of FSO, TPrA oxidation occurred in the potential region where the electrode surface oxides start to be formed and the oxidation current overlapped completely with that of the gold surface. The ECL peak appeared at the potential more positive than potential of TPrA oxidation and more likely at the potential of eventual oxidation of  $[\text{Ru}(\text{bpy})_2(\text{phen-Si})]^{2+}$  species indicating that ECL was produced *via* the conventional emission routes. From other hand, when FSO was present in the solution, the initial growth of the electrode surface oxides was significantly suppressed, and TPrA oxidation was more efficient. In this case, ECL signal appeared along with the TPrA oxidation. This peak was 110-fold enhanced in comparison with the ECL peak obtained in the previous case, which shows the importance of mechanism based on  $\text{TPrA}^{*+}$  in the efficiency of bead based experiments.

The understanding of ECL mechanism and its influence on ECL emission at the single bead level is of great importance considering numerous bead based analysis. ORIGEN Analyser provided by IGEN International, Inc. (now BioVers, part of Roche Diagnostic corp.), is the first commercialised system based on ECL as detection method.<sup>30</sup> The use of ECL detection has many advantages over other detection systems. The labels are not radioactive and they are stable compared with those of most other chemiluminescent systems. The detection limits for label are extremely low (200 fmol/L) with dynamic range of quantification over six orders of magnitude.<sup>15</sup> The ORIGEN Analyser is adapted to measure ECL labels presented on the surface of magnetic beads. The instrument consists of flow cell containing a reusable platinum electrode and a PMT for light detection.

The ECL labels are usually  $\text{Ru}(\text{bpy})_3^{2+}$  derivatives which can bind to biomolecules. The binding of ECL label to the magnetic beads depends on assay format. In sandwich immunoassay, for example, antibody coated magnetic beads are used to bind the detection antigen and secondary ECL labeled antibody. The binding is usually running offline. Then, each individual sample is drawn into the flow cell, where the paramagnetic beads are magnetically captured on the electrode surface. By this way the labels attached to the beads



are concentrated on the electrode surface which increases the sensitivity. A solution containing TPrA is then drawn through the flow cell to wash the beads and supply coreactant for ECL, which is initiated by applying potential between the working and counter electrodes. The emitted light is detected using a PMT. The beads are then washed from the cell, and a cleaning solution is drawn into the cell to leave the surfaces of the electrodes in a reproducible state, ready for the next measurement.<sup>31</sup>

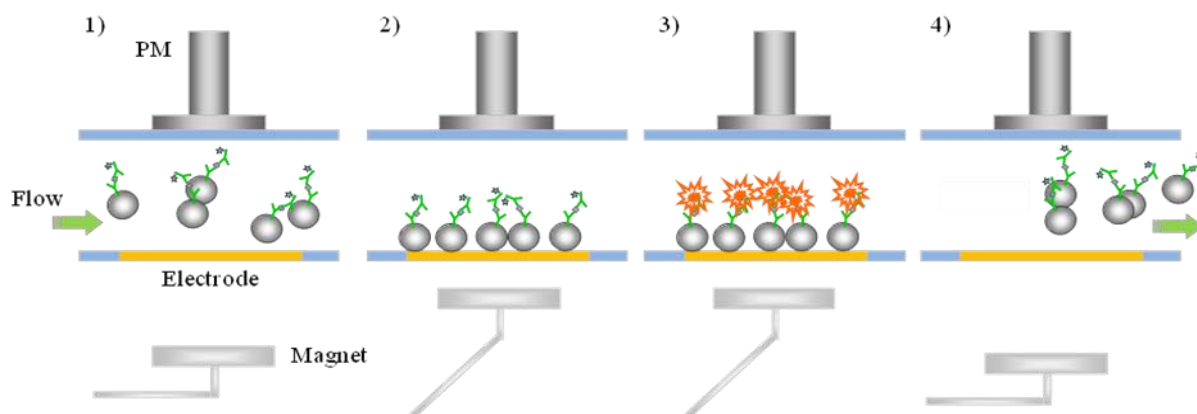


Figure 1. Generic process for measuring magnetic bead-based ECL assays in flow cells. 1) Introducing magnetic beads with bound assay component; 2) Capturing of magnetic particles with magnetic field, introducing the TPrA buffer; 3) Applying the electrode potential to induce ECL; 4) Washing out of the beads

Now, there are several commercial systems that are based on ORIGIN technology.

These instruments are designed for a variety of applications in life sciences, high-throughput drug screening, and food, water, and animal health testing. Roche Diagnostics markets different analyzers based on ORIGIN technology for clinical immunoassay testing. These systems feature an expansive menu of over 50 immunoassay tests in the areas of cardiology, fertility, thyroid function, oncology, anemia, infectious disease, and osteoporosis.<sup>31</sup>

In the research field, beads based ECL assays have been also reported. A very sensitive immunoassay based on the similar instrumentation as in commercial systems have been reported. The application of the system was presented on detection of alpha-fetoprotein (AFP).<sup>32</sup> The magnetic beads coated with anti-AFP antibodies was used for binding of AFP in sandwich type immunoassay with  $\text{Ru}(\text{bpy})_3^{2+}$ -NHS labelled secondary anti-AFP antibodies. Employing ECL detection of beads confined to the electrode surface the detection reached sensitivity to the level of 5 pg/mL of the AFP with wide dynamic range.<sup>32</sup>

Miao and Bard reported an ultrasensitive DNA hybridisation detection based on the use of magnetic beads as support and polystyrene microspheres/beads (PSB) as the carrier of the ECL labels.<sup>18</sup> Probe single-stranded DNA (p-ssDNA) was attached to the surface of magnetic

beads (~ 1.0 and 2.8  $\mu\text{m}$  diameter) and hybridised with target-ssDNA (t-ssDNA) immobilised on PSB. The 10  $\mu\text{m}$  diameter PSB were loaded with large amount of tris(2,2-bipyridyl)ruthenium(II) tetrakis(pentafluorophenyl)borate ( $\text{Ru}(\text{bpy})_3\text{-}[\text{B}(\text{C}_6\text{F}_5)_4]_2$ ) species.

With this approach a large amplification factor of  $\text{Ru}(\text{bpy})_3\text{[B(C}_6\text{F}_5)_4]_2$  molecules for each t-ssDNA can be achieved, when each PSB is attached to a limited number of t-ssDNA. The formed conjugates were magnetically separated from reaction solution and dissolved in acetonitrile. The ECL intensity was measured during potential scan in acetonitrile in the presence of TPrA. The ECL intensity showed linear dependence of t-ssDNA in the range 1.0 fM to 10 nM. It was found that ECL signals associated with two base pairs mismatched ssDNA and non-complementary ssDNA can be distinguished well from the ECL signal related to the complementary DNA hybridisation.

The same group reported the detection of C-reactive protein (CRP), an acute-phase protein found in human serum, using the same polystyrene microspheres as the carrier of the ECL labels.<sup>33</sup> Biotinylated anti-C-reactive protein (CRP) species were attached to the surface of streptavidin-coated magnetic beads (MB) to form Anti-CRP $\leftrightarrow$ MB. To be labeled biotinylated Anti-CRP was attached to avidin-coated polystyrene microspheres (PSB) in which was entrapped the large number of  $\text{Ru}(\text{bpy})_3\text{-}[\text{B}(\text{C}_6\text{F}_5)_4]_2$  forming Ru(II)-PSB $\leftrightarrow$ Anti-CRP. When PSB is used there is no need of the direct attachment of the ECL labels to the antibody, so that the loading capacity of the ECL labels per PSB can be very high which amplify the ECL signal for each molecule of analyte. The sandwich assay was performed by mixing Anti-CRP $\leftrightarrow$ MB and Ru(II)-PSB $\leftrightarrow$ Anti-CRP in the presence of C-reactive protein (CRP). This leads to the formation of sandwich format and Ru(II)-PSB $\leftrightarrow$ Anti-CRP<CRP>Anti-CRP $\leftrightarrow$ MB. The beads were magnetically separated from reaction solution and dissolved in acetonitrile containing TPrA. ECL signal was measured by PMT during a potential scan. ECL intensity was found to be proportional to the analyte CRP concentration over the range 0.010-10  $\mu\text{g/mL}$ .<sup>33</sup>

Zhou et al. reported the application of magnetic bead-based assay for detection of telomerase activity.<sup>34, 35</sup> Human telomerase is a ribonucleoprotein complex which is inactivated in most somatic cells and reactivated in most cancer cells. The ECL detection was developed with and without telomere repeat amplification protocol (TRAP). The direct detection of telomerase activity was accomplished by the hybridization of ECL nanoprobe to telomerase reaction products. The assay was immobilised on the streptavidin coated magnetic beads that were used as both separation tool and immobilization matrix. The measured ECL intensity directly reflects the quantity of telomerase reaction products, thus telomerase activity.<sup>34</sup>

A different approach of immunoassay which employs beads was reported by Deiss et al.<sup>13</sup> In this case 3.1  $\mu\text{m}$  polystyrene microspheres were immobilised on the surfaces of gold coated optical fibre bundle. To perform sandwich immunoassay, the beads modified with antigen were incubated first with antigen and then with secondary labelled antibody. The beads were then loaded in the wells of etched and gold-coated optical fibre bundle which act as working electrode. The ECL intensity was detected using a CCD camera to perform ECL imaging of immobilised beads. This detection is different from previously reported examples where in the follow cell beads are magnetically attracted to the electrode surface and ECL emission is detected using PMT and displayed as intensity curve. The main advantage of this system is the possibility of multiplexing assays which is explained in the paragraph 3.1.2. of this thesis. The simultaneous detection of antigens VEGF, IL-8, and TIMP-1 was reported.<sup>13</sup>

#### 4.2. THE CONCEPT OF SINGLE BEAD IMAGING

Since there are numerous examples of bead based assays, the study of ECL mechanism is of great importance for improving the system efficiency and developing new protocols. When  $\text{Ru}(\text{bpy})_3^{2+}$  modified beads are immobilised on the electrode surface and immersed in the TPrA solution, ECL emission can be generated via different routes. The direct oxidation of  $\text{Ru}(\text{bpy})_3^{2+}$  species can occur only in the electron tunnelling distance from the electrode surface. Thus, if ECL emission appears only due to mechanism which involves direct oxidation of  $\text{Ru}(\text{bpy})_3^{2+}$ , most of the label on the bead would not contribute to the ECL response. However, the high sensitivity of the bead based assays indicated that most of the labels on the beads participate to the reaction. This leads to the conclusion that revisited mechanism which involves  $\text{TPrA}^{*+}$  species may have an important contribution. To visualise the distribution of ECL emission from the beads surface and thus the contribution of different mechanisms, PL and ECL were both imaged at single bead level. To simulate the assay, 6  $\mu\text{m}$  diameter polystyrene beads were used. The surface of the beads was modified with  $\text{Ru}(\text{bpy})_3^{2+}$  labels. The size of the beads was chosen in respect to the reported experiments that  $\text{TPrA}^{*+}$  species may diffuse up to 6  $\mu\text{m}$  from electrode surface before they undergo deprotonation.<sup>23</sup> Thus, if the ECL emission appears only via routes based on direct oxidation of  $\text{Ru}(\text{bpy})_3^{2+}$  labels, the light will be emitted only from the narrow part of the bead close to the electrode surface (Figure 2A). Besides, if revisited mechanism is involved, ECL emission will appear from whole bead surface which intensity will depend on the gradient of  $\text{TPrA}^{*+}$  concentration (Figure 2B).

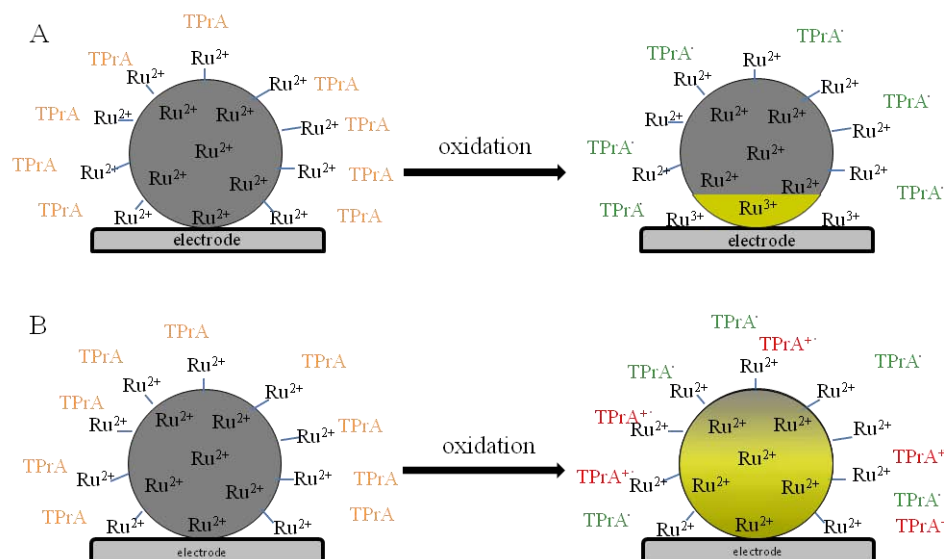


Figure 2. Expected ECL bead profile if A) the revisited mechanism does not take part; b) the revisited mechanism is involved in the ECL reaction

The ECL emission from the bead surface depends on different parameters such as TPrA concentration and electrode material. ECL imaging can give direct overview on efficiency of the system and thus may be used as a convenient approach for monitoring the optimisation of an assay.

To demonstrate the concept, -NH<sub>2</sub> functionalised 6  $\mu$ m diameter polystyrene beads were modified with Ru(bpy)<sub>3</sub><sup>2+</sup>-NHS ester (bis(2,2'-bipyridine)-4'-methyl-4-carboxybipyridine-ruthenium N-succinimidyl ester-bis(hexafluorophosphate)).

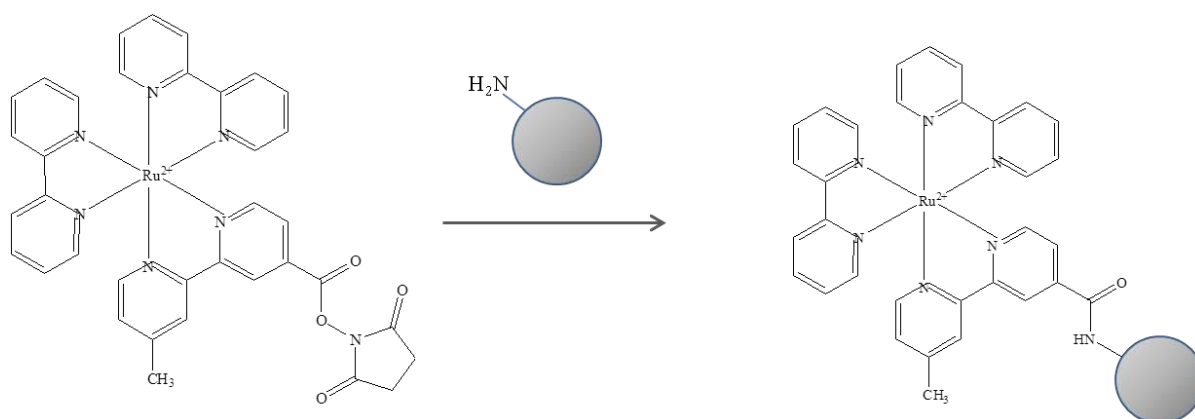


Figure 3. Modification of beads surface by Ru(bpy)<sub>3</sub><sup>2+</sup>-NHS ester

Ru(bpy)<sub>3</sub><sup>2+</sup>-NHS ester is often used as an ECL label because it can easily bind to -NH<sub>2</sub> groups forming the amide bond and its ECL behaviour is very similar to that of Ru(bpy)<sub>3</sub><sup>2+</sup>.

#### 4.2.1. Electrochemical characterisation

The beads which surface were modified with  $\text{Ru}(\text{bpy})_3^{2+}$  complex was deposited on the electrode surface by drop-coating and let to dry on the room temperature, protected from the light. The electrochemical response of deposited  $\text{Ru}(\text{bpy})_3^{2+}$  modified beads was studied on GC electrode using cyclic voltammerty. The characterisation was performed in a 100 mM phosphate buffer (pH=7.4). CV curves obtained for bare GC electrode (red) and  $\text{Ru}(\text{bpy})_3^{2+}$  modified beads deposited on the GC electrode (blue) are compared on Figure 4.

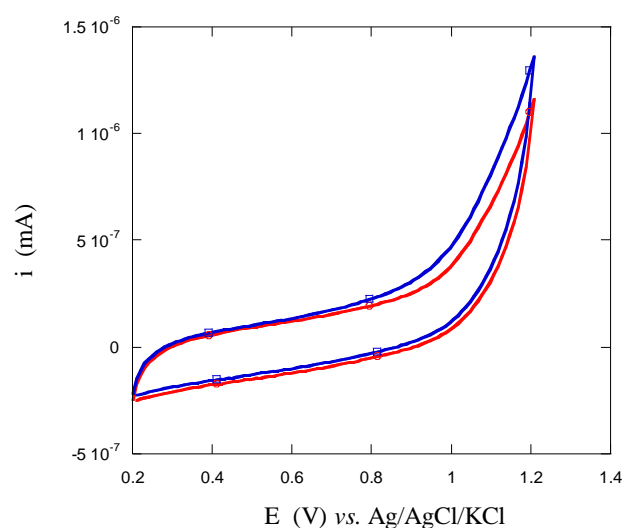


Figure 4. Cyclic voltammograms of bare GC electrode (red) and  $\text{Ru}(\text{bpy})_3^{2+}$  modified beads deposited on the GC electrode (blue) in 100 mM phosphate buffer (pH=7.4), scan rate 50 mV/s

The curves are very similar. On the blue curve, which correspond to GC electrode with deposited beads, no clear oxidation peak can be observed. This may be explained by distribution of  $\text{Ru}(\text{bpy})_3^{2+}$ -centres on the electrode surface. Namely, the direct oxidation of  $\text{Ru}(\text{bpy})_3^{2+}$  occurs only when they are in contact with electrode and in the electron tunnelling distance. Concerning the spherical geometry of the beads, only a small part of the bead is in contact with electrode. Electron tunnelling usually appears at a distance of few nanometres. As a result, a small number of  $\text{Ru}(\text{bpy})_3^{2+}$  molecules are directly oxidised on the electrode surface which was in our case, under the detection limit.

#### 4.2.2. Photoluminescence imaging

The spectral characteristic of  $\text{Ru}(\text{bpy})_3^{2+}$  are presented in Chapter 1 of this thesis.  $\text{Ru}^{2+}$  centre has electron configuration  $[\text{Kr}] 4d^6$ . When it is coordinated with three bidentate polypyridine ligands it shows characteristic photoluminescent emission at  $\sim 610 \text{ nm}$ .<sup>36-38</sup> The emission comes from one electron excitation from metal HOMO (highest occupied molecular orbital) to ligand LUMO (lowest unoccupied molecular orbital), which results in MLCT (metal-to-ligand charge transfer). When  $\text{Ru}(\text{bpy})_3^{2+}$  is oxidised,  $\text{Ru}^{3+}$  has electron configuration  $[\text{Kr}]4d^5$ . In electron deficient  $d^5$  centre the charge transfer occurs by excitation of the electron localised in ligand network with low extinction coefficient.<sup>37</sup> Thus, the oxidation of  $\text{Ru}(\text{bpy})_3^{2+}$  to  $\text{Ru}(\text{bpy})_3^{3+}$  results in a decrease of photoluminescent emission which is known as oxidative quenching.<sup>36</sup> For this reason, the photoluminescence (PL) imaging may be used for investigation of direct oxidation of bead labelled  $\text{Ru}(\text{bpy})_3^{2+}$  species. As the direct oxidation occurs only close to the electrode surface, in the absence of electron-hopping, the decreasing of PL from the bead surface is expected in the narrow part of the bead in the direct contact to electrode surface.

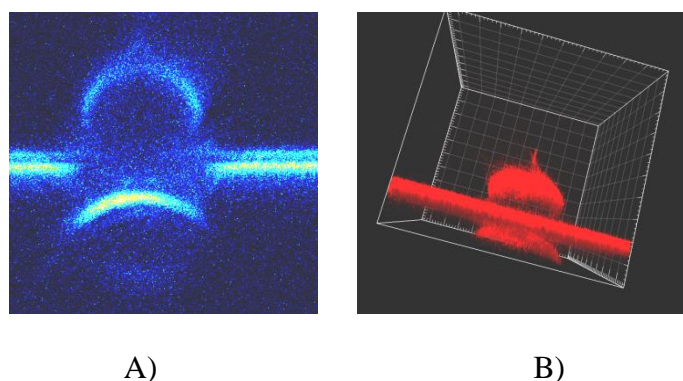


Figure 5. PL images of  $6 \mu\text{m}$   $\text{Ru}(\text{bpy})_3^{2+}$  modified beads on gold plate A) 2D profile image B) 3D reconstruction obtained by confocal microscope

Figure 5 shows a profile PL image of a  $6 \mu\text{m}$  diameter polystyrene  $\text{Ru}(\text{bpy})_3^{2+}$  modified bead immobilised on gold plate electrode.

Using confocal microscopy, images are obtained by scanning the sample with focused light beam. When series of images are obtained for different focal plane they may be used for 3D reconstruction. In this case, optical set-up was parallel with microscope objective and images were collected from the top of the bead toward to electrode surface. The presented image was obtained by reconstruction of Z-stacking. It can be observed that  $\text{Ru}(\text{bpy})_3^{2+}$  is attached to the

polystyrene beads surface, with no entrapment of  $\text{Ru}(\text{bpy})_3^{2+}$ -NHS ester inside the beads (Figure 5A). Nevertheless, the image shows irregular shape due to reflection of the gold surface. The effect of reflection is well visible on the 3D reconstruction (Figure 5B). Despite these problems, to verify whether the PL emission decrease in the region of the bead close to electrode surface, series of PL images were recorded during different step potentials (Figure 6).

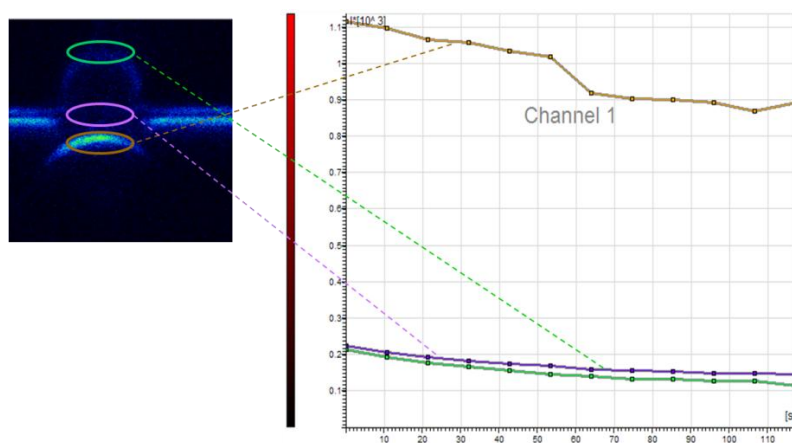


Figure 6. Time monitoring of PL intensity of a bead on gold electrode in PBS. Step 1: 30 s at 0 V; Step 2: 60 s at 1.2 V; Step 3: 30 s at 0 V *vs.* Ag wire

Even if the problem of optical reflection on the sphere can affect the results, the PL intensity of different regions of the bead has been compared. It can be seen that intensity of PL emission from the top and the bottom of the bead decrease slowly with no noticeable difference when the potential was changed (at 30 and 90 s). The slightly decreasing of PL intensity can be attributed to photobleaching. From the region that correspond to the bead reflection the intensity decrease faster but again without any correlation with potential change. Using this technique the influence of ruthenium oxidation on the intensity of PL emission was not possible to observe probably because the oxidation appears in the distance of few nm from the electrode surface which is not observable with resolution provided by confocal microscopy.

#### 4.2.3. ECL imaging

Confocal microscopy is optical imaging technique with improved resolution. It offers several advantages over the conventional optical microscopy including reduce out-of-focus light detection and the ability to collect serial optical sections from thick specimens. The last one is especially important in bead imaging because it allows the construction of profile image from

any orientation of the electrode surface toward the objective. The illumination is achieved by scanning the focused beam, usually from a laser passing through a pinhole. Only the light that is produced by fluorescence very close to the focal plane can be detected. Thus, the out-of-focus light detection is avoided and optical resolution of the image is much better than that of wide-field microscopes. However, as much of the light from sample is blocked at the pinhole, the resolution increases while the signal intensity decreases. This can be a limiting factor in using confocal microscopy in ECL imaging. Several attempts to obtain the ECL image in the conditions similar to PL images (figure 5A) have been performed but the recording was not sensitive enough and no ECL image was obtained.

Thus, a conventional wide-field epifluorescent microscope was used. The disadvantage is that there is no possibility of 3D reconstruction and profile imaging from any orientation of the electrode surface toward the objective. For the other side, classic epifluorescent microscope was equipped with EM-CCD camera providing high sensitivity, exceptional stability and extremely low noise. The first experiments were done with direct view on the beads at the electrode surface. The glassy carbon electrode with immobilised beads was placed in special electrochemical cell with transparent window. The electrode surface was orientated parallel with objective lens. A Pt wire and Ag/AgCl/KCl were the counter and reference electrode, respectively. The cell was filled up with solution of 100 mM TPrA. To obtain the position of the beads on the surface, the photoluminescent mode was used with excitation at 485 nm and emission at 605 nm. The ECL image of the same focal plane was realised in the same configuration with no use of excitation light but with applied potential at 1.2 V vs. Ag/AgCl/KCl during the exposure. The EM-CCD mode of camera and 20 s of exposure were used to record the image. Figure 7 displays a PL and ECL images of the same beads.

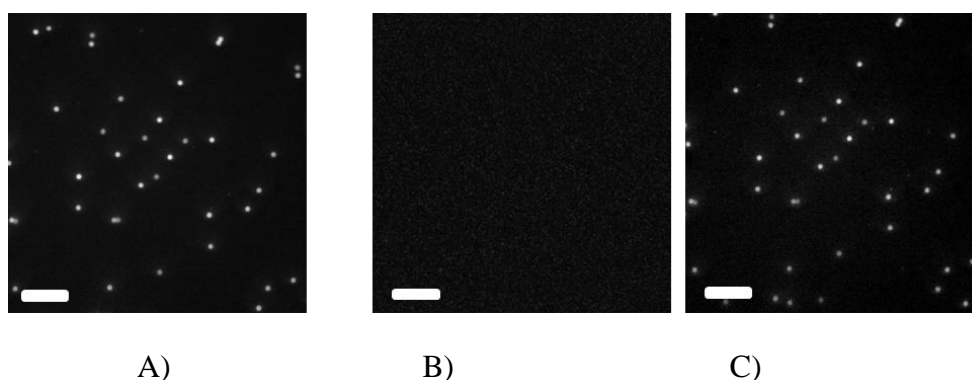


Figure 7. A) PL image; B) ECL images without potential application and C) with potential application at 1.2 V vs. Ag/AgCl/KCl in 100 mM TPrA, white bar 50  $\mu\text{m}$



It can be seen that PL and ECL images correspond one to the other. Further, from control ECL image, it is obvious that when potential is not applied no emission of light occurs. To study the dependence of the ECL emission on the electrode potential, a series of ECL images were recorded during a cyclic voltammetric scan (Figure 8).

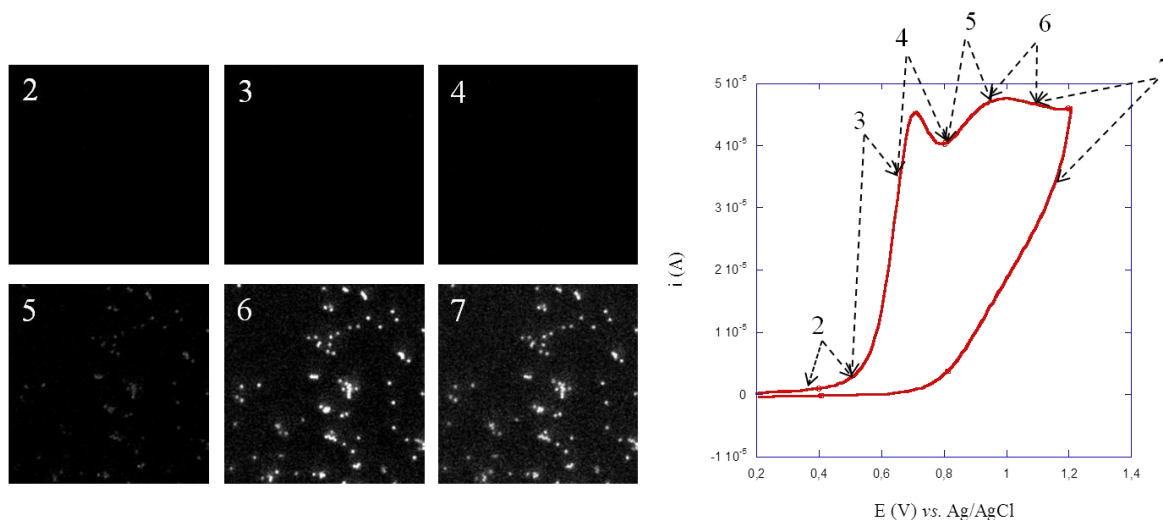


Figure 8. Series of ECL images obtained during votammetric cycle. Exposure time of each image is 3 s which corresponds to certain part of cyclic voltammogram. ECL performed on glassy carbon electrode in 100 mM TPrA. Scan rate 50 mV/s. All images presented in the same intensity range.

In anodic part of the cycle two separated current peaks appear. The first peaks at +0.7 V vs. Ag/AgCl/KCl corresponds to the direct oxidation of TPrA at the electrode surface. The second one appears at the oxidation potential of ruthenium centre at +1.0 V vs. Ag/AgCl/KCl. Regarding the ECL images with respect to the cyclic voltammogram, there is no ECL emission detected during the direct oxidation of TPrA (Figure 8, image 4). However, a weak ECL image was obtained in the part of the voltammogram after the TPrA oxidation and before the oxidation of  $\text{Ru}(\text{bpy})_3^{2+}$  (Figure 8, image 5). Finally, after the oxidation of  $\text{Ru}(\text{bpy})_3^{2+}$  the light intensity on the ECL images drastically increased (Figure 8, images 6 and 7). The results obtained in this experiment lead to conclusion that in this case the mechanisms based on direct oxidation of ruthenium centres have greater contribution on ECL emission that one based on  $\text{TPrA}^{*+}$  as the reactive reagent.

The contribution of each involved mechanism has a great influence on the distribution of light emission from the bead surface. If the ECL reaction involves only mechanisms which are based on direct oxidation of  $\text{Ru}^{2+}$  centres, the ECL will be emitted only in the electron hopping distance. However, if the revisited mechanism is involved in the reaction, the ECL

will be generated in the distance which depends on the diffusion of  $\text{TPrA}^{*+}$ . This distance may be estimated from comparison of bead diameter on PL and ECL image. On figure 9 are compared diameters of a bead on PL and ECL images. It can be notice that for 6  $\mu\text{m}$  bead the diameter is the same on PL and ECL image which indicate that at least half part of the bead emit ECL. This means that diffusion distance of  $\text{TPrA}^{*+}$  is at least 3  $\mu\text{m}$ . By repeating the experiment using the beads with different size it could be possible to estimate up to which size of the bead the diameters are the same on PL and ECL images and thus up to which distance from the electrode surface  $\text{TPrA}^{*+}$  can diffuse. Taking in account that these beads are transparent and, due to spherical geometry, have specific optical properties this approach may be used only for estimation.

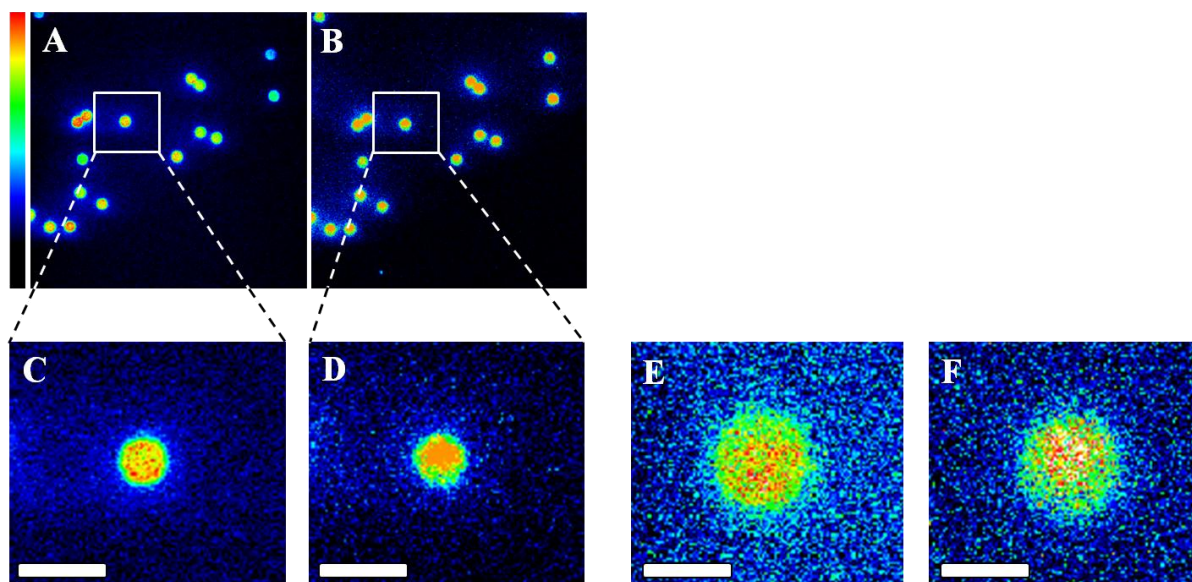


Figure 9. PL and ECL images of 6  $\mu\text{m}$  diameter beads. A and B PL and ECL images, respectively, magnification 50x; C and D particular view on one bead from image A and B, respectively; E and F PL and ECL image of 6  $\mu\text{m}$  diameter beads, magnification 100x.

To visualise the  $\text{TPrA}^{*+}$  diffusion distance and light distribution on the bead surface, the profile ECL bead image should be realised. For this, the working electrode with immobilised beads was orientated so that surface of the electrode was perpendicular toward the microscope objective.

Figure 10 shows pairs of PL and ECL images obtained with 20x and 50x objective magnification, respectively. The images using 100x objective magnification have also been recorded but probably due to low numerical aperture (0.80) the ECL signal on direct view ECL images was very low while in profile view images no ECL response have been detected.

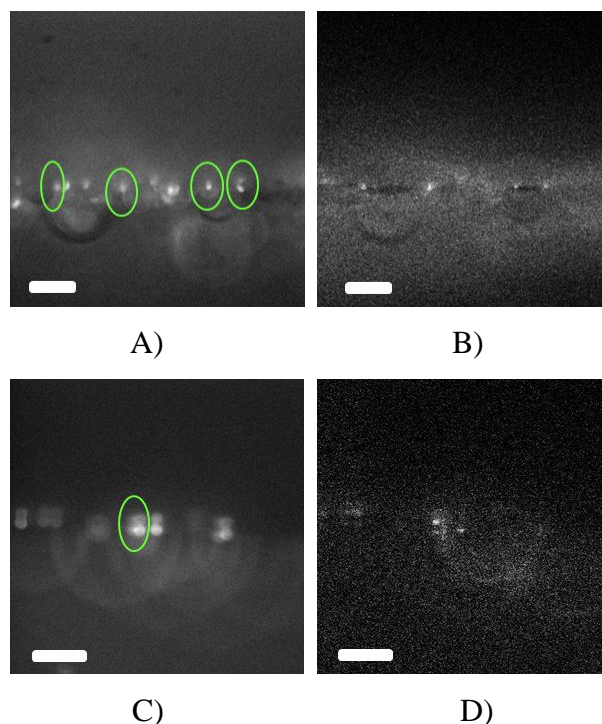


Figure 10. A and B: PL and ECL images respectively obtained with objective 20x, white bar 50  $\mu\text{m}$ ; C and D: PL and ECL images respectively obtained with objective 50x, white bar 20  $\mu\text{m}$ . Green marks show the beads on PL images which appear on ECL images (Images realised on glassy carbon electrode at + 1.2 V vs. Ag/AgCl/KCl in 100 mM TPrA)

Due to perpendicular orientation of the electrode surface to the objective, imaging the beads is more difficult than in the previous case. The reflections of beads on the electrode surface that appear on the PL images make them less clear. By comparing the PL and ECL image, one can observe that not all beads recorded by PL appear in the ECL image. The surface of the beads that emit the light in ECL image is the most important information but it cannot be concluded from ECL images obtained up to now. As the light spots on the ECL images are at least few  $\mu\text{m}$  diameter, it can be assumed that the emission does not occur only because of direct oxidation of  $\text{Ru}(\text{bpy})_3^{2+}$  but also due to  $\text{TPrA}^+$  reactivity and contribution of the revisited ECL mechanism. According to the previous experiments which show that direct oxidation of  $\text{Ru}(\text{bpy})_3^{2+}$  is of great importance, but weak ECL emission occurs also before it, can be suggested that all three mechanisms are involved in the ECL emission. However, the quality of profile beads ECL images is not satisfactory and important improvements in resolution and sensitivity should be realised to be able to use these images like reliable results.

### 4.3. CONCLUSION

In this work we presented the ECL imaging at a single bead level as a new approach in studying the ECL mechanism. The approach consists in simple recording of ECL images of a bead from different angles which provide the information about the distribution of light emission on the bead surface. This information correlated with other experiment results such as cyclic voltammogram and facts such as concentration of  $\text{Ru}(\text{bpy})_3^{2+}$ -like complex and TPrA can help in determination of involved mechanism and its impact on ECL emission. Further, as the method allows visualisation of an ECL process it can be applied for evaluation of ECL efficiency for a bead based assays and can help in optimisation of the system. Even for the assays in which the ECL intensity is analytical signal, the ECL imaging performed in the same conditions like intensity measurement may help in choosing the parameters such as electrode material, solution concentration or beads size.

The results presented so far show promise in application of this approach. Photoluminescent experiments indicate that electron-hopping is not significant and that oxidation of  $\text{Ru}(\text{bpy})_3^{2+}$  occurs only on the electrode surface. On the other hand, by comparison of PL and ECL images it was observed the same diameter of the beads indicating that entire bead emits ECL light rather than only the small region in contact with the electrode. Although the obtained ECL images from the profile of a bead have low resolution it is obvious that majority of the bead surface emit the light. This leads to conclusion that revisited route has an important significance on ECL emission from the bead surface.

Since the quality of obtained ECL images is not satisfying, many other experiments have been performed using different optical set-ups and fluorescent microscope. This work is still in progress in order to find the conditions for performing quality images from any angle of the single bead.

## REFERENCES

1. W. Miao, *Chem. Rev.*, 2008, **108**, 2506.
2. M. M. Richter, *Chem. Rev.*, 2004, **104**, 3003.
3. L. Hu and G. Xu, *Chem. Soc. Rev.*, 2010, **39**, 3275.
4. I. Rubinstein, C. R. Martin and A. J. Bard, *Anal. Chem.*, 1983, **55**, 1580.
5. I. Rubinstein and A. J. Bard, *J. Am. Chem. Soc.*, 1981, **103**, 512.
6. T. M. Downey and T. A. Nieman, *Anal. Chem.*, 1992, **64**, 261.
7. A. F. Martin and T. A. Nieman, *Anal. Chim. Acta*, 1993, **281**, 475.
8. M. Milutinovic, S. Sallard, D. Manojlovic, N. Mano and N. Sojic, *Bioelectrochem.*, 2011, **82**, 63.
9. J. K. Leland and M. J. Powell, *J. Electrochem. Soc.*, 1990, **137**, 3127.
10. J. B. Noffsinger and N. D. Danielson, *Anal. Chem.*, 1987, **59**, 865.
11. L. Dennany, E. J. O'Reilly, T. E. Keyes and R. J. Forster, *Electrochem. Commun.*, 2006, **8**, 1588.
12. X. Liu, L. Shi, W. Niu, H. Li and G. Xu, *Angew. Chem. Int. Edit.*, 2007, **46**, 421.
13. F. Deiss, C. N. LaFratta, M. Symer, T. M. Blicharz, N. Sojic and D. R. Walt, *J. Am. Chem. Soc.*, 2009, **131**, 6088.
14. Y. Shan, J.-J. Xu and H.-Y. Chen, *Chem. Commun.*, 2010, **46**, 5079.
15. G. F. Blackburn, H. P. Shah, J. H. Kenten, J. Leland, R. A. Kamin, J. Link, J. Peterman, M. J. Powell, A. Shah and D. B. Talley, *Clin Chem*, 1991, **37**, 1534-1539.
16. L. Dennany, R. J. Forster and J. F. Rusling, *J. Am. Chem. Soc.*, 2003, **125**, 5213.
17. Y. Shan, J.-J. Xu and H.-Y. Chen, *Chem. Commun.*, 2009, 905.
18. W. Miao and A. J. Bard, *Anal. Chem.*, 2004, **76**, 5379.
19. X.-H. Xu and A. J. Bard, *J. Am. Chem. Soc.*, 1995, **117**, 2627.
20. J. H. Kenten, S. Gudibande, J. Link, J. J. Willey, B. Curfman, E. O. Major and R. J. Massey, *Clin Chem*, 1992, **38**, 873-879.
21. Y. Zu and A. J. Bard, *Anal. Chem.*, 2000, **72**, 3223.
22. F. Kanoufi, Y. Zu and A. J. Bard, *J. Phys. Chem. B*, 2000, **105**, 210.
23. W. Miao, J.-P. Choi and A. J. Bard, *J. Am. Chem. Soc.*, 2002, **124**, 14478.
24. R. M. Wightman, S. P. Forry, R. Maus, D. Badocco and P. Pastore, *J. Phys. Chem. B*, 2004, **108**, 19119.
25. E. M. Gross, P. Pastore and R. M. Wightman, *J. Phys. Chem. B*, 2001, **105**, 8732.

26. D. Badocco, F. Zanon and P. Pastore, *Electrochim. Acta*, 2006, **51**, 6442.
27. M. Zhou, J. Heinze, K. Borgwarth and C. P. Grover, *ChemPhysChem*, 2003, **4**, 1241.
28. S. Zanarini, E. Rampazzo, L. D. Ciana, M. Marcaccio, E. Marzocchi, M. Montalti, F. Paolucci and L. Prodi, *J. Am. Chem. Soc.*, 2009, **131**, 2260.
29. M.-J. Li, Z. Chen, V. W.-W. Yam and Y. Zu, *ACS Nano*, 2008, **2**, 905-912.
30. [www.roche.com](http://www.roche.com).
31. B. Sigal George, E. Glezer, J. Leland, J. Wohlstadter and J. Debad, in *Electrogenerated Chemiluminescence*, CRC Press, 2004, pp. 359-396.
32. Y. Namba, M. Usami and O. Suzuki, *Anal. Sci.*, 1999, **15**, 1087.
33. W. Miao and A. J. Bard, *Anal. Chem.*, 2004, **76**, 7109.
34. X. Zhou, D. Xing, D. Zhu and L. Jia, *Anal. Chem.*, 2008, **81**, 255.
35. X. Zhou, D. Xing, D. Zhu and L. Jia, *Electrochem. Commun.*, 2008, **10**, 564.
36. A. Juris, V. Balzani, F. Barigelletti, S. Campagna, P. Belser and A. von Zelewsky, *Coord. Chem. Rev.*, 1988, **84**, 85-277.
37. K. K., *Coord. Chem. Rev.*, 1982, **46**, 159-244.
38. S. J. Woltman, W. R. Even and S. G. Weber, *Anal. Chem.*, 1999, **71**, 1504-1512.

## GENERAL CONCLUSION

---

The work presented in this doctoral dissertation was focused on the study of ECL and its application in development of new analytical techniques for different bioanalytical applications.

Generally, the first step in the development of new ECL assay is the immobilisation of ECL luminophore. A lot of efforts have been made in order to invent new techniques for immobilisation of  $\text{Ru}(\text{bpy})_3^{2+}$  or its derivatives.

Here we presented the optimisation and development of new techniques for immobilisation of an ECL exhibited polymer and its application in biorelated systems. Also, the contribution of ECL mechanisms in the efficiency of an ECL-based assay was investigated.

The first part of this work was focused on the optimisation of electrochemical immobilisation of a ruthenium metallopolymer and its application in detection enzymatic systems. The ruthenium containing polymer PVP- $\text{Ru}(\text{bpy})_2$  was immobilised on the electrode surface using cyclic voltammetry. This method provides the polymer deposition in rapid, reproducible and well-controlled one-step procedure. The obtained redox hydrogel films with micrometric thickness showed reversible, surface confined electrochemistry. Immobilised hydrogel was permeable to water soluble compounds such as coreactant and coenzymes. The ECL studies in the presence of NADH indicate that oxidative-reductive mechanism leads to light emission in the hydrogel film. The application of electrodeposited film in enzymatic reaction was demonstrated on the example of glucose detection in the presence of glucose dehydrogenase. The enzymatically generated NADH is oxidised at the electrode surface and reacts with hydrogel's  $\text{Ru}^{2+}$  centres leading to the ECL emission. Glucose detection with the ECL hydrogel is demonstrated at much lower anodic potential than with the model  $\text{Ru}(\text{bpy})_3^{2+}$  complex. It is interesting to notice that the immobilised luminophore in the hydrogel is regenerated during the ECL process and that the coreactant is also regenerated by the enzymatic reaction. This leads to the amplification of ECL intensity and an improvement of the sensitivity.

The second part of this work describes photodeposition and photopatterning as novel method of immobilisation of an ECL luminophore. The method is simple and rapid providing ultrathin films. Moreover, it requires cheap equipment for photolithography. Electrochemical

and ECL properties of obtained nanometric films are comparable with those of electrodeposited films. This indicates that there is no change in the structure of the ruthenium complex and in the excited state due to entrapment in PEGDA hydrogel or to the UV light illumination. The ultrathin photodeposited film showed linear dependence on the TPrA concentration. The advantage of photodeposition over other previously reported methods is that it allows region-selective immobilisation of active centres. Using photolithographic methods, the figures from the mask are projected on the electrode surface. This results in formation of photopatterns which size, shape and thickness can be modulated depending on fabrication parameters. As they contain ECL-exhibiting  $\text{Ru}^{2+/3+}$  centers which show strong ECL response, they can be used for ECL imaging. The development of such process presents the first and the essential step in developing of micrometric ECL spots arrays and allows multiplexed detection by ECL imaging.

The third part of this work was dedicated to study the ECL mechanisms that lead to ECL emission from a single microbead. A new approach which combines spectroelectrochemistry and ECL imaging was presented. The study was performed on 6  $\mu\text{m}$  diameter polystyrene microbeads which surface was modified with  $\text{Ru}(\text{bpy})_3^{2+}$  complex to simulate the labelled beads which are used in bioassays. The light emission was monitored at the single bead level performing PL and ECL images from different angles (mainly direct and profile view). Using this approach the distribution of electroactive and ECL sites has been highlighted. From this study we can clarify the mechanism that leads to ECL emission at the single bead level which is of great importance for understanding and improving the ECL emission in bead-based assays.

Concerning the obtained results it can be concluded that both electrodeposited and photodeposited ruthenium metallopolymer show efficient ECL emission. Electrodeposited redox hydrogel shows linear dependence on the substrate (glucose) concentration. In the same time, photodeposition allows successful photopatterning and fabrication of microspot arrays which size, shape and thickness can be modulated. Thus, the future work should be focalised on the development of a complete multiplexed assay. In most of the multiplexed assays, the ECL label concentration is determined. In contrast to that, in our case, the ECL luminophore is immobilised on the electrode surface and ECL intensity shows dependence on coreactant concentration. For this reason, if on different spots of a pattern are immobilised different dehydrogenase, for example, the NADH will be produced locally and ECL will be emitted only from the spots which enzyme corresponds to present substrate. This concept can be applicable



in all recognition reactions in which the coreactant is brought or produced locally near to individual spot.

The ECL imaging at the single bead level shows a promise in studying the mechanism in an ECL process. The future work should be dedicated on optimisation of imaging conditions to obtain clear, reliable ECL image under the any angle of acquisition. The combination of spectroelectrochemistry and ECL imaging should be developed to serves as rapid and efficient method for investigation of involved ECL mechanisms. The same approach may be also applied for determination of experimental conditions for an efficient bead-based assay.

~ ~ ~

## EXPERIMENTAL PART

~ ~ ~

The work presented in this thesis is focused on electrogenerated chemiluminescence detection. The first two parts deal with advanced techniques of immobilisation of a ruthenium containing polymer like an ECL luminophore while the third part is dedicated to the study of the ECL reaction mechanism based on ECL imaging. Thus, this work employs different methods of immobilisation and characterisation including different types of microscopy, spectroscopy and electrochemical techniques which are presented here.

**Materials.** Glucose dehydrogenase (EC1.1.1.47, from *Thermoplasma acidophilum*),  $\beta$ -nicotinamide adenine dinucleotide hydrate ( $\text{NAD}^+$ ),  $\beta$ -nicotinamide adenine dinucleotide reduced dipotassium salt (NADH), sodium phosphate dibasic heptahydrate, sodium phosphate monobasic monohydrate, poly(ethylene glycol) diacrylate (PEGDA), 2,2-dimethoxy-2-phenylacetophenone (DMPA), tri-*n*-propylamine and bis(2,2'-bipyridine)-4'-methyl-4-carboxybipyridine-ruthenium N-succinimidyl ester-bis(hexafluorophosphate) were purchased from Sigma. D-(+)-Glucose anhydrous was from Fluka. The latex beads were purchased from Polysciences. The synthesis of  $[\text{poly}(4\text{-vinylpyridine})\text{Ru}(2,2'\text{-bipyridine})_2\text{Cl}]^{+/2+}$  has been reported previously.<sup>1</sup>

**Apparatus.** All electrochemical and ECL experiments were performed with a  $\mu$ -Autolab Type III and PGSTAT30 electrochemical stations. ECL intensity was measured using Hamamatsu photomultiplier tube R4632 while ECL spectra were recorded with a Princeton Instruments spectrograph SpectraPro 2300i. SEM imaging was realized by Hitachi TM-1000 scanning electron microscope. Spin-coating was performed using a Caframo BDC6015-220 apparatus. UV light illumination for the photodeposition step was done with a X-Cite 120 lamp. Imaging instrumentation was an epifluorescence microscope Olympus BXFM-ILHSPU equipped with a Hamamatsu EM-CCD camera and Leica DMR TCS SP2 confocal microscope. All Atomic Force Microscopy observations were recorded using a Veeco Nanoscope Multimode 8 with ScanAsyst.

## 1. ELECTROGENERATED CHEMILUMINESCENCE ON ELECTRODEPOSITED REDOX HYDROGEL

### 1.1. Electrodeposition of $[\text{poly}(4\text{-vinylpyridine})\text{-Ru}(2,2'\text{-bipyridine})_2\text{Cl}]^{+/2+}$ on the electrode surface

The  $[\text{poly}(4\text{-vinylpyridine})\text{-Ru}(2,2'\text{-bipyridine})_2\text{Cl}]^{+/2+}$  (PVP-Ru(bpy)<sub>2</sub><sup>2+</sup>) was previously synthesised<sup>1</sup> and it was received like 10 mg/mL water solution. The solution for

electrodeposition was prepared by dissolving the polymer in 10 mM phosphate buffer to a final concentration 0.95 mg/mL. The electrodeposition was carried out at glassy carbon (GC) and home-made graphite electrodes. The GC electrodes were commercially available. The graphite electrodes were made by placing a graphite disc on the top of the body of commercial electrode. The connection was provided with a mercury drop (Figure 1A). Polishing procedure was different for the different kinds of electrode. Glassy carbon electrodes were polished with 0.5  $\mu\text{m}$  alumina powder, sonicated in Milli-Q water for 2 minutes and dried with compressed air. Home-made graphite electrodes were polished using silicon carbide grinding paper (P4000, Buehler), washed with Milli-Q water and dried with compressed air. Both types of electrodes were plasma pre-oxidised (oxygen or air, 0.5 Torr, 10 min).

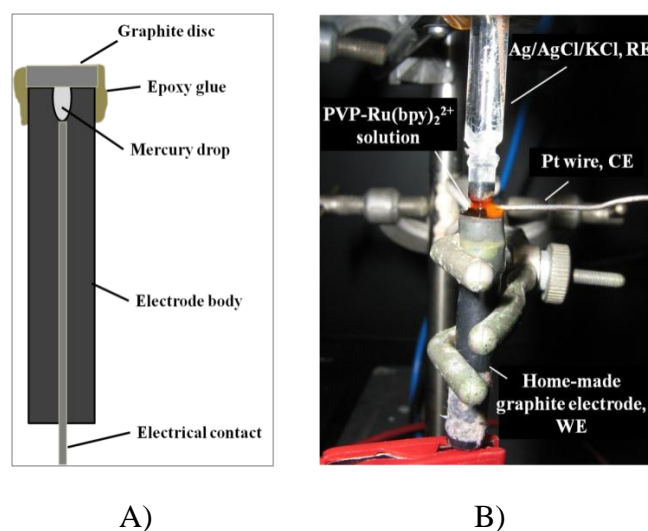


Figure 1. A) Scheme of home-made graphite electrode; B) Image of set up for electrodeposition of  $\text{PVP-Ru}(\text{bpy})_2^{2+}$

The electrode modification was carried out in three-electrode cell with GC or home-made graphite electrode as working one and  $\text{Ag/AgCl/KCl}$  3 M saturated electrode and a platinum wire as reference and counter electrodes, respectively. Because of small amount of synthesised  $\text{PVP-Ru}(\text{bpy})_2^{2+}$  the whole electrodeposition process was realised in a drop (Figure 1A).

The electrodeposition of the polymer was performed by cycling the polymer solution between +0.2 V and +1.1 V vs.  $\text{Ag/AgCl/KCl}$  at scan rate 100 mV/s. In the first experiments the electrodeposition was running for 100-500 scans to find to optimal number of scans. It was

found that ECL emission shows the maximum intensity for the films immobilised during 400 scans and this conditions was kept in all further experiments.

## 1.2. Electrochemical characterisation

The electrochemical characterisation of immobilised redox hydrogel was performed by cyclic voltammetry from +0.2 V to +1.1 V *vs.* Ag/AgCl/KCl at scan rate 10 mV/s in 100 mM phosphate buffer solution (pH=7.4).

## 1.3. ECL experiments

ECL detection presents a marriage between electrochemical and spectroscopic methods thus the set-up for an ECL experiment consist of both electrochemical work station and light detection device. In this case, ECL intensity measurements were carried out in home-made electrochemical cell with transparent window made of cover glass slide which allows that emitted light is detected with minimum loss. The three-electrode system was consisting of glassy carbon or graphite electrode modified with electrodeposited ruthenium containing polymer as working electrode and Ag/AgCl/KCl 3 M saturated electrode and a platinum wire as reference and counter electrodes, respectively. The whole electrochemical cell was set in front of photomultiplier tube (PMT) with the surface of working electrode orientated toward the detector. The measured signal strongly depends on the distance between the detector and the emitting surface, thus the surface of working electrode was always kept at the same distance from the detector (5 mm). The whole set-up was placed in a dark box to prevent incoming of any other light on the detector except of photons emitted in the ECL reaction. The light emission was measured by PMT which was triggered with the potentiostat to record the light emission simultaneously with cyclic voltammogram.

### 1.3.1. ECL characterisation of the electrodeposited film

To study the ECL behaviour of electrodeposited redox film, the ECL signal was detected in the presence of NADH like coreactant. The measurements were done in the solutions with different concentration of NADH in 100 mM phosphate buffer (pH=7.4). The ECL responses were recorded by PMT during the cyclic voltammetry between +0.2 V and +1.05 V *vs.* Ag/AgCl/KCl.

### 1.3.2. ECL detection of glucose

The graphite electrode modified with ruthenium polymer during 400 scans was used as working one. Ag/AgCl/KCl 3 M saturated electrode and a platinum wire as reference and counter electrodes, respectively. Like in the case of ECL detection of NADH, the electrodes were placed in electrochemical cell with transparent window with surface of working electrode orientated toward the PMT. The solution which consists of enzyme, substrate and  $\text{NAD}^+$  was incubated for 30 minutes at  $37^\circ\text{C}$  to allow enzymatic reaction to take place. After the incubation the solution was rapidly placed in electrochemical cell for the detection. The ECL intensity was measured during cycling between +0.2 V and +1.05 V vs. Ag/AgCl/KCl at scan rate 30 mV/s.

To optimise the condition of glucose detection, the influence of pH of the solution has been studying. For this investigation, the examined solution was consisting of 10 mM  $\text{NAD}^+$  and 9.28 U/mL of GDH and 30 mM glucose prepared in the different buffer solutions. For pH=6-7.4 were prepared phosphate buffer solutions, while for pH=8 and pH=9 was tris buffer solutions. The preparation of the buffer solutions is summarised in Table 1.

Table 1. Composition of buffer solutions

Phosphate buffer solutions		
pH	g of $\text{NaH}_2\text{PO}_4 \cdot \text{H}_2\text{O}$ in 100 mL of buffer solution	g of $\text{Na}_2\text{HPO}_4 \cdot 7\text{H}_2\text{O}$ in 100 mL of buffer solution
6	1.2142	0.3218
6.5	0.9643	0.8078
7	0.5836	1.5466
7.4	0.3117	2.0747
Tris buffer solutions		
pH	mL of 0.1 M Tris in 100 mL of buffer solution	mL of 0.1 M HCl in 100 mL of buffer solution
8	50	29.2
9	50	5.7

Solutions with different concentrations of glucose have been analysed. The solutions were consisting of 9.28 U/mL GDH, 10 mM  $\text{NAD}^+$  and glucose with concentration in range from 1 to 30 mM, prepared in the phosphate buffer solution (pH=7.4). The experimental set up was the same like in the previous cases. The ECL intensity was measured during cycling between +0.2 V and +1.05 V vs. Ag/AgCl/KCl at scan rate 30 mV/s.

### 1.3.3. The ECL spectra recording

The ECL spectra were performed using SpectraPro 2300i spectrograph. The spectrograph was designed for the spectral analysis of emitted light and it was equipped with CCD camera with low working temperature ( $-125^{\circ}\text{C}$ ) which decrease the noise and improves the sensitivity. The experimental setup was similar as for ECL experiments where ECL intensity is measured except that photomultiplier tube was replaced by optical fibre input of the spectrograph. The ruthenium polymer modified graphite electrode, Pt wire and Ag/AgCl/KCl reference electrode were placed in the cell with transparent window. The optical fibre input of the spectrograph was placed in front of the working electrode to collect the emitted light and transfer it to the detector. The set-up was placed in dark box and the spectra were recorded by applying constant step potential of 1.2 V vs. Ag/AgCl/KCl during the spectrum acquisition in 10 mM TPrA solution in phosphate buffer (pH=7.4).

## 2. PHOTODEPOSITION AND PHOTOPATTERNING

### 2.1. Preparation of electrodes

Photodeposition of the ruthenium containing polymer was performed on GC disc electrodes, gold disc electrodes and gold coated plates. All disc electrodes were polished using 0.05  $\mu\text{m}$  alumina powder, rinsed and sonicated in Milli-Q water for 2 minutes before use. The commercially available gold coated plates were cut using the equipment for glass cutting to form the plates with size up to 1x1 cm. Before the photodeposition the gold coated plates were cleaned with Piranha solution in order to obtain clean gold surface with hydrophilic properties. Piranha solution was prepared by mixing  $\text{H}_2\text{SO}_4$ (98%) and  $\text{H}_2\text{O}_2$ (30%) in ratio 3:1 (v.v). The Piranha solution is very corrosive and all experiments were done carefully. The gold plates were immersed in the Piranha solution for at least two hours and then abundantly rinsed with Milli-Q water. To avoid the post-treatment pollution, the gold plates were kept in the Milli-Q water and dried with compressed air just before using.

### 2.2. Polymer solution preparations

The redox polymer hydrogel precursor solution contains poly(ethylene glycol) diacrylate (PEGDA) as macromer, 2,2'-dimethoxy-2-phenylacetophenone (DMPA) as photoinitiator and PVP-Ru(bpy) $_2^{2+}$ .

First, PEGDA and DMPA were mixed in desired ratio and then this solution was mixed with 5 mg/ml water solution of PVP-Ru(bpy)<sub>2</sub><sup>2+</sup> in volume ratio 1:1. Different mass ratios of PEGDA/DMPA were tested including 200:1, 100:1, 50:1 and 15:1. The 100:1 ratio leads to the highest ECL intensity and it was used in all further experiments. All solutions were freshly prepared and protected from the light using the aluminium foil.

### **2.3. Photodeposition and photopatterning**

Freshly prepared photopolymer solution was dropped on the electrode surface and spin coated during 20 s with different rotational speed from 2000 to 10000 rpm. The electrode was then rapidly placed in front of UV light during 5 s. The distance from the light source was 6.5 cm. By this way we obtained smooth thin films of photopolymer. By modifying the rotational speed we were able to tune the thickness of the photodeposited layers. The procedure for photopatterning was the same with addition of photolithography mask placed 1 mm above the electrode surface. After the UV exposure, electrode surface was abundantly rinsed with Milli-Q water to remove the part of the photopolymer which was in the shadow part of the mask and remained nonpolymerised during the process. Obtained photopatterns were dried and kept at the ambient temperature.

### **2.4. Electrochemical characterisation**

Photopolymer modified electrodes were characterised by cyclic voltammetry. Three-electrode electrochemical cell consists of Ag/AgCl/KCl like reference, Pt wire like contra electrode and photopolymer modified electrode as a working one. Characterisation was performed by cyclic voltammetry between +0.5 V and +1.0 V at scan rate 50 mV/s in 100 mM phosphate buffer solution (pH = 7.4).

### **2.5. PL and ECL imaging**

The PL and ECL imaging were performed using horizontal epifluorescence microscope. Figure 2 presents scheme of the epifluorescence microscope that was used.



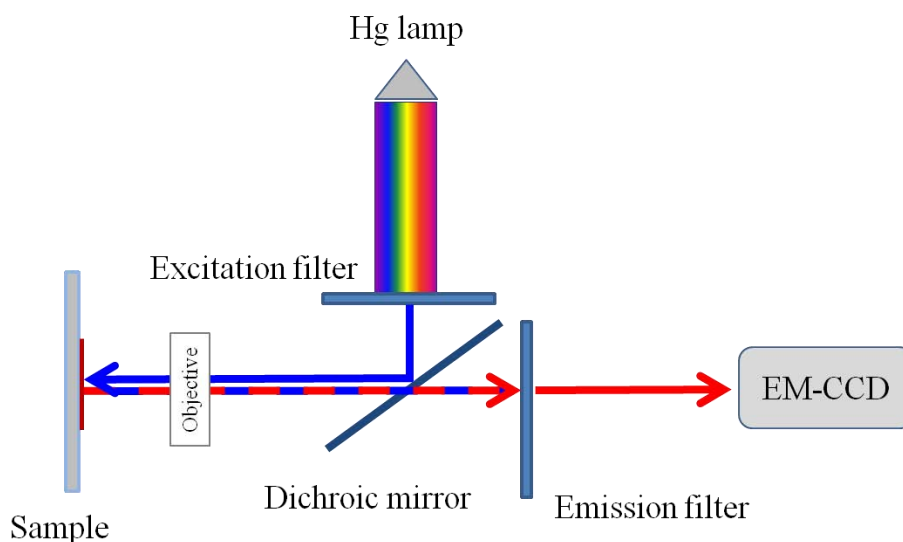


Figure 2. Scheme of epifluorescence microscope

The microscope was equipped with mercury lamp. Specific set of filters was used to select the excitation and emission wavelength of  $\text{Ru}(\text{bpy})_3^{2+}$ -fluorophore. Only the light that correspond to the excitation of luminophore passes through and is reflected by dichroic mirror toward the sample. A dichroic mirror (dichroic beam splitter) reflects shorter wavelengths of light and allows longer wavelengths to pass. A dichroic mirror is required because the objective acts as both a condenser lens (excitation light) and objective lens (emission light) therefore the beam splitter isolates the emitted light from the excitation wavelength. The wavelength at which a beam splitter allows the longer wavelengths to pass must be set between the excitation and emission wavelengths so that excitation light is reflected and emission light is allowed to pass through it (Figure 3). In all experiments the set of filters which correspond to ruthenium complex as luminophore was used. The components of the set and the transmission spectra of the filters are presented in Table 2 and Figure 3 respectively.

Table 2. Set of filters for ruthenium complex PL imaging

Filter type	Label	Wavelength
Excitation filter	485DF22	485 nm
Dichroic filter	540DRLP	540 nm
Emission filter	605DF50	605 nm

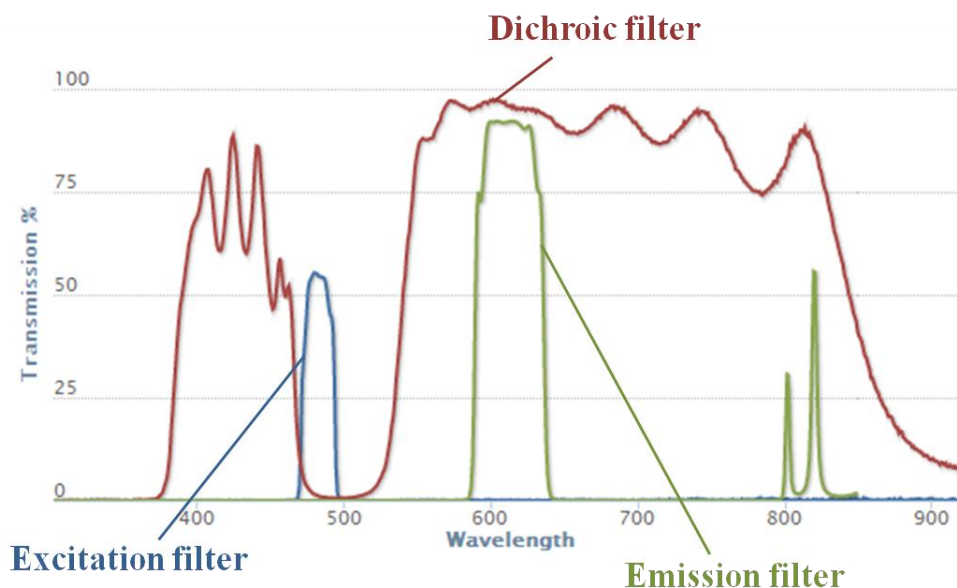


Figure 3. Transmission spectra of the set of filters for ruthenium complex fluorore (from [www.omegafilters.com](http://www.omegafilters.com))

The microscope was equipped with 5x, 10x, 20x, 50x and 100x (Olympus) from which last three were long working distance objectives. The detection was provided by Electron Multiplying CCD (Hamamatsu EM-CCD digital camera).

The PL imaging was often performed just before ECL imaging (to allow the comparison of the two images) thus the experimental set-up was the same. The three-electrode home-made cell with transparent window was placed in front of microscope objective. The reaction solution was consisting of 100 mM TPrA in the 100 mM phosphate buffer (pH=7.4).

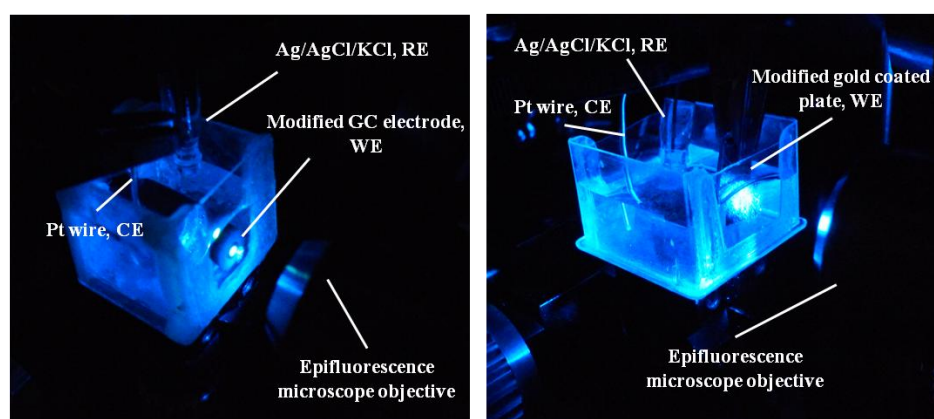


Figure 4. Experimental setup for PL and ECL imaging for A) disc and B) gold coated plate electrode (images obtained during PL exposure)

The electrodes were connected to potentiostat. For PL imaging no potential was applied.

In contrast, for ECL imaging there is no need of excitation light source but the application of the potential is required. The ECL reaction was generated by applying constant potential at +1.2 V vs. Ag/AgCl/KCl and the emitted light was detected by the EM-CCD. No filter was used to diminish the loss of emitted light. For ECL imaging, the whole set-up including microscope and camera was placed in dark box to avoid surround light which intensity may be higher than ECL to reach the detector. Also, images with no application of potential were recorded to check that there is no background light.

## 2.6. AFM imaging

To obtain information about the topography and the thickness of the photopatterns, atomic force microscopy was used. Veeco Nanoscope Multimode 8 with ScanAsyst is a new generation AFM microscope which utilises new Peak Force Tapping mode. In peak force tapping mode, similar to the tapping mode, the probe and sample are intermittently brought together to contact the surface for a short period, eliminating lateral forces. Unlike tapping mode, in which the feedback loop keeps the cantilever vibration amplitude constant, peak force tapping controls maximum force applied by the tip. Peak force tapping is a technique that generates force/distance curves at each pixel. Information concerning different mechanical properties (elasticity, deformation, adhesion, dissipation) can be extracted during the course of scanning the entire cell using built-in software.

For AFM imaging the photopatterns were deposited on the surface of gold plate electrodes to be able to fit in sample holder. For the imaging, the redox hydrogel was in the dry state. Thickness and roughness was analysed by depth and roughness analysis available by software NanoScope Analysis.

## 3. ECL IMAGING AT THE SINGLE BEAD LEVEL

### 3.1. Beads surface modification

Polystyrene beads size 6  $\mu\text{m}$  diameter were used. The beads surface was  $-\text{NH}_2$  modified which allows further functionalisation of the beads surface. In order to add the ECL exhibiting ruthenium complex on the bead surface, the beads were functionalised by  $\text{Ru}(\text{bpy})_3^{2+}$ -NHS ester (bis(2,2'-bipyridine)-4'-methyl-4-carboxybipyridine-ruthenium N-succinimidyl ester-

bis(hexafluorophosphate, abbreviated  $\text{Ru}(\text{bpy})_2(\text{mcbpy-O-Su-ester})(\text{PF}_6)_2$ ) whose ECL behaviour is very similar to that of  $\text{Ru}(\text{bpy})_3^{2+}$ .

10  $\mu\text{L}$  of beads suspension (2.5% solid-latex) was washed with phosphate buffer solution,  $\text{pH}=7.4$  and resuspended in 1 mL of PB. In the same time, 1 mg of  $\text{Ru}(\text{bpy})_2(\text{mcbpy-O-Su-ester})(\text{PF}_6)_2$  was dissolved in 100  $\mu\text{L}$  of dimethyl sulfoxide and this solution was added to the beads suspension. This mixture was incubated on  $+4^\circ\text{C}$  for 3 hours with periodical stirring. After the incubation the beads were washed from reaction solution with phosphate buffer 10-15 times by the centrifugation for 10 min at 10000 rpm to separate the beads from the solution. Finally, beads were suspended in 1 mL phosphate buffer and kept at  $4^\circ\text{C}$ .

### 3.2. Beads immobilisation at the electrode surface

In the first experiments glassy carbon, gold and platinum disc electrode and ITO and gold coated plates were used. As the highest intensity and stability of ECL was found at GC electrode in the most of ECL experiments were performed with CG electrode. In PL imaging with confocal microscope due to microscope design, gold coated plates was utilised. The GC electrode was polished using 0.05  $\mu\text{m}$  alumina powder, rinsed and sonicated in Milli-Q water for 2 minutes and dried with compressed air. The gold coated plates were sonicated for 2 min in acetone, ethanol and Milli-Q water respectively and dried with compressed air.

To immobilise the beads at the electrode surface the drop of beads suspension was applied and was let to dry on the room temperature. The electrode with immobilised beads was dried and stored in the dark to avoid the photobleaching by ambient light.

### 3.3. PL and ECL imaging by epifluorescence microscopy

PL and ECL imaging was realised by the same epifluorescence microscope like the one presented in the paragraph 5.2.6. The setup was similar like for imaging of photodeposited redox hydrogel (Image 4A). The three electrodes were placed in home-made cell with transparent window in the presents of 100 mM TPrA solution in phosphate buffer,  $\text{pH}=7.4$ . The GC disc electrode was placed in front of microscope objective with the surface parallel with the objective for the direct view and with the surface perpendicular with the objective for the profile view imaging. The PL imaging was performed by the same set of filters for ruthenium complex presented previously. The ECL emission was provided by applying a potential of  $+1.2\text{ V vs. Ag/AgCl/KCl}$ .

### 3.4. PL imaging by confocal microscopy

The PL properties of the beads before and after the applying the potential was performed by confocal microscopy. In a conventional wide-field microscope, the entire specimen is bathed in light from a mercury or xenon source, and the image can be viewed directly by eye or projected onto an image capture device. In contrast, the method of image formation in a confocal microscope is fundamentally different. Illumination is achieved by scanning one or more focused beams of light, usually from a laser, across the specimen. This point of illumination is brought to focus in the specimen by the objective lens. The sequences of points of light from the specimen are detected by a photomultiplier tube through a pinhole and the output from the PMT is built into an image and displayed by the computer. For comparison of two types of microscopy, Figure 5 shows the scheme of wide-field A and confocal microscope B. Confocal microscopy offers several advantages over conventional wide-field optical microscopy, including the elimination or reduction of background information away from the focal plane and the capability to collect serial optical sections from thick specimens. Using digital image processing techniques, these serial images can be reassembled to form 3D representation of the structures that is studied.

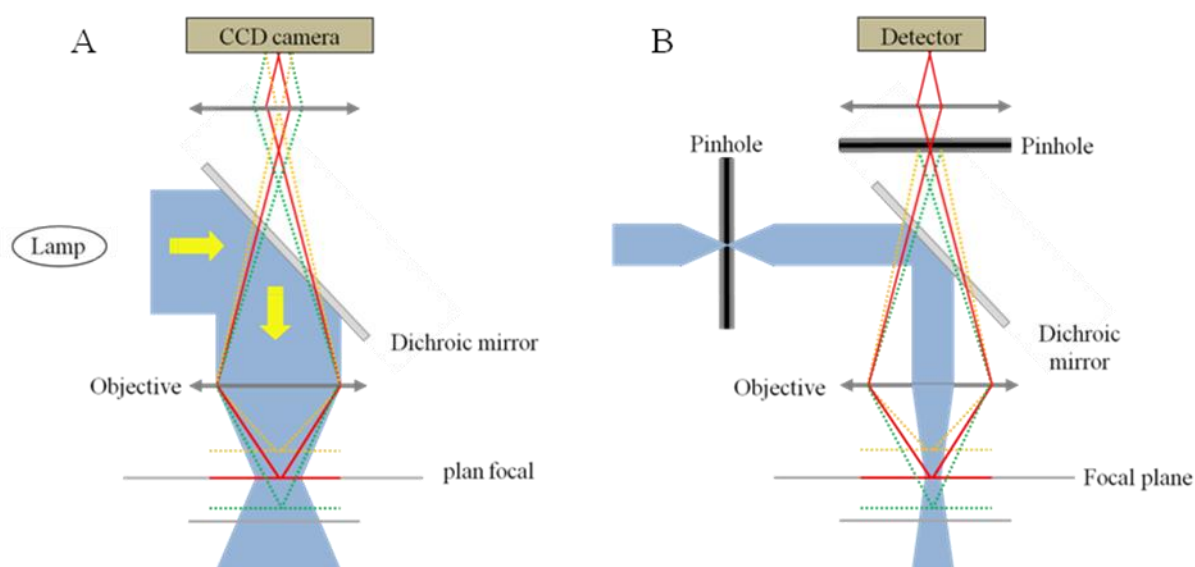


Figure 5. Scheme of A) wide-field epifluorescence microscope and B) confocale microscope

The beads modified by  $\text{Ru}(\text{bpy})_3^{2+}$ -NHS ester were imaged by PL with a confocal microscope. The plate was parallel with the objective of the vertical confocal microscope. The images were performed with application of different potential steps. In the electrode cell the gold coated plate was the working electrode while Ag wire was used as counter electrode.. All

images were done with objective of magnification 63x, with numeric aperture  $N=0.90$ . The excitation laser was set at 514 nm while detection was in range from 520-560 nm.

## References

1. S. Sallard, J. Patole, V. Soukharev, A. Heller, N. Mano and N. Sojic, *Electrochem. Commun.*, 2009, **11**, 599.